



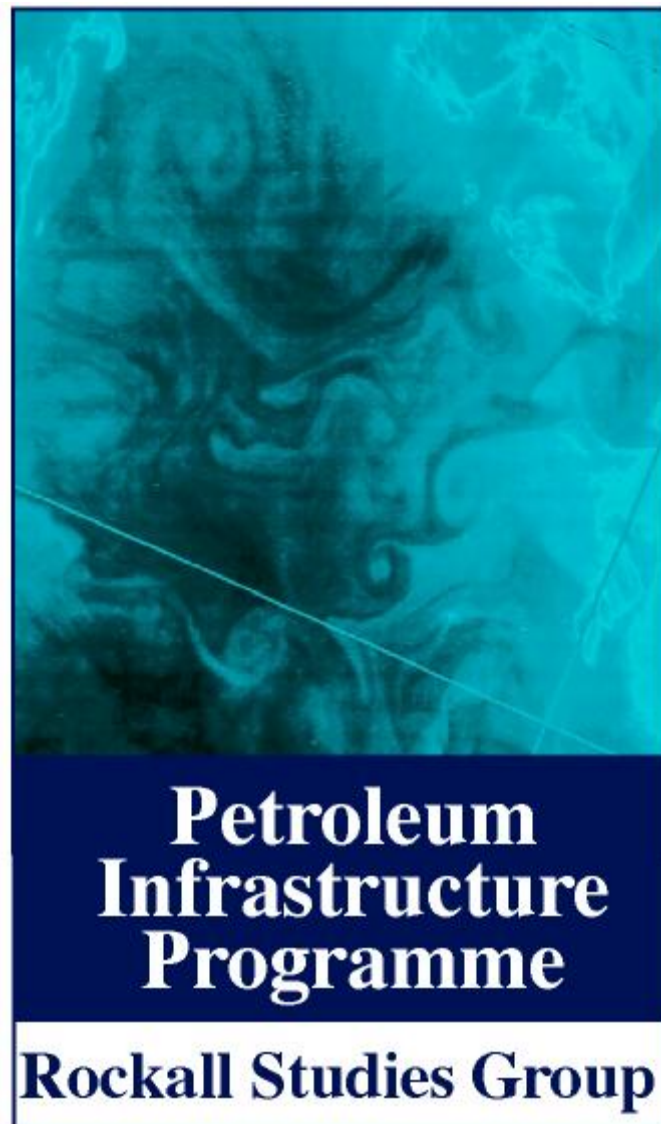
**THERMAL HISTORY RECONSTRUCTION IN IRISH ROCKALL
TROUGH BOREHOLES 16/28-sb01, 83/20-sb01, 83/24-sb02
USING AFTA[®], VR AND FLUID INCLUSION DATA**

GEOTRACK REPORT #777

**A report prepared for the Rockall Studies Group
through Dr John Parnell, University of Aberdeen**

Report prepared by:	P.F. Green
AFTA determinations by:	P.F. Green

January 2001



AFTA ANALYSIS OF ROCKALL CORE SAMPLES

RSG PROJECT 00/1

SEA BED TECHNICAL COMMITTEE



"This Project, including data and survey results acquired for the purpose, has been undertaken on behalf of the Rockall Studies Group (RSG) of the Irish Petroleum Infrastructure Programme Group 2 which was established by the Petroleum Affairs Division of the Department of the Marine and Natural Resources on 4 June, 1997 in conjunction with the award of exploration licences under the Rockall Trough Frontier Licensing Round. The RSG comprises: Agip (UK) Ltd, Anadarko Ireland Company, ARCO Ireland Offshore Inc, BG Exploration & Production Ltd, BP Exploration Operating Company Ltd, British-Borneo International Ltd, Elf Petroleum Ireland BV, Enterprise Energy Ireland Ltd, Mobil Oil North Sea Ltd, Murphy Ireland Offshore Ltd, Phillips Petroleum Exploration Ireland, Saga Petroleum Ireland Ltd, Shell EP Ireland B.V., Statoil Exploration (Ireland) Ltd, Total Oil Marine plc, Union Texas Petroleum Ltd and the Petroleum Affairs Division of the Department of the Marine and Natural Resources."

"The ownership of and copyright to all the data and interpretations contained herein resides with PIPCo RSG Ltd."

Geotrack International Pty Ltd and its officers and employees assume no responsibility and make no representation as to the productivity or profitability of any mineralisation, oil, gas or other material in connection with which this report may be used.

AFTA[®] and Geotrack[®] are registered trademarks owned and maintained by Geotrack International Pty Ltd.



THERMAL HISTORY RECONSTRUCTION IN IRISH ROCKALL TROUGH BOREHOLES 16/28-sb01, 83/20-sb01, 83/20-sb02 USING AFTA®, VR AND FLUID INCLUSION DATA

GEOTRACK REPORT #777

CONTENTS

	Page
Executive Summary	i
Technical Summary	ii
AFTA and VR paleotemperature analysis summary - Table i	iv
ZFTA Data Summary Table ii	v

1. Introduction	
1.1 Aims and Objectives	1
1.2 Report Structure	2
1.3 Data Quality	3
1.4 Apatite Compositions	4
2. Interpretation strategy	
2.1 Thermal history interpretation of AFTA data	5
2.2 Thermal history interpretation of VR data	7
2.3 Comparison of paleotemperature estimates from AFTA and VR	8
2.4 Estimates of paleogeothermal gradients and removed section	9
2.5 Determination of removed section	10
3. Thermal history interpretation of data from Borehole 16/28-sb01	
3.1 Geological background	12
3.2 Thermal history interpretation of AFTA data	13
3.3 Comments on igneous rock near TD	14
3.4 Fluid inclusion results	15
4. Thermal history interpretation of data from Borehole 83/20-sb01	
4.1 Geological background	22
4.2 Thermal history interpretation of AFTA data	22
4.3 Fluid inclusion results	24
5. Thermal history interpretation of data from Borehole 83/24-sb02	
5.1 Geological background	33
5.2 Thermal history interpretation of AFTA data	34
5.3 Fluid inclusion results	35



CONTENTS continued

6.	Thermal history synthesis	
6.1	Mechanisms of cooling and heating	43
6.2	Amounts of removed section	44
6.3	Timescales of hot fluid pulses	47
7.	ZFTA data: sediment provenance and depositional age constraints	
7.1	Introduction	53
7.2	Borehole 16/28-sb	53
7.3	Borehole 83/20-sb01	54
7.4	Borehole 83/24-sb02	55
7.5	Synthesis of ZFTA data	56
	References	57
Appendix A	- Sample Details, Geological Data and Apatite Compositions	A.1 -A.6
Appendix B	- Sample Preparation, Analytical Details and Data Presentation	B.1-B.32
Appendix C	- Principles of Interpretation of AFTA & ZFTA Data in Sedimentary Basins	C.1-C.25
Appendix D	- Vitrinite Reflectance Measurements	D.1-D.13

TABLES

	Page
Table i - AFTA paleotemperature analysis summary	iv
Table ii - ZFTA data	v
Table 3.1 - Apatite Fission Track data summary; Borehole 16/28-sb01	16
Table 3.2 - Thermal history interpretation summary; Borehole 16/28-sb01	17
Table 3.3 - Estimates of timing and magnitude of elevated paleo-temperatures from AFTA; Borehole 16/28-sb01	18
Table 3.4 - Maximum temperatures from VR ; Borehole 16/28-sb01	19
Table 4.1 - Apatite Fission Track data summary; Borehole 83/20-sb01	26
Table 4.2 - Thermal history interpretation summary; Borehole 83/20-sb01	27
Table 4.3 - Estimates of timing and magnitude of elevated paleo-temperatures from AFTA; Borehole 83/20-sb01	28
Table 4.4 - Maximum temperatures from VR ;	



CONTENTS continued

Table 5.1 - Apatite Fission Track data summary; Borehole 83/24-sb02	37
Table 5.2 - Thermal history interpretation summary; Borehole 83/24-sb02	38
Table 5.3 - Estimates of timing and magnitude of elevated paleo- temperatures from AFTA; Borehole 83/24-sb02	39
Table 5.4 - Maximum temperatures from VR ; Borehole 83/24-sb02	40
Table 6.1 - Key samples for burial estimation	45
Table 6.2 - Removed section estimates	46
Table A.1 - Details of AFTA samples and apatite yields	A.4
Table A.2 - Summary of stratigraphy	A.5
Table A.3 - Lower limits of detection for apatite analyses	A.6
Table A.4 - Percent errors in chlorine content	A.6
Table B.1 - Apatite fission track analytical results	B.10
Table B.2 - Length distribution summary data	B.11
Table B.3 - AFTA data in compositional groups	B.12 - B.14
Table B.4 - ZFTA data	B.15
Glossary	B.18
Analytical data	B.19 - B.32
Table D.1 - Paleotemperature - vitrinite reflectance nomogram	D.6
Table D.2 - Vitrinite reflectance sample details and results supplied by Client and Keiraville Konsultants	D.7-D.13

FIGURES

Figure i - Reconstructed thermal history	iv
Figure 3.1 - AFTA and ZFTA parameters plotted against sample depth and present temperature; Borehole 16/28-sb01	20
Figure 3.2 - Paleotemperature constraints; Borehole 16/28-sb01	21
Figure 4.1 - AFTA and ZFTA parameters plotted against sample depth and present temperature; Borehole 83/20-sb01	31
Figure 4.2 - Paleotemperature constraints; Borehole 83/20-sb01	32
Figure 5.1 - AFTA and ZFTA parameters plotted against sample depth and present temperature; Borehole 83/24-sb02	41
Figure 5.2 - Paleotemperature constraints; Borehole 83/24-sb02	42
Figure 6.1 - Timing summary	49
Figure 6.2 - AFTA modelling; preferred thermal history interpretation sample GC777-2	50
Figure 6.3 - AFTA modelling; with addition of short term heating	51
Figure 6.4 - AFTA modelling summary	52



CONTENTS continued

Figure A.1 - Present-day temperature profile	A.9
Figure B.1 - Construction of a radial plot	B.16
Figure B.2 - Simplified structure of radial plots	B.17
Figure C.1a - Comparison of mean length in Otway Basin reference wells with predictions of Laslett et al. (1987) model	C.18
Figure C.1b - Comparison of mean length in apatites of the same Cl content as Durango from Otway Group samples with predictions of Laslett et al. (1987) model	C.18
Figure C.2 - Comparison of mean length in apatites of differing chlorine compositions	C.19
Figure C.3 - Comparison of mean length in Otway Basin reference wells with predictions of new multi-compositional annealing model	C.19
Figure C.4 - Histogram of Cl contents in typical samples	C.20
Figure C.5 - Comparison of mean length in Otway Basin reference wells with predictions of Crowley et al. (1991) model for F-apatite	C.21
Figure C.6 - Comparison of mean length in Otway Basin reference wells with predictions of Crowley et al. (1991) model for Durango apatite	C.21
Figure C.7 - Changes in radial plots of post-depositional annealing	C.22
Figure C.8 - Typical AFTA parameters: a. Maximum temperatures now b. Hotter in the past	C.23
Figure C.9 - Constraint of paleogeothermal gradient	C.24
Figure C.10 - Estimation of section removed	C.25



THERMAL HISTORY RECONSTRUCTION IN IRISH ROCKALL TROUGH BOREHOLES 16/28-sb01, 83/20-sb01, 83/24-sb02 USING AFTA[®], VR AND FLUID INCLUSION DATA

GEOTRACK REPORT #777

EXECUTIVE SUMMARY

Introduction and Objectives

Apatite Fission Track Analysis (AFTA[®]), Zircon Fission Track Analysis (ZFTA[™]) and vitrinite reflectance (VR) have been applied to core samples from **Irish Rockall Trough Boreholes 16/28-sb01, 83/20-sb01, 83/24-sb02**. The study was commissioned by **Dr John Parnell**, Dept. of Geology and Petroleum Geology, University of Aberdeen, on behalf of the **Rockall Studies Group (RSG)**. Results from these analyses have been integrated with fluid inclusion results from Dr John Parnell, University of Aberdeen, to provide a thermal history framework for understanding the burial/uplift and fluid flow history of the sedimentary sections intersected in these boreholes.

Summary Conclusions

AFTA data in samples from all three boreholes show consistent evidence of maximum post-depositional paleotemperatures in the general range 50 to 75°C, from which cooling began sometime in the last 40 Ma (assuming synchronous cooling at all three borehole sites). This interval coincides with a major regional unconformity, and we suggest that these paleotemperatures were most likely the result of deeper burial, probably by between 500 and 2000 metres (depending on the paleogeothermal gradient) of additional section, removed during mid to Late Tertiary exhumation. A VR value in a single sample from one of the boreholes is highly consistent with the thermal history indicated by the AFTA data.

Fluid inclusion homogenisation temperatures vary from values close to those indicated by AFTA and VR to much higher values, up to 200°C. Integration of AFTA and VR data from similar depths suggests that these higher homogenisation temperatures represent the effects of short term hot fluid pulses, and allows limits to be placed on the maximum timescales of heating, varying from ~0.1 Ma for homogenisation temperatures of ~125°C to ~10 years or less for temperatures of 200°C.



TECHNICAL SUMMARY

Thermal history interpretation

1. AFTA data in individual samples can be explained by a single episode of cooling, with maximum paleotemperatures and times of cooling derived from the AFTA data in each sample summarised in Table i. If all data represent a single, regionally synchronous cooling paleo-thermal episode, then combining results from all samples suggests that cooling began some time between 40 and 0 Ma.
2. AFTA data in the sample are of variable quality, largely reflecting the variable yields of apatite. Reasonable quality data were obtained in five samples while two samples provided lesser quality data. Overall, the thermal history interpretations of the AFTA data, summarised in Table i, are considered to be extremely reliable.
3. VR measurements in a sample of Jurassic sediment from borehole 83/20-sb01 reveal the presence of two populations of vitrinite. A population with higher reflectance represents re-worked coal of Carboniferous age, while a lower reflectance population represents organic matter indigenous to the sample. The mean reflectance of this population is highly consistent with the thermal history of AFTA data from other samples in this borehole (Table i).

Mechanisms of heating and cooling

4. With samples available from only a narrow range of depths in each borehole, the results provide no direct insight into mechanisms of heating and cooling. The time interval 40 to 0 Ma, during which AFTA suggests cooling began, coincides with a prominent regional unconformity (see Figure 6.1). Thus, it is likely that at least some degree of deeper burial was involved in producing the observed heating

Integration of AFTA, VR and fluid inclusion results

5. In all three boreholes, while AFTA and VR give very consistent results, homogenisation temperatures (T_{hom}) from fluid inclusions in quartz and calcite are generally much higher than the maximum paleotemperatures indicated by AFTA and VR at similar depths. However in most cases, a population of fluid inclusions is also present giving homogenisation temperatures closer to the paleotemperatures indicated by AFTA and VR. We suggest that the pervasive paleo-thermal effects identified by AFTA and VR data, together with the lower T_{hom} values, most likely represent the effects of heating due to deeper burial, while most of the T_{hom} values represent localised effects of hot fluid movement.



Former depths of burial

6. For likely values of paleogeothermal gradient and paleo-surface temperature, the maximum paleotemperatures derived from AFTA and VR data allows constraints on amounts of former burial (equal to the amount of section removed during subsequent uplift and erosion) required to explain the observed paleotemperatures in each borehole, as summarised in Table 6.1. Values generally fall in the range 0.5 to 2 km, for likely values of paleogeothermal gradient and paleo-surface temperature. Note that estimation of amounts of removed section depends on certain assumptions, as outlined in the text.

Likely timescales of hot fluid pulses

7. Integration of the AFTA data with fluid inclusion homogenisation temperatures allows investigation of likely timescales of heating to temperatures indicated by fluid inclusion results, such that no detectable effects are produced in the AFTA data. Quantitative analysis of this question suggests that the timescale of heating to temperatures around 200°C must have been less than 10 years (10^{-5} Ma), while for a maximum temperature of 125°C, a duration of 0.1 Ma or more is required before a detectable change in the AFTA parameters is produced.

Sediment provenance information from zircon fission track ages

8. Zircon fission track age data in five samples are summarised in Table ii. Three samples of Early to Mid Cretaceous or older units show two dominant age populations, as shown. A younger population of grains gives ages close to the depositional age in each sample. The pooled age of grains in these populations provides a maximum limit to the depositional age of these samples (as the host units have not been sufficiently hot for the fission track ages to be thermally disturbed).
9. Two samples of Late Cretaceous to Early Tertiary age from borehole 16/28-sb01 each contains a single population of zircon fission track ages which are similar to the older group of ages in the three samples of Early to Mid Cretaceous or older units. These older ages in the range 200 to 250 Ma suggest a dominant source for these sediments from a terrain dominated by Triassic to Late Permian cooling, probably representing the effects of late-stage Variscan cooling. The presence of reworked coals of Carboniferous age in one sample (see point 3, above), provides support for this scenario.
10. The absence of zircons with ages close to depositional ages in units younger than Mid Cretaceous suggests an absence of Late Cretaceous to Early Tertiary volcanism in the region, possibly due to migration of igneous activity to the northeast, or alternatively may reflect a switch to basaltic volcanism producing no detrital zircons.



Table i: Paleotemperature analysis summary: AFTA data from Irish Rockall Trough Shallow Boreholes (Geotrack Report #777)

Sample number	Mean depth (mkb)	Stratigraphic age (Ma)	Present temperature ^{*1} (°C)	Maximum paleotemperature ^{*2} (°C)	Onset of cooling ^{*2} (Ma)
16/28-sb01					
GC777-1&9	60.45	55-39	6	<70	post-deposition
				<60	30-0
GC777-2	147.2	70-65	7	50-60	40-0
83/20-sb01					
GC777-3	117.8	97-89	9	55-65	60-0
GC777-4	153.2	146-112	10	45-60	75-0
GC777-5	177.0	208-146	10	<110	80-0
				unconstrained	pre-80 Ma
GC777-5.1	177.0	208-146	100	59 ^{*3}	-
83/24-sb02					
GC777-6	39.9	130-65	6	no apatite	-
GC777-7	44.8	130-65	6	50-70	85-0
GC777-11	45.1	130-65	6	no apatite	-
GC777-8&12	70.9	>178	7	60-75	50-0
				(60-90) ^{*4}	90-50) ^{*4}
				(60-125) ^{*4}	170-90) ^{*4}
				(>90) ^{*4}	>170) ^{*4}

^{*1} Present temperature estimate based on an assumed mean sea bed temperature of 5°C

^{*2} Thermal history interpretation of AFTA data is based on an assumed heating rate of 1°C/Ma and a cooling rate of 10°C/Ma (see Section 2). Quoted ranges correspond to ±95% confidence limits.

^{*1} Maximum paleotemperature from VR data

^{*4} Conditions in brackets are allowed but not definitely required by the data in sample GC777-8&12.



Table ii: Zircon fission track age data from Irish Rockall Trough Shallow Boreholes (Geotrack Report #777)

Sample number	Mean depth (mkb)	Stratigraphic age (Ma)	Pooled fission track age of younger population ^{*1} (Ma)	Pooled fission track age of older population ^{*1} (Ma)
16/28-sb01				
GC777-9	60.45	55-39	-	260 ± 23 (11)
GC777-2	147.2	70-65	-	245 ± 43 ^{*2} (7)
16/28-sb01				
GC777-3	118	89-97	96 ± 8 (3)	218 ± 14 (12)
GC777-4	153.5	146-112	152 ± 13 (3)	234 ± 12 (12)
16/28-sb01				
GC777-11	45.1	130-65	89 ± 9	233 ± 11 (18)

^{*1} Numbers in brackets show the number of tracks counted

^{*2} Central age, for data showing a significant spread of ages. Other values refer to “pooled ages” where all grains are consistent with a single population of ages.

Notes: All errors quoted at ± 1 sigma.
Basic data and analytical details in Appendix B.

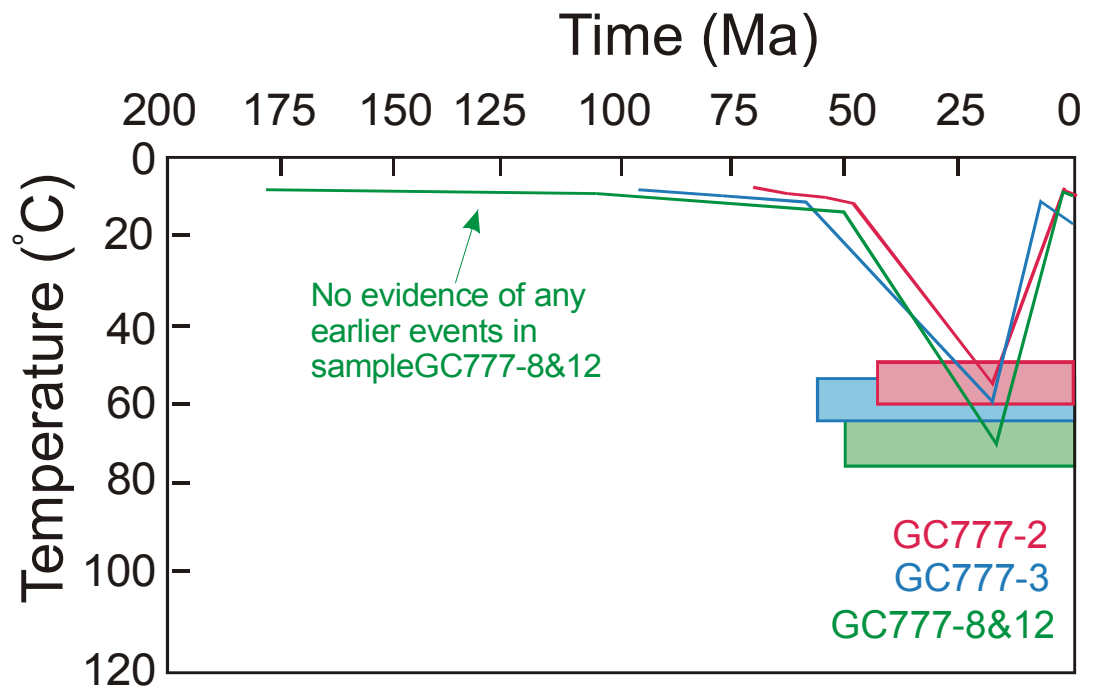


Figure i: Schematic illustration of the thermal history interpretation of AFTA data in selected samples from **Irish Rockall Trough Shallow Boreholes 16/28-sb01 (GC777-2), 83/20-sb01 (GC777-3) and 83/24-sb02 (GC777-8&12)**. The coloured boxes illustrate the range of maximum paleotemperatures and time of cooling allowed by the AFTA data in each sample within 95% confidence limits. Data from all samples are consistent with cooling beginning some time between 40 and 0 Ma (see summary in Table i). Possible mechanisms of heating and cooling are discussed in the text.



1. Introduction

1.1 Aims and objectives

This report describes a Thermal History Reconstruction study of **Irish Rockall Trough Boreholes 16/28-sb01, 83/20-sb01, 83/24-sb02**. The study was commissioned by **Dr John Parnell**, Dept. of Geology and Petroleum Geology, University of Aberdeen, on behalf of the **Rockall Studies Group (RSG)**. The report was completed in November 2000.

Apatite Fission Track Analysis (AFTA[®]) and vitrinite reflectance (VR) have been applied to core samples from the three boreholes. Results from these analyses have been integrated with fluid inclusion results from Dr John Parnell to provide a thermal history framework for understanding the burial/uplift and fluid flow history of the sedimentary sections intersected in these boreholes. In addition, Zircon Fission Track Analysis (ZFTA) has been applied to selected samples, in order to provide sediment provenance information as well as possibly providing improved depositional age constraints on the host sediments.

Using Geotrack's Thermal History Reconstruction methodology, described elsewhere in this report, AFTA and vitrinite reflectance (VR) data can be used to identify, characterise and quantify any episodes of heating and cooling which have affected a sedimentary section. AFTA allows determination of the magnitude of maximum paleotemperatures in individual samples, and the time at which each sample began to cool from the paleo-thermal maximum. VR data can also provide independent estimates of maximum paleotemperatures, the timing of which is interpreted on the basis of information provided by AFTA. This information is then synthesised to define the timing of the major episodes of heating and cooling. The variation of paleotemperature with depth in individual paleo-thermal episodes can be used to constrain paleogeothermal gradients, and to characterise the mechanisms of heating and cooling in each episode. Where appropriate, extrapolation of paleogeothermal gradients to assumed paleo-surface temperatures allows estimation of amounts of section removed by uplift and erosion.

Because samples are available only from a very restricted depth range in each borehole for this report, this type of detailed assessment is not possible, and observed paleo-thermal effects are converted to former burial depths based on a range of assumed paleogeothermal gradients.



1.2 Report structure

The main conclusions of this report are summarised in the Executive Summary. The thermal history interpretation of AFTA data is summarised in Table i. Figure i presents a schematic illustration of the thermal history interpretation of data in selected samples from each borehole.

In Section 1, introductory aspects of the report are discussed, including comments on data quality. The approach to thermal history reconstruction employed in this report is also described in Section 1. Section 2 presents a discussion of the general principles involved in thermal history interpretation of AFTA and VR data, use of the resulting paleotemperatures to determine paleogeothermal gradients, and how this information can be used (with some caveats) to estimate amounts of eroded section. In Sections 3, 4 and 5, the thermal history interpretation of the AFTA and VR data in boreholes 16/28-sb01, 83/20-sb01, 83/24-sb02, respectively, is discussed in detail, and compared with fluid inclusion homogenisation temperatures. In Section 6, results from all three boreholes are synthesised to provide a regional thermal history framework, including discussion of likely mechanisms of heating and cooling, assessment of former burial depths, and timescales of hot fluid flow, together with a brief discussion of the results within the regional context. In section 7, ZFTA results are discussed, together with provenance aspects of the AFTA data. Finally, Section 8 discusses recommendations for further work, which might allow further insight into the topics discussed in preceding sections.

Supporting information is provided in four Appendices. Details of all AFTA and ZFTA samples analysed for this study, including stratigraphic details, sample depths and present temperatures in each well, are presented in Appendix A, together with the yields of detrital apatite obtained after mineral separation, apatite grain morphologies and apatite compositions (Cl contents). Sample preparation and analytical details are described in Appendix B, followed by the presentation of all AFTA data, including data summary sheets containing raw track counts, fission track ages and chlorine contents for individual grains. Details of the presentation of data in the form of Tables and Figures throughout the report are also discussed in detail in Appendix B. Appendix C outlines the principles employed in interpreting the AFTA data in terms of thermal history. The VR data discussed in this report are presented in Appendix D, together with sample details. Appendix D also discusses the principles involved in integrating AFTA and VR data to provide coherent thermal history interpretations.



1.3 Data quality

AFTA data

The AFTA data generated for this report are very variable in quality, largely reflecting the variable yields of apatite obtained from the samples (see Appendix A). Reasonable quality data were obtained from only four of the twelve samples analysed, with between 17 and 20 single grain fission track ages and between 23 and 82 track lengths measured (cf. the usual “targets” of 20 ages and 100 track lengths), while lesser quality data were obtained from five samples (between 2 and 6 ages and between 1 and 16 track lengths). No apatite was obtained from three samples. By compositing data from samples from similar depths (samples GC777-8 and -12, and samples GC777-1 and -9), data quality was improved, giving a total of five samples with reasonable quality and two with lesser quality data.

Quality of the etched surfaces of the apatites obtained for analysis was generally high, allowing confident measurement of fission track age and length data in all samples.

The five samples with reasonable data quality provide quite well-defined thermal history constraints, as summarised in Table i, while data from the other two samples provide broader constraints. The width of the 95% confidence intervals on paleotemperatures and timing quoted in Table i provides an indication of the overall quality of the thermal history interpretation of AFTA data. Generally, this does not always correlate with apatite yields, since AFTA data from a Tertiary sample which has not been appreciably heated after deposition may only give a broad paleotemperature constraint (e.g. $<100^{\circ}\text{C}$), despite an excellent yield of apatite, if the data are dominated by tracks inherited from sediment source terrains. In contrast, data from a relatively small number of apatite grains may be sufficient to reveal evidence of a paleotemperature around 110 to 120°C, due to the severe fission track age reduction achieved at that paleotemperature.

ZFTA data

ZFTA data are of high quality, with between 7 and 20 individual grains analysed in each ZFTA sample. Etched surfaces of all zircons analysed were of high quality, allowing track counting to be carried out with confidence.



VR data

While three samples were submitted for VR analysis, data were obtained from only one sample. Quality of the data in this sample is extremely high, with measurements in 39 fields (see results and maceral descriptions in Appendix D for full details).

1.4 Apatite Compositions

The annealing kinetics of fission tracks in apatite are affected by chemical composition, specifically the Cl content, as explained in more detail in Appendix C. Chlorine compositions were determined for all individual apatite grains analysed for this study (i.e. all grains in which fission track ages were determined and/or lengths were measured). Knowledge of chlorine contents is essential in interpreting AFTA data, and provides both improved accuracy and precision in establishing the time and magnitude of thermal events.

The measured ranges of chlorine contents of dated grains and/or grains used for confined track length measurements are shown in histogram format in the Fission Track Age Data Sheet at the end of Appendix B. Table B.3 (Appendix B) contains single grain fission track age and track length data collected into discrete compositional groups, on the basis of the chlorine contents of the grains from which the data were derived. In addition, a plot of single grain age versus weight % chlorine is shown in the Fission Track Age Data Sheet, which also lists the chlorine contents of individual age grains.



2. Thermal history interpretation strategy

2.1 Thermal history interpretation of AFTA data

Basic principles

Interpretation of AFTA data in this report begins by assessing whether the fission track age and track length data in each sample could have been produced if the sample has never been hotter than its present temperature at any time since deposition. To this end, we consider a "Default Thermal History" for each sample, which forms the basis of interpretation. "Default Thermal Histories" are derived from the stratigraphy of the preserved sedimentary section, combined with constant values for paleogeothermal gradient and paleo-surface temperature which are adopted from present-day values.

Using this history, AFTA parameters are predicted for each sample. If the measured data show a greater degree of fission track annealing (in terms of either fission track age reduction or track length reduction) than expected on the basis of this history, the sample must have been hotter at some time in the past. In this case, the AFTA data are analysed to provide estimates of the magnitude of the maximum paleotemperature in that sample, and the timing of cooling from the thermal maximum (as explained below).

Because of the possible presence of tracks inherited from sediment source terrains, it is possible that track length data might show definite evidence that the sample has been hotter in the past while fission track ages are still greater than predicted from the Default Thermal History (which only refers to tracks formed after deposition). Similarly, in samples in which all or most fission tracks were totally annealed in a paleo-thermal episode, and which have subsequently been cooled and then reheated (e.g. due to further burial), fission track age data might show clear evidence of exposure to higher temperatures in the past while track length data may be dominated by the present-day thermal regime and will not directly reveal the paleo-thermal effects. In circumstances such as these, evidence from either track length or fission track age data alone is sufficient to establish that a sample has been hotter in the past.

As AFTA data provide no information on the approach to a thermal maximum, they cannot independently constrain the heating rate and a value must therefore be assumed in order to interpret the data. The resulting paleotemperature estimates are therefore conditional on this assumed value. AFTA data do provide some control on



the history after cooling from maximum paleotemperatures, through the lengths of tracks formed during this period.

Wherever possible, data from each sample are interpreted in terms of two episodes of heating and cooling, using assumed heating and cooling rates during each episode, with the maximum paleotemperature being reached during the earlier episode. The timing of the onset of cooling and the peak paleotemperatures during the two episodes are varied systematically, and by comparing predicted and measured parameters the range of conditions which are compatible with the data (within $\pm 95\%$ confidence limits) is defined using rigorous statistical methods. Resolution of one additional episode of heating and cooling after the onset of cooling from maximum paleotemperature is usually straightforward from a typical AFTA data set, provided that peak paleotemperatures in the two episodes were separated by $\sim 30^\circ\text{C}$ or more and the timing of each cooling episode differ sufficiently (which depends on the uranium content and size of the apatite grains and the absolute timing). In some cases the data may be explained by a single episode of heating and cooling, in which case fixed heating and cooling rates are assumed and the range of values of maximum paleotemperature and the time of cooling defined as before. Two events closely spaced in time may give the illusion of a single event, particularly where samples yield data of lesser quality, while two event solutions may represent more complex histories involving multiple heating and cooling episodes, in which case the resulting interpretation may represent the two most dominant events or alternatively may represent simply an approximation to the overall history. In rare circumstances, AFTA data in a single sample may allow three events to be identified (alternatively combination of AFTA and VR may reveal three episodes).

If AFTA data show a lower degree of fission track annealing (age and/or length reduction) than expected on the basis of the Default Thermal History, this suggests either present temperatures may be overestimated or temperatures have increased very recently. In such cases, AFTA may allow a more realistic estimate of the present temperature, or an estimate of the time over which temperatures have increased.

AFTA data are predicted using a multi-compositional kinetic model for fission track annealing in apatite developed by Geotrack, described in more detail in Appendix C.

Specific to this report

For the samples analysed for this report, Cl content has been determined in every grain analysed (i.e. for both fission track age and track length measurement), as



explained in more detail in Appendix A, and the data have been grouped into 0.1 wt% Cl divisions for interpretation (see Table B.3, Appendix B).

In this report, AFTA data have been interpreted using heating rates of 1°C/Ma and cooling rates of 10°C/Ma. These assumed values are arbitrary but geologically reasonable, and all paleotemperature estimates are conditional on the assumed rates. For the kinetics characterising both AFTA and VR, increasing or decreasing heating rates by an order of magnitude is equivalent to raising or lowering the required maximum paleotemperature by about 10°C.

2.2 Thermal history interpretation of VR data

Basic principles

Interpretation of VR data follows similar principles to those used in interpreting the AFTA data (Section 2.1). If a measured VR value is higher than the value predicted from the Default Thermal History (making due allowance for analytical uncertainty), the sample must have been hotter at some time in the past. In this case, VR data provide an independent estimate of maximum paleotemperature, which can be calculated using an assumed heating rate and timing information provided from AFTA data, if available (otherwise, assumed). Cooling rates do not significantly affect VR values, which are dominated by the maximum paleotemperature provided that cooling occurs immediately after reaching the thermal maximum. If both AFTA and VR data are available from the same sample or well, then identical heating and rates must be used to obtain consistent paleotemperature estimates.

If a measured VR value is lower than expected on the basis of the Default Thermal History, either present temperatures have been overestimated or temperatures have increased very recently. In such cases, the measured VR value may allow an estimate of the true present-day temperature. Alternatively, the measured VR value may underestimate the true maturity for some other reason, e.g. suppression of reflectance in certain organic macerals, misidentification of true "in-situ" vitrinite, presence of caved material, etc. Comparison of AFTA and VR data usually allows such factors to be identified, and where applicable they are discussed in the relevant section of text.

Vitrinite reflectance data are predicted using the distributed activation energy model describing the evolution of VR, with temperature and time developed by Burnham



and Sweeney (1989) (see also Sweeney and Burnham, 1990), as implemented in the BasinMod™ software package of Platte River Associates.

Values of VR less than 0.32% and greater than 4% cannot be assigned to a specific maximum paleotemperature with confidence, and such values are given a maximum limit of 50°C and a minimum limit of 250°C, respectively.

Further discussion of the methodology employed in interpreting VR data are given in Appendix D, which also briefly discusses the benefits of integrating AFTA and VR data.

Specific to this report

For this report, VR data in all samples have been interpreted using heating and cooling rates of 1 and 10°C/Ma (respectively), for consistency with interpretation of the AFTA data, as specified in Section 2.1. Maximum paleotemperatures determined for the VR samples are attributed to specific paleo-thermal episodes on the basis of comparison of the VR-derived maximum paleotemperature with observed paleo-heating of a similar style in adjacent AFTA samples.

2.3 Comparison of paleotemperature estimates from AFTA and VR

Maximum paleotemperatures derived from AFTA and VR using the strategies outlined above are usually highly consistent. Estimates of maximum paleotemperature from AFTA are often quoted in terms of a range of paleotemperatures, as the data can often be explained by a variety of scenarios. Paleotemperature estimates from VR are usually quoted to the nearest degree Celsius, as the value which predicts the exact measured reflectance. This is not meant to imply VR data can be used to estimate paleotemperatures to this degree of precision. VR data from individual samples typically show a scatter equivalent to a range of between ± 5 and $\pm 10^\circ\text{C}$. Estimates from a series of samples are normally used to define a paleotemperature profile in samples from a well, or a regional trend in paleotemperatures from outcrop samples.



2.4 Paleogeothermal gradients, and mechanisms of heating and cooling

Basic principles

A series of paleotemperature estimates from AFTA and/or VR over a range of depths can be used to reconstruct a paleotemperature profile through the preserved section. The slope of this profile defines the paleogeothermal gradient. As explained by Bray et al. (1992), the shape of the paleotemperature profile and the magnitude of the paleogeothermal gradient provides unique insights into the origin and nature of the heating and cooling episodes expressed in the observed paleotemperatures.

Linear paleotemperature profiles with paleogeothermal gradients close to the present-day geothermal gradient provide strong evidence that heating was caused by greater depth of burial with no significant increase in basal heat flow, implying in turn that cooling was due to uplift and erosion. Paleogeothermal gradients significantly higher than the present-day geothermal gradient suggest that heating was due, at least in part, to increased basal heat flow, while a component of deeper burial may also be important as discussed in the next section. Paleogeothermal gradients significantly lower than the present-day geothermal gradient suggest that a simple conductive model is inappropriate, and more complex mechanisms must be sought for the observed heating. One common cause of low paleogeothermal gradients is transport of hot fluids shallow in the section. However the presence of large thicknesses of sediment with uniform lithology dominated by high thermal conductivities can produce similar paleotemperature profiles and each case has to be considered individually.

A paleotemperature profile can only be characterised by a single value of paleogeothermal gradient when the profile is linear. Departures from linearity may occur where strong contrasts in thermal conductivities occur within the section, or where hot fluid movement or intrusive bodies have produced localised heating effects. In such cases a single value of paleogeothermal gradient cannot be calculated, and different values (possibly negative) may apply through different parts of the section. However it is important to recognise that the validity of the paleotemperatures determined from AFTA and/or VR are independent of these considerations, and can still be used to control possible thermal history models.

Estimation of paleogeothermal gradients in this report

As samples were analysed over a narrow range of depths in each borehole for this report, determination of paleogeothermal gradients was not possible.



2.5 Determination of removed section

Basic principles

Subject to a number of important assumptions, extrapolation of a linear paleotemperature profile to a paleo-surface temperature allows estimation of the amount of eroded section represented by an unconformity, as explained in more detail in Section C.9 (Appendix C).

Specifically, this analysis assumes:

- The paleotemperature profile through the preserved section is linear
- The paleogeothermal gradient through the preserved section can be extrapolated linearly through the missing section.
- The paleo-surface temperature is known.
- The heating rate used to estimate the paleotemperatures defining the paleogeothermal gradient is correct

It is important to realise that any method of determining the amount of eroded section based on thermal methods is subject to these and/or additional assumptions. For example methods based on heat-flow modelling must assume values of thermal conductivities in the eroded section, which can never be known with confidence. Such models also require some initial assumption of the amount of eroded section to allow for the effect of compaction on thermal conductivity. Methods based on geothermal gradients, as used in this study, are unaffected by this consideration, and can therefore provide independent estimates of the amount of eroded section. But these estimates are always subject to the assumptions set out above, and should be considered with this in mind.

The analysis used to estimate paleogeothermal gradients is easily extended to provide maximum likelihood values of eroded section for an assumed paleo-surface temperature, together with $\pm 95\%$ confidence limits. These parameters are quoted for each well in which the paleotemperature profile suggests that heating may have been due, at least in part, to deeper burial.

Estimates of paleogeothermal gradient and eroded section derived from fitting linear profiles to paleotemperature data as a function of depth are highly correlated, since the profile is constrained to pass through the main body of the data. Thus, higher paleo-gradients within the allowed range correspond to lower amounts of section removed, while lower paleo-gradients correspond to higher amounts of removed



section. In plots of paleogeothermal gradient against removed section, paired values of each parameter which are consistent with the paleotemperature data can be defined, thus allowing the range of allowed values at various levels of statistical significance to be contoured. In general, the greater the depth interval over which paleotemperature constraints are available, the tighter the resulting constraints on both the paleogeothermal gradient and the amount of removed section.

However, it is emphasised that reconstructed burial histories produced in this way do not produce unique solutions, and alternative interpretations are always possible. For instance, where the eroded section was dominated by units with high thermal conductivities the paleogeothermal gradient through the missing section may have been much higher than in the preserved section, and extrapolation of a linear gradient will lead to overestimation of the eroded section.

Specific to this report

As samples were analysed over a narrow range of depths in each borehole for this report, rigorous determination of paleogeothermal gradients, and hence amounts of removed section, was not possible. Instead, we have estimated amounts of removed section required to account for the thermal history constraints obtained from AFTA on the basis of a range of assumed values of paleogeothermal gradient, as set out in Section 6. Values of removed section derived in this way are conditional on a number of additional assumptions, viz:

- Heating rates of $1^{\circ}\text{C}/\text{Ma}$ and cooling rates of $10^{\circ}\text{C}/\text{Ma}$, as assumed in interpreting the AFTA data in terms of thermal history.
- A constant paleo-surface temperature of 5°C (equal to the assumed present-day value)
- A linear paleogeothermal gradient at the time of the paleo-thermal maximum.

The effects of higher paleo-surface temperatures can be simply allowed for by subtracting the depth increment corresponding to the increase in temperature, for the appropriate value of paleogeothermal gradient. For instance, if the paleogeothermal gradient was $50^{\circ}\text{C}/\text{km}$ and the paleo-surface temperature was 10°C higher than the value assumed in this report, the estimated eroded section should be *reduced by 200 metres*. Different heating rates can be allowed for in similar fashion, with an order of magnitude change in heating rate equivalent to a 10°C change in paleotemperature (paleotemperatures increase for higher heating rates, and decrease for lower heating rates). (Changes in heating rate do not affect determination of the timing of cooling from maximum paleotemperature profile significantly).



3. Thermal history interpretation of data from Borehole 16/28-sb01

3.1 Geological background

This borehole intersected 14.5 metres of Quaternary sediments unconformably overlying ~131 metres of Upper Paleocene to Middle Eocene fine grained calcareous sandstones, silts and muds. These sediments are separated from underlying sandy limestone of ?Maastrichtian age by an erosional unconformity. Within 1 metre of TD (reached at a depth of 148.3 m below sea bed), the borehole intersected fractured, altered basalt, thought to represent an intrusive sill (but see discussion in Section 3.3).

Prominent unconformities thus occur at Middle Eocene to Quaternary and ?Maastrichtian to Late Paleocene levels, representing the approximate time intervals 65 Ma to 60 Ma and 39 to 2 Ma. The detailed stratigraphic succession in this borehole is summarised in Table A.2. No information is available on present-day geothermal gradients in the vicinity of the borehole. A present-day sea bed temperature of 5°C has been assumed, together with a present-day geothermal gradient of 30°C/km, although these assumptions do not affect the thermal history interpretations presented here, because of the very minor present-day burial depths.

Three samples were provided from this borehole for AFTA (Table A.1), from depths of 40.9 metres (GC777-1), 40.9 to 80.0 metres (GC777-9) and 147.2 metres (GC777-2). Sample GC777-9 was collected in a second round of sampling, in order to supplement results from sample GC777-1, and data from these two samples were combined for thermal history interpretation. Results from this combined sample, GC777-1&9, and those from sample GC777-2, provide extremely reliable thermal history constraints, as described below.

Fission track ages were also determined in zircons from samples GC777-2 and -9, in order to provide provenance information and also to possibly obtain depositional age constraints on the host sediments. These results are discussed in Section 7.

A single sample, GC777-2.1 from the ?Maastrichtian section in this well, was sent for VR analysis, but no material suitable for analysis was present in the sample. Fluid inclusion data from this well were provided by Dr John Parnell and are discussed in Section 3.3.



3.2 Thermal history interpretation of AFTA data

Introduction

Fission track age and mean track length data in samples analysed from this well are summarised in Table 3.1 and plotted as a function of depth and present temperature in Figure 3.1, where the fission track age data are contrasted with the variation of stratigraphic age through the section. Zircon fission track ages are also plotted in Figure 3.1. Discussion of the zircon data is provided in Section 7.

In interpreting the AFTA data from this well, results from samples GC777-1 and GC777-9, collected over adjacent intervals, have been combined into a single dataset, characterised by the sample number GC777-1&9. Note that although the fission track ages reported for samples GC777-1 and GC777-9 in Table 3.1 appear quite different, results for the two samples are actually quite consistent, as sample GC777-9 contains grains with a large spread of ages including several grains with ages similar to those of the two grains analysed from sample GC777-1 (see data summary sheets in Appendix B).

Interpretation of the AFTA data in terms of evidence that the samples may have been hotter in the past is summarised in Table 3.2. Following the strategy outlined in Section 2.1, estimates of the magnitude and timing of maximum paleotemperatures allowed by the AFTA data in each sample are summarised in Table 3.3.

Evidence for elevated paleotemperatures from AFTA

Taking the deepest sample first, AFTA parameters in sample GC777-2 show clear evidence that the sample has been hotter than its present-day temperature at some time after deposition (Table 3.2). This evidence comes from the track length data, which show a greater degrees of reduction than expected on the basis of the Default Thermal History. The fission track age data show that the sample retains a large proportion of tracks formed prior to deposition, and post-depositional heating has not been sufficiently pronounced to significantly reduce the fission track age.

In contrast, AFTA data from the combined sample, GC777-1&9, do not require that the sample has been hotter in the past, due to the combination of the dominance of tracks formed prior to deposition and the modest degree of post-depositional heating. But the data would allow the possibility within certain limits (see below).



Magnitude of paleotemperatures and timing of cooling from AFTA

As detailed in Table 3.3, AFTA data in sample GC777-2 can be explained by a single paleo-thermal episode, involving cooling from a maximum paleotemperature between 50 and 60°C beginning some time between 40 and 0 Ma. AFTA data from sample GC777-1&9 provide only an upper limit of 70°C for the maximum post-depositional paleotemperature, with a lower limit of 60°C over the last 30 Ma.

The timing constraint from sample GC777-2 for the onset of cooling correlates closely with the unconformity between Middle Eocene and Quaternary units recognised in this well (Section 3.1), representing the approximate time interval 39 to 2 Ma. The significance of this is discussed in greater detail in Section 6.

Thermal history constraints derived from AFTA data in samples GC777-1&9 and GC777-2 are summarised in Table i. Figure i provides a schematic illustration of the thermal history interpretation of AFTA data from sample GC777-2, as representative of results from this well.

Equivalent maturity values from AFTA

As also detailed in Table 3.3, the AFTA data in sample GC777-1&9 suggest an equivalent R_0 max value of less than 0.42%, while data from sample GC777-2 suggest a value in the range 0.33 to 0.37%. These values are calculated from the thermal history interpretation derived from the AFTA data, using the algorithm presented by Burnham and Sweeney (1989) and Sweeney and Burnham (1990).

3.3 Comments on igneous rock near TD

The summary log of this borehole reports the presence of basalt at a depth of 147.3 metres below sea bed, which is thought to represent an igneous sill of post-Maastrichtian age. The sill occupies the deepest 1 metre of the borehole.

AFTA data from sample GC777-2 shows no obvious thermal effects due to this “sill”. Since this sample was taken from a depth of 147.2 metres (i.e. within 10 cm of the sill contact), then given the “sill” thickness of over 1 metre, paleotemperatures in sample GC777-2 due to sill intrusion should have been sufficiently high to totally reset the fission track age of this sample. Instead, the sample gives a fission track age of 161 ± 11 Ma which is much older than the age of the host sediment, and thermal history interpretation suggests a maximum paleotemperature of only 50 to 60°C,



which is similar to values observed in other boreholes in which no igneous rocks are recognised. On this basis it is clear that this sample shows no evidence of contact heating effects, and we conclude that the most likely explanation is that the basalt is extrusive in origin.

Major reasons presented on the summary log for the assignment as a sill include lack of eroded basalt fragments in overlying sediments and the lack of autobrecciation or bole on the surface of the igneous unit. However since the summary log notes that the contact of this unit with the overlying sediments has not been recognised, the impact of these comments is lessened, and we suggest that a possible extrusive origin should be re-examined.

3.4 Fluid inclusion results

Homogenisation temperatures (T_{hom}) in fluid inclusions from this borehole are summarised in Table 3.4, and are plotted against depth in Figure 3.2. Paleotemperature constraints from AFTA are also plotted against depth in Figure 3.2. Fluid inclusion measurements are focussed at two depth horizons close to those of AFTA samples GC777-1 and GC777-2, which affords direct comparison of results from both techniques.

At the shallower horizon around 41 metres below sea bed, homogenisation temperatures measured from trails in quartz and in calcite cements (see Table 3.4) are much higher than the paleotemperatures derived from AFTA. At the deeper horizon, around 147 metres below sea bed, a sub-set of T_{hom} values, measured in calcite cements, overlap with the paleotemperatures derived from AFTA, while values from other calcite cements and from trails in quartz are much higher.

The significance of these observations in the context of the thermal and fluid flow histories at the borehole site are discussed in detail in Section 6.3.



Table 3.1: Summary of AFTA parameters in samples from Irish Rockall Trough Borehole 16/28-sb01 (Geotrack Report #777)

Sample number	Average depth (m)	Present temperature ^{*1} (°C)	Stratigraphic age (Ma)	Mean track length (μm)	Predicted mean track length ^{*2} (μm)	Fission track age (Ma)	Predicted fission track age ^{*2} (Ma)
GC777-1	40.9	6	50-39	12.16 ± 0.11	15.0	58.2 ± 32.6	51.2
GC777-9	60.5	7	55-39	13.68 ± 0.17	15.0	180.6 ± 21.1	50.9
GC777-1&9 ^{*3}	60.5	7	55-39	13.6 ± 0.2	15.0	171.2 ± 19.8	51.0
GC777-2	147.2	9	70-65	13.31 ± 0.16	14.9	161.5 ± 10.8	70.8

^{*1} See Appendix A for discussion of present temperature data.

^{*2} Values predicted from the Default Thermal History (Section 2.1); i.e. assuming that each sample is now at its maximum temperature since deposition. The values refer only to tracks formed after deposition. Samples may contain tracks inherited from sediment provenance areas. Calculations refer to apatites within the measured compositional range for each sample, as discussed in Appendix A.

^{*3} Data from samples GC777-1 and GC777-9 combined.

Note: all depths quoted are TVD with respect to sea bed.

**Table 3.2: Summary of thermal history interpretation of AFTA data in Irish Rockall Trough Borehole 16/28-sb01 (Geotrack Report #777)**

Sample Details Sample No. Depth Present temp Strat. Age	Do AFTA data require any revision of present temperature?	Evidence of higher temperatures in the past from length data?	Evidence of higher temperatures in the past from fission track age data?	Conclusion
GC777-1&9 40.9 – 80.0 m 6°C 55-39 Ma High quality data: 22 age grains 84 track lengths	No	Equivocal [The mean length is 1.4 μm less than predicted on the basis of the Default Thermal History. Modelling the AFTA parameters through likely thermal history scenarios shows that the track length data in this sample can be explained either by post-depositional heating or by inheritance of shorter tracks from sediment source terrains (because data in this sample are dominated by tracks formed prior to deposition – see age data).]	No [The central fission track age of this sample and most of the single grain ages are significantly greater than that predicted on the basis of the Default Thermal History.]	AFTA data do not require that this sample has been hotter in the past, although they would allow the possibility within certain limits.
GC777-2 147.2 m 7°C 70-65 Ma Good quality data: 17 age grains 43 track lengths	No	Yes [The mean length is 1.6 μm less than predicted on the basis of the Default Thermal History. Modelling the AFTA parameters through likely thermal history scenarios shows that the track length data in this sample cannot be explained by inheritance of shorter tracks from sediment source terrains, and must be due to the effects of higher paleotemperatures at some time after deposition.]	No [The pooled fission track age of this sample is greater than that predicted on the basis of the Default Thermal History.]	Track length data show that this sample has been hotter in the past, while the lack of significant age reduction suggests only a moderate degree of paleo-heating.

Note: Interpretation of AFTA data is based on comparison of measured AFTA parameters with values predicted from "Default Thermal History" (Section 2.1); i.e., assuming that each sample is now at its maximum temperature since deposition. The predicted values for each sample are summarised in Table 3.1, and refer only to tracks formed after deposition. Samples may also contain tracks inherited from sediment provenance areas, which must be allowed for in interpreting the data. Calculations refer to apatites with the compositional range appropriate to each sample, as explained in Appendix A.



Table 3.3: Estimates of timing and magnitude of elevated paleotemperatures from AFTA data in Irish Rockall Trough Borehole 16/28-sb01 (Geotrack Report #777)

Sample Details	Paleo-thermal episodes			Comments
	Event	Maximum paleo-temperature (°C)	Onset Of Cooling (Ma)	
GC777-1&9 40.9 – 80.0 m 6°C 55-39 Ma High quality data: 22 age grains 84 track lengths	Single	<70 <60	post-deposition 30-0	AFTA data from this sample can be explained either solely in terms of inheritance of shorter tracks from source terrains, with no additional post-depositional heating, or by a single episode of post-depositional heating to a maximum paleotemperature less than 70°C some time after deposition (less than 60°C over the last 30 Ma). Because the AFTA parameters in this sample are dominated by tracks formed prior to deposition, coupled with the modest degree of post-depositional heating, these alternative scenarios cannot be resolved, despite the high quality of the AFTA data in this sample. Equivalent R_omax <0.42%
GC777-2 147.2 m 7°C 70-65 Ma Good quality data: 17 age grains 43 track lengths	Single	50-60	40-0	AFTA data from this sample can be explained by a single episode of heating to a maximum paleotemperature between 50 and 60°C, from which cooling began some time between 40 and 0 Ma, as summarised left. At these relatively low maximum paleotemperatures, AFTA data often do not provide rigorous thermal history constraints, but in this sample, high quality data result in well-defined timing and paleotemperature constraints. No VR data are available from depths adjacent to this AFTA sample. Equivalent R_omax 0.33-0.37%

All thermal history constraints are based on assumed heating rates of 1°C/Ma and cooling rates of 10°C/Ma.

Events shown in brackets are not required by the AFTA data, though they are allowed within the limits shown.



Table 3.4: Fluid inclusion homogenisation temperatures in Irish Rockall Trough Borehole 16/28-sb01 (Geotrack Report #777)

		Quartz					Calcite			
Depth (m)	Stratigraphic age	Cement	Trail 1	Trail 2	Trail 3	Trail 4	Cement	Recryst.	Cement 2	Vein
40.87	Eocene		89.7 (5)	143.9 (4)			101.3 (1)			
41.0	Eocene						98.3 (8)			
147.08	?Maastrichtian				161.3 (11)		80.3 (4)		<50 (6)	
147.18	?Maastrichtian		94 (2)		154.7 (1)	190.2 (5)	104.5 (3)		67.5-<50 (11)	
147.2	?Maastrichtian				163.9 (9)	198.3 (9)	79.3 (7)		<50 (4)	

Numbers shown in brackets show the numbers of inclusions in each population.

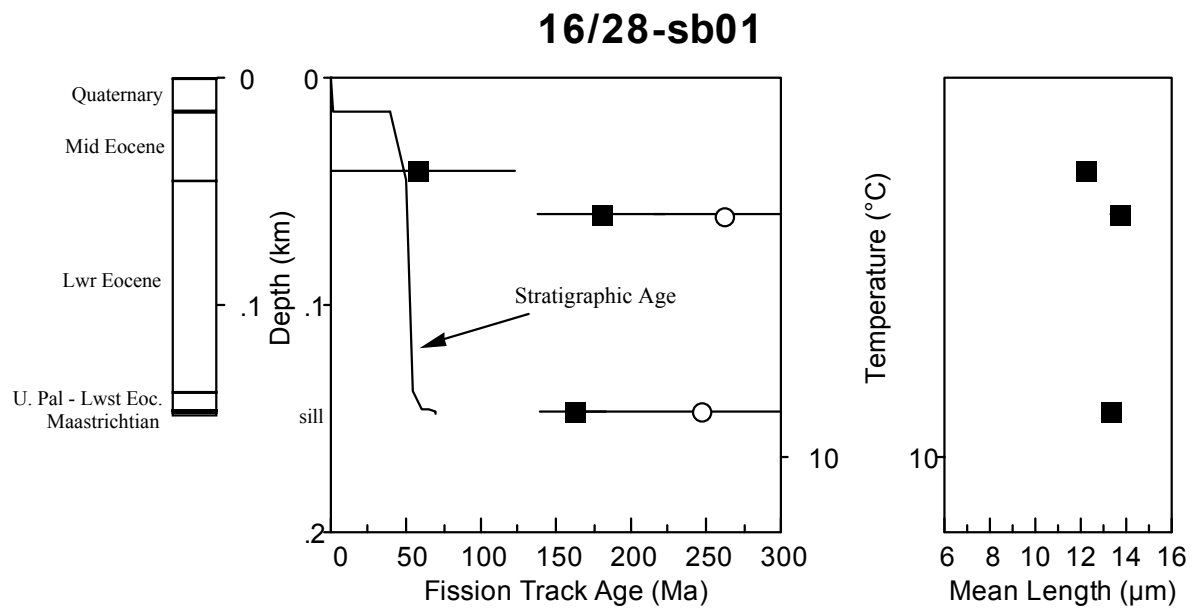


Figure 3.1: AFTA (filled squares) and ZFTA (open circles) parameters plotted against sample depth and present temperature for samples from **borehole 16/28-sb01, Irish Rockall Trough**. The variation of stratigraphic age with depth is also shown, as the solid line in the central panel.



16/28-sb01

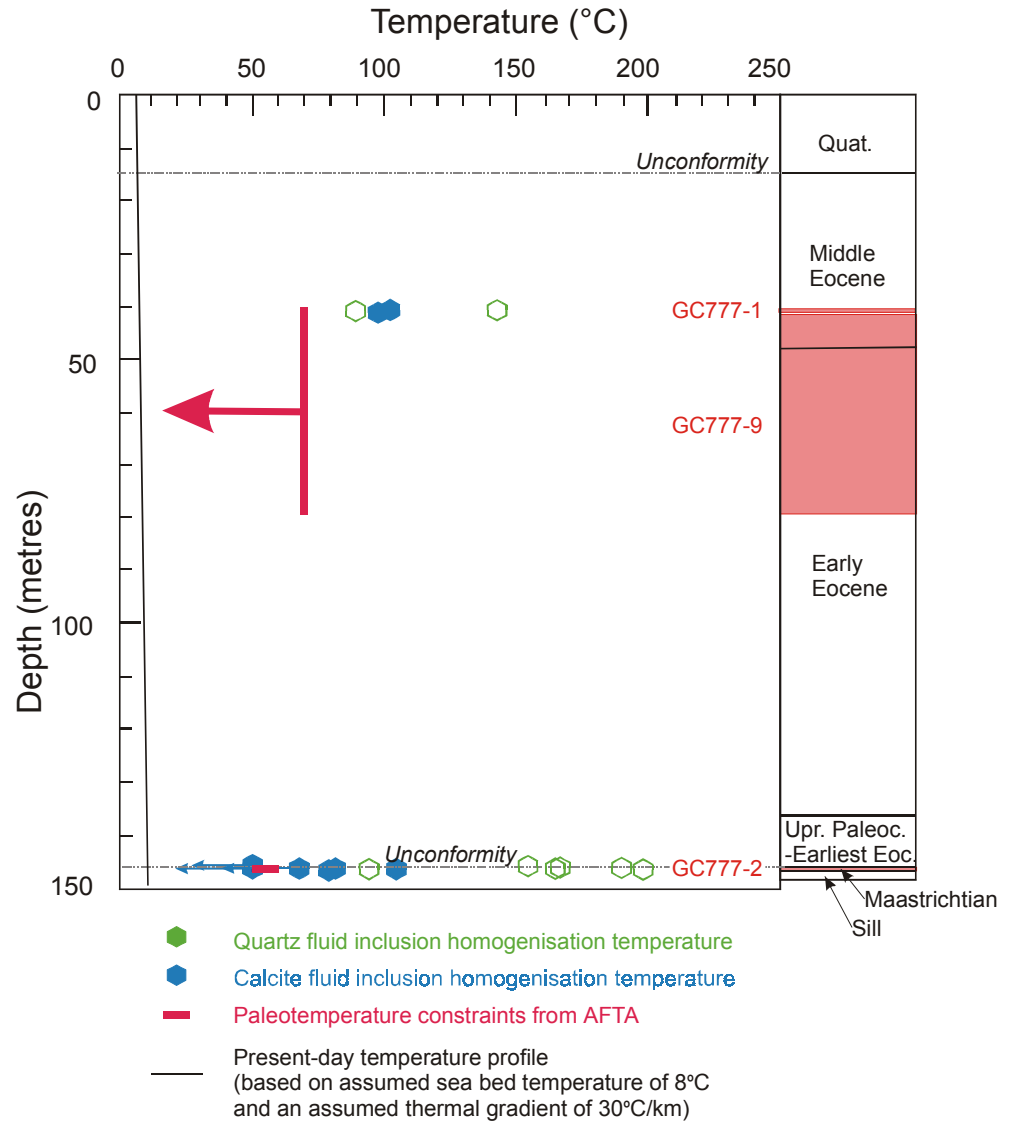


Figure 3.2:

Paleotemperature constraints derived from AFTA in **borehole 16/28-sb01, Irish Rockall Trough**, plotted against depth (below sea bed). Fluid inclusion homogenisation temperatures from Dr John Parnell (summarised in Table 3.4) are also plotted against depth. Open symbols represent veins and trails, while filled symbols represent cements. The assumed present-day temperature profile in the well is also shown. AFTA data from this well define a single paleo-thermal episode, from which cooling began some time between 40 and 0 Ma. Fluid inclusion homogenisation temperatures are generally much higher than paleotemperatures indicated by AFTA. See text for further discussion.



4. Thermal history interpretation of data from Borehole 83/20-sb01

4.1 Geological background

This borehole intersected 72 metres of Pliocene to Recent sediments unconformably overlying 14 metres of Middle Miocene sediments, which in turn unconformably overlie a Cretaceous to ?Jurassic sequence, with the borehole reaching TD at a depth of 177 metres below sea bed

Prominent unconformities thus occur at Middle Miocene to Pliocene and Maastrichtian to Middle Miocene levels, representing the approximate time intervals 10 to 5 Ma and 65 to 15 Ma. Minor unconformities may also be present within the Mesozoic sequence. The detailed stratigraphic succession in this borehole is summarised in Table A.2. No information is available on present-day geothermal gradients in the vicinity of the borehole. A present-day sea bed temperature of 5°C has been assumed, together with a present-day geothermal gradient of 30°C/km, although these assumptions do not affect the thermal history interpretations presented here, because of the very minor present-day burial depths.

Four samples were provided from this borehole for AFTA (Table A.1), from depths of 117.8 metres (GC777-3), 150.8 to 155.6 metres (GC777-4), 176.7 to 177.3 metres (GC777-5) and 177.3 metres (GC777-10). Sample GC777-10 was collected in a second round of sampling, in order to supplement results from sample GC777-5, but failed to yield any apatite, and thus sample GC777-10 is not discussed further.

Fission track ages were also determined in zircons from samples GC777-3 and -4, in order to provide provenance information and also to possibly obtain depositional age constraints on the host sediments. These results are discussed in Section 7.

A single sample (GC777-5.1) from the Jurassic section in this well was sent for VR analysis. Fluid inclusion data from this well were provided by Dr John Parnell and are discussed in Section 4.4.

4.2 Thermal history interpretation of AFTA data

Introduction

Fission track age and mean track length data in samples analysed from this well are summarised in Table 4.1 and plotted as a function of depth and present temperature



in Figure 4.1, where the fission track age data are contrasted with the variation of stratigraphic age through the section. Zircon fission track ages are also plotted in Figure 4.1. Discussion of the zircon data is provided in Section 7.

Interpretation of the AFTA data in terms of evidence that the samples may have been hotter in the past is summarised in Table 4.2. Following the strategy outlined in Section 2.1, estimates of the magnitude and timing of maximum paleotemperatures allowed by the AFTA data in each sample are summarised in Table 4.3.

Evidence for elevated paleotemperatures from AFTA

AFTA parameters in samples GC777-3 and -4 both show clear evidence that the samples have been hotter than their present-day temperatures at some time after deposition (Table 3.2). In both samples, this evidence comes from the track length data, which show a greater degree of reduction than expected on the basis of the Default Thermal History. The fission track age data show that the samples retain a large proportion of tracks formed prior to deposition, and post-depositional heating has not been sufficiently pronounced to significantly reduce the fission track age.

The deepest sample, GC777-5, yielded insufficient apatite grains to provide a detailed interpretation, as summarised in Table 3.2, but the data in this sample would allow some degree of post-depositional heating (see below).

Magnitude of paleotemperatures and timing of cooling from AFTA

As detailed in Table 4.3, AFTA data in both samples GC777-3 and -4 can be explained by a single paleo-thermal episode. Results from sample GC777-3 indicate cooling from a maximum paleotemperature between 55 and 65°C beginning some time between 60 and 0 Ma, while results from sample GC777-4 indicate cooling from a maximum paleotemperature between 45 and 60°C beginning some time between 75 and 0 Ma. AFTA data from sample GC777-5 indicate only that the sample must have been at temperatures less than 125°C over the last 80 Ma, due to the poor data quality in this sample.

Assuming that results from both samples GC777-3 and -4 represent a common paleo-thermal episode, then the combined timing constraint on the time of cooling, at between 60 and 0, can reasonably be extended to both samples. (This quite broad range of timing allowed by the data in these samples results largely from the relatively low maximum paleotemperatures, which has produced only a moderate degree of length reduction.) This timing for the onset of cooling correlates closely with the unconformity between ?Maastrichtian and Middle Miocene units recognised



in this well (Section 4.1), representing the approximate time interval 65 to 15 Ma, while also overlapping with the later unconformity between Middle Miocene and Pliocene units (~10 to 5 Ma). The significance of this is discussed in greater detail in Section 6.

Thermal history constraints derived from AFTA data in samples GC777-3, -4 and GC777-5 are summarised in Table i. Figure i provides a schematic illustration of the thermal history interpretation of AFTA data from sample GC777-3, as representative of results from this well.

Equivalent maturity values from AFTA

Also detailed in Table 4.3 are equivalent $R_{o,max}$ values for each sample, calculated from the thermal history interpretation derived from the AFTA data, using the algorithm presented by Burnham and Sweeney (1989) and Sweeney and Burnham (1990).

4.3 Vitrinite reflectance results

A single sample from this borehole was submitted for vitrinite reflectance measurements. VR results in sample GC777-5.1, from the ?Jurassic section, are summarised in Table D.2, and maceral descriptions and discussion of the results is also provided in Appendix D. Two populations of vitrinite were identified in this sample, a primary in-situ population with a well-defined mean $R_{o,max}$ of 0.36% (based on 39 measurements) and a higher reflecting population (mean $R_{o,max}$ 1.37% but with a large range from 0.87 to 2.30%), which is identified by the analyst as re-worked coal of Carboniferous age.

Based on the thermal history interpretation strategy outlined in Section 2.2, the in-situ VR value of 0.36% is equivalent to a maximum post-depositional paleotemperature of 59°C (for assumed heating and cooling rates of 1°C/Ma and 10°C/Ma, respectively). AFTA sample GC777-5, from a similar depth range to VR sample GC777-5.1, did not provide very tight thermal history constraints (Section 4.2). But the maximum paleotemperature of 45 to 60°C indicated by AFTA data in sample GC777-4, from the overlying Early Cretaceous section, is highly consistent with the value indicated by the VR data from sample GC777-5.1, as noted in Table 4.3 and it seems clear that the measured VR value represents the same episode as revealed by the AFTA data from this borehole.



4.4 Fluid inclusion results

Homogenisation temperatures (T_{hom}) in fluid inclusions from this borehole are summarised in Table 4.4, and are plotted against depth in Figure 4.2. Paleotemperature constraints from AFTA and VR are also plotted against depth in Figure 4.2. Fluid inclusion measurements are available from a range of depths through the pre-Campanian section, overlapping with the depth intervals of AFTA samples GC777-3 and -4, and VR sample GC777-5.1. Direct comparison of results from all three techniques is therefore possible in this well.

In units of Santonian to Jurassic? age, homogenisation temperatures measured from cements and trails in quartz and from calcite cements and veins and recrystallised calcite (see Table 4.4) are generally much higher than the paleotemperatures derived from AFTA. However, throughout this section a sub-set of T_{hom} values measured in calcite cements and veins overlap with the paleotemperatures derived from AFTA and VR. No obvious trend is evident in the T_{hom} values throughout the borehole, with a wide range of values present at all depths.

The significance of these observations in the context of the thermal and fluid flow histories at the borehole site are discussed in detail in Section 6.3.



Table 4.1: Summary of AFTA parameters in samples from Irish Rockall Trough Borehole 83/20-sb01 (Geotrack Report #777)

Sample number	Average depth (m)	Present temperature ^{*1} (°C)	Stratigraphic age (Ma)	Mean track length (µm)	Predicted mean track length ^{*2} (µm)	Fission track age (Ma)	Predicted fission track age ^{*2} (Ma)
GC777-3	117.8	9	89-87	13.11 ± 0.25	15.0	142.2 ± 18.5	91.4
GC777-4	153.2	10	146-112	12.59 ± 0.30	14.9	216.6 ± 41.6	121.0
GC777-5	177.0	10	208-146	13.84	14.8	182.0 ± 98.5	163.0
GC777-10	177.3	10	208-146		no apatite		

^{*1} See Appendix A for discussion of present temperature data.

^{*2} Values predicted from the Default Thermal History (Section 2.1); i.e. assuming that each sample is now at its maximum temperature since deposition. The values refer only to tracks formed after deposition. Samples may contain tracks inherited from sediment provenance areas. Calculations refer to apatites within the measured compositional range for each sample, as discussed in Appendix A.

Note: all depths quoted are TVD with respect to sea bed.



Table 4.2: Summary of thermal history interpretation of AFTA data in Irish Rockall Trough Borehole 83/20-sb01 (Geotrack Report #777)

Sample Details Sample No. Depth Present temp Strat. Age	Do AFTA data require any revision of present temperature?	Evidence of higher temperatures in the past from length data?	Evidence of higher temperatures in the past from fission track age data?	Conclusion
GC777-3 117.8 m 9°C 89-97 Ma Good quality data: 20 age grains 23 track lengths	No	Yes [The mean length is 1.8 μm less than predicted on the basis of the Default Thermal History. Modelling the AFTA parameters through likely thermal history scenarios shows that the track length data in this sample cannot be explained by inheritance of shorter tracks from sediment source terrains, and must be due to the effects of higher paleotemperatures at some time after deposition.]	No [The central fission track age of this sample and many of the single grain ages are significantly greater than that predicted on the basis of the Default Thermal History.]	Track length data show that this sample has been hotter in the past, while the lack of significant age reduction suggests only a moderate degree of paleo-heating.
GC777-4 150.8-155.6 m 10°C 146-112 Ma Good quality data: 18 age grains 57 track lengths		Yes [The mean length is 2.2 μm less than predicted on the basis of the Default Thermal History. Modelling the AFTA parameters through likely thermal history scenarios shows that the track length data in this sample cannot be explained by inheritance of shorter tracks from sediment source terrains, and must be due to the effects of higher paleotemperatures at some time after deposition.]	No [The central fission track age of this sample and several single grain ages are significantly greater than that predicted on the basis of the Default Thermal History.]	Track length data show that this sample has been hotter in the past, while the lack of significant age reduction suggests only a moderate degree of paleo-heating.
GC777-5 176.7-177.3 m 10°C 208-146 Ma Poor quality data: 2 age grains 1 track lengths	No	Insufficient data [Only one track length was measured in this sample, precluding a detailed thermal history interpretation.]	No [The pooled fission track age of this sample is consistent with predictions on the basis of the Default Thermal History. Since only two single grains ages were measured, the data do not provide a detailed thermal history interpretation.]	Insufficient data for detailed interpretation.

Note: Interpretation of AFTA data is based on comparison of measured AFTA parameters with values predicted from "Default Thermal History" (Section 2.1); i.e., assuming that each sample is now at its maximum temperature since deposition. The predicted values for each sample are summarised in Table 4.1, and refer only to tracks formed after deposition. Samples may also contain tracks inherited from sediment provenance areas, which must be allowed for in interpreting the data. Calculations refer to apatites with the compositional range appropriate to each sample, as explained in Appendix A.



Table 4.3: Estimates of timing and magnitude of elevated paleotemperatures from AFTA data in Irish Rockall Trough Borehole 83/20-sb01 (Geotrack Report #777)

Sample Details	Paleo-thermal episodes			Comments
	Event	Maximum paleo-temperature (°C)	Onset Of Cooling (Ma)	
GC777-3 117.8 m 9°C 89-97 Ma Good quality data: 20 age grains 23 track lengths	Single	55-65	60-0	AFTA data from this sample can be explained by a single episode of heating to a maximum paleotemperature between 55 and 65°C, from which cooling began some time between 60 and 0 Ma. No VR data are available from depths adjacent to this AFTA sample. Equivalent R_0max 0.34 to 0.39%.
GC777-4 150.8-155.6 m 10°C 146-112 Ma Good quality data: 18 age grains 57 track lengths	Single	45-60	75-0	AFTA data from this sample can be explained by a single episode of heating to a maximum paleotemperature between 45 and 60°C, from which cooling began some time between 75 and 0 Ma. Equivalent R_0max 0.32 to 0.37%. This is highly consistent with a measured VR value of 0.36% from the underlying Jurassic section (Table D.2).
GC777-5 176.7-177.3 m 10°C 208-146 Ma Poor quality data: 2 age grains 1 track lengths	Single	<110 unconstrained	80-0 pre-80 Ma	Poor quality AFTA data in this sample provide only very broad constraints on the maximum post-depositional paleotemperature to less than 125°C since 80 Ma, based on lack of detectable age reduction in two apatite grains. Equivalent R_0max not constrained from AFTA.

All thermal history constraints are based on assumed heating rates of 1°C/Ma and cooling rates of 10°C/Ma.

Events shown in brackets are not required by the AFTA data, though they are allowed within the limits shown.



Table 4.4: Fluid inclusion homogenisation temperatures in Irish Rockall Trough Borehole 83/20-sb01 (Geotrack Report #777)

Depth (m)	Stratigraphic age	Quartz					Calcite			
		Cement	Trail 1	Trail 2	Trail 3	Trail 4	Cement	Recryst.	Cement 2	Vein
107.75	Late Cretaceous		90.4 (5)		168 (6)	201.1 (7)			54.4-<50 (10)	
130.95	Late Cretaceous							92.8 (10)		
131.25	Late Cretaceous		74.5 (1)	129.1 (16)	162.5 (14)		85.3 (19)		<50 (2)	
131.4	Late Cretaceous				158.9 (11)	197.9 (3)	82.1 (7)		<50 (4)	
137.35	Late Cretaceous				155.7 (12)	197 (6)		91.1 (8)		
137.95	Late Cretaceous	101.1 (8) 149.9 (3)			165.5 (14)			123.5 (8)		
142.0	Albian- Cenomanian							81.7-164.7 (13)		
146.7	Early Cretaceous			126.1 (4)		185.8 (23)	118.5 (3)	154.3 (7)		
151	Early Cretaceous				167.5 (27)			160.3 (6)		
155.6	Early Cretaceous		94.7 (1)	141 (2)	169.5 (13)	207.6 (7)	94.1 (5)			
156.3	Early Cretaceous		65.3 (6)	106.2 (11)					<50 (5)	
161.5	Early Cretaceous		94.2 (1)	132.9 (6)		191.1 (8)			35.4 (5)	
166.2	Early Cretaceous		80.1 (4)			183 (27)		165.8 (5)		

Numbers shown in brackets show the numbers of inclusions in each population.

**Table 4.4: Continued (Geotrack Report #777)**

Depth (m)	Stratigraphic age	Quartz					Calcite			
		Cement	Trail 1	Trail 2	Trail 3	Trail 4	Cement	Recryst.	Cement 2	Vein
176.7	Jurassic									57.8-<50 (7)
176.7	Jurassic				156.6 (11)					
177	Jurassic		99.4 (8)	135.4 (15)						75.1 (11)
177	Jurassic		90.0 (5)	119.4 (6)	148.6 (6)	179.6 (5)		140.5 (5)		
177.15	Jurassic									<50-33.8 (8)
177.32	Jurassic			107.1 (9)	167.7 (4)					

Numbers shown in brackets are the numbers of inclusions in each population.

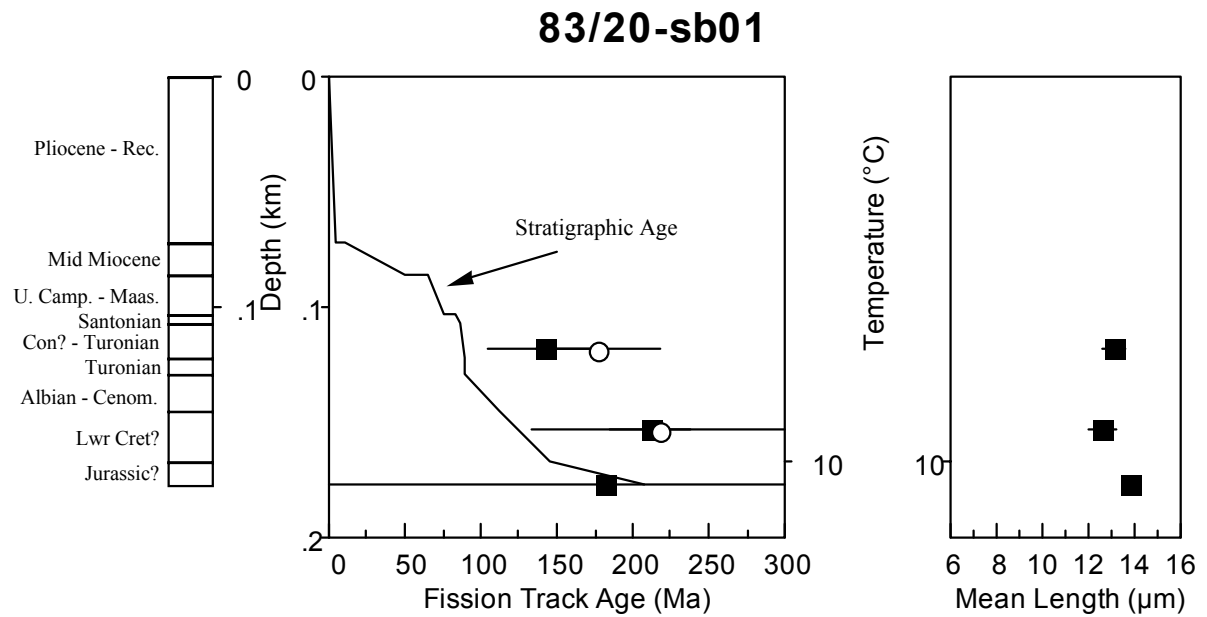


Figure 4.1: AFTA (filled squares) and ZFTA (open circles) parameters plotted against sample depth and present temperature for samples from **borehole 83/20-sb01, Irish Rockall Trough**. The variation of stratigraphic age with depth is also shown, as the solid line in the central panel.

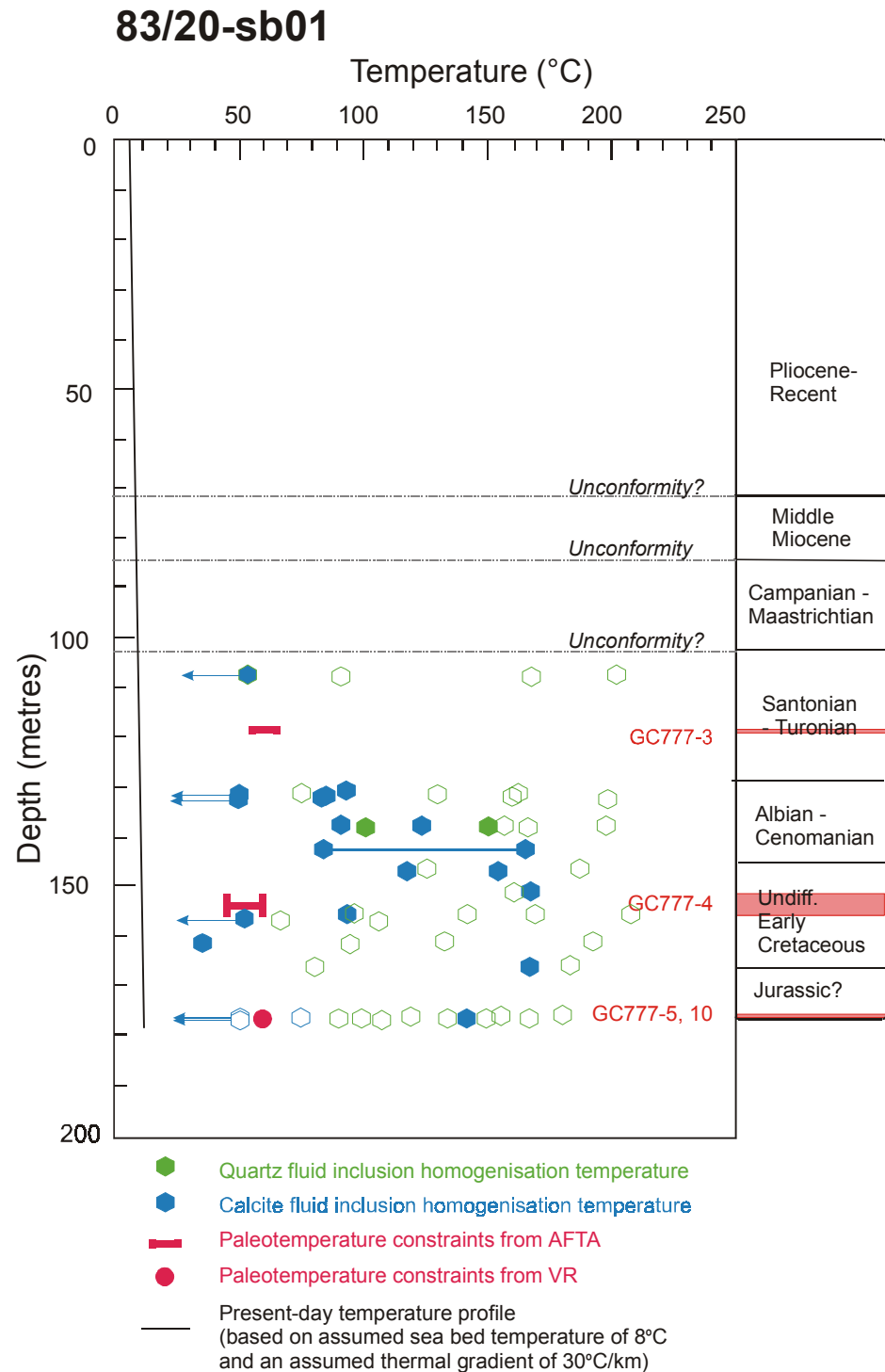


Figure 4.2: Paleotemperature constraints derived from AFTA in **borehole 83/20-sb01, Irish Rockall Trough**, plotted against depth (below sea bed). Fluid inclusion homogenisation temperatures from Dr John Parnell (summarised in Table 4.4) are also plotted against depth. Open symbols represent veins and trails, while filled symbols represent cements and recrystallised calcite. The assumed present-day temperature profile in the well is also shown. AFTA data from this well define a single paleo-thermal episode, from which cooling began some time between 40 and 0 Ma. Fluid inclusion homogenisation temperatures are generally much higher than paleotemperatures indicated by AFTA. See text for further discussion.



5. Thermal history interpretation of data from Borehole 83/24-sb02

5.1 Geological background

This borehole intersected a 20 metre thickness of Pliocene to Recent sediments uncomfortably overlying 18.1 metres of Middle and Lower Eocene limestones, which in turn unconformably overlie calcareous sandstones and sandy limestone of Mid to Upper Cretaceous age. These are separated by an unconformity from underlying muds and very fine grained sands of ?Middle to Late Jurassic age, which again unconformably overlie a sequence of fine grained sands and silts of indeterminate age, with TD reached at a depth of 72 metres below sea bed.

Prominent unconformities thus occur at Middle Eocene to Pliocene, Upper Cretaceous to Eocene, Late Jurassic to Mid-Cretaceous and sub-Middle Jurassic levels, representing the approximate time intervals 39 to 5 Ma, 65 Ma to 56 Ma, 146 to 130 Ma and pre-178 Ma, respectively. The detailed stratigraphic succession in this borehole is summarised in Table A.2, where the section of indeterminate age is designated as of Early Jurassic age, for convenience. No information is available on present-day geothermal gradients in the vicinity of the borehole. A present-day sea bed temperature of 5°C has been assumed, together with a present-day geothermal gradient of 30°C/km, although these assumptions do not affect the thermal history interpretations presented here, because of the very minor present-day burial depths.

Five samples were provided from this borehole for AFTA (Table A.1), from depths of 39.9 metres (GC777-6), 44.8 metres (GC777-7) and 44.8 to 45.4 metres (GC777-11), within the Middle to Upper Cretaceous section, and from 70.8 metres (GC777-8) and 70.8 to 71.0 metres (GC777-12) within the section of indeterminate age. Samples GC777-11 and -12 were collected in a second round of sampling, in order to supplement results from sample GC777-7 and -8, respectively, due to poor apatite yields in the earlier samples, and data from these respective sample pairs were combined for thermal history interpretation. Sample GC777-11 failed to yield any apatite, but sample GC777-12 provided sufficient additional apatite that, when combined with data from sample GC777-8, results from the combined sample (referred to as GC777-8&12) provide reliable thermal history constraints, as described below.

Fission track ages were also determined in zircons from sample GC777-11, in order to provide provenance information and also to possibly obtain depositional age constraints on the host sediments. These results are discussed in Section 7.



A single sample, GC777-11.1, from the Middle to Upper Cretaceous section in this well, was sent for VR analysis, but no material suitable for analysis was identified in the sample. (A collection of small black grains that resembled coal in hand specimens were reported to be iron oxide grains by the analyst.) Fluid inclusion data from this well were provided by Dr John Parnell and are discussed in Section 5.3.

5.2 Thermal history interpretation of AFTA data

Introduction

Fission track age and mean track length data in samples analysed from this well are summarised in Table 5.1 and plotted as a function of depth and present temperature in Figure 5.1, where the fission track age data are contrasted with the variation of stratigraphic age through the section. Zircon fission track ages are also plotted in Figure 5.1. Discussion of the zircon data is provided in Section 7.

In interpreting the AFTA data from this well, results from samples GC777-8 and GC777-12, collected over adjacent intervals, are quite consistent (Tables 5.1, B.1) and these have been combined into a single dataset, characterised by the sample number GC777-8&12, for detailed thermal history interpretation.

Interpretation of the AFTA data in terms of evidence that the samples may have been hotter in the past is summarised in Table 5.2. Following the strategy outlined in Section 2.1, estimates of the magnitude and timing of maximum paleotemperatures allowed by the AFTA data in each sample are summarised in Table 5.3.

Evidence for elevated paleotemperatures from AFTA

AFTA parameters in both samples from this borehole which yielded apatite, GC777-7 and -8&12, show clear evidence that the samples have been hotter than their present-day temperature at some time after deposition (Table 5.2). This evidence comes from the track length data alone in sample GC777-7, and from both fission track age and track length data in sample GC777-8&12.

Magnitude of paleotemperatures and timing of cooling from AFTA

As detailed in Table 5.3, AFTA data in both samples GC777-7 and -8&12 can be explained by a single episode of heating and cooling after deposition. Data from sample GC777-7 suggest cooling from a maximum paleotemperature between 50 and 70°C beginning some time between 85 and 0 Ma, while the higher quality data from



sample GC777-8&12 provide tighter constraints on the time of cooling, at between 50 and 0 Ma (from a maximum paleotemperature between 60 and 75°C).

Results from sample GC777-8&12 would also allow an earlier episode, as summarised in Table 5.3. In the absence of tighter constraints on the age of this section it is not possible to comment further on this possibility. Unfortunately, no zircons were obtained from this section, which might have helped in improving stratigraphic age constraints.

Assuming that results from both samples GC777-7 and -8&12 represent a common paleo-thermal episode, the combined timing constraint on the time of cooling, at between 50 and 0, can reasonably be extended to both samples. This timing for the onset of cooling correlates closely with the unconformity between Middle Eocene Pliocene units recognised in this well (Section 5.1), representing the approximate time interval 39 to 5 Ma. The significance of this is discussed in greater detail in Section 6.

Thermal history constraints derived from AFTA data in samples GC777-7 and GC777-8&12 are summarised in Table i. Figure i provides a schematic illustration of the thermal history interpretation of AFTA data from sample GC777-8&12, as representative of results from this well.

Equivalent maturity values from AFTA

Also detailed in Table 5.3 are equivalent $R_{o,max}$ values for each sample, calculated from the thermal history interpretation derived from the AFTA data, using the algorithm presented by Burnham and Sweeney (1989) and Sweeney and Burnham (1990). Values are generally in the range 0.33 to 0.45%, although the possibility of an earlier episode in the pre-Middle Jurassic section might indicate higher maturities in this part of the section.

5.3 Fluid inclusion results

Homogenisation temperatures (T_{hom}) in fluid inclusions from this borehole are summarised in Table 5.4, and are plotted against depth in Figure 5.2. Paleotemperature constraints from AFTA are also plotted against depth in Figure 5.2. Fluid inclusion measurements are focussed at similar depths to AFTA samples GC777-6, -7 and -8&12, allowing direct comparison of results from the two techniques.



At depths around 40 metres below sea bed, in units of Middle to Late Cretaceous age, calcite cements show a population of homogenisation temperatures which are very close to the paleotemperatures indicated by AFTA in sample GC777-7, while other calcite cements and recrystallised calcite, trails in quartz and a quartz cement also give much higher values. At deeper levels, at depths around 70 metres, only the higher values are present.

The significance of these observations in the context of the thermal and fluid flow histories at the borehole site are discussed in detail in Section 6.3.



Table 5.1: Summary of AFTA parameters in samples from Irish Rockall Trough Borehole 83/24-sb02 (Geotrack Report #777)

Sample number	Average depth (m)	Present temperature ^{*1} (°C)	Stratigraphic age (Ma)	Mean track length (μm)	Predicted mean track length ^{*2} (μm)	Fission track age (Ma)	Predicted fission track age ^{*2} (Ma)
GC777-6	39.9	6	130-65		no apatite		
GC777-7	44.8	6	130-65	13.44 ± 0.36	14.9	127.6 ± 13.7	111
GC777-11	45.1	6	130-65		no apatite		
GC777-8	70.8	7	>178	12.80 ± 0.99	14.8	115.4 ± 40.4	197
GC777-12	70.9	7	>178	12.76 ± 0.35	14.9	147.1 ± 13.7	197
GC777-8&12 ^{*3}	70.9	7	>178	12.77 ± 0.27	14.9	145.3 ± 12.6	197

^{*1} See Appendix A for discussion of present temperature data.

^{*2} Values predicted from the Default Thermal History (Section 2.1); i.e. assuming that each sample is now at its maximum temperature since deposition. The values refer only to tracks formed after deposition. Samples may contain tracks inherited from sediment provenance areas. Calculations refer to apatites within the measured compositional range for each sample, as discussed in Appendix A.

^{*3} Data from samples GC777-8 and GC777-12 combined.

Note: all depths quoted are TVD with respect to sea bed.



Table 5.2: Summary of thermal history interpretation of AFTA data in Irish Rockall Trough Borehole 83/24-sb02 (Geotrack Report #777)

Sample Details Sample No. Depth Present temp Strat. Age	Do AFTA data require any revision of present temperature?	Evidence of higher temperatures in the past from length data?	Evidence of higher temperatures in the past from fission track age data?	Conclusion
GC777-6 39.9 m 6°C 130-65 Ma	-	-	-	No apatite
GC777-7 44.8 m 6°C 130-65 Ma Low quality data: 2 age grain 8 track lengths	No	Yes [The mean length is ~1.5 µm less than predicted on the basis of the Default Thermal History. Modelling the AFTA parameters through likely thermal history scenarios shows that the track length data in this sample cannot be explained by inheritance of shorter tracks from sediment source terrains, and must be due to the effects of higher paleotemperatures at some time after deposition.]	No [The pooled fission track age of this sample is greater than that predicted on the basis of the Default Thermal History.]	Track length data show that this sample has been hotter in the past, while the lack of significant age reduction suggests only a moderate degree of paleo-heating.
GC777-11 44.8-45.4 m 6°C 130-65 Ma	-	-	-	No apatite
GC777-8&12 70.8-71.0 m 7°C >178 Ma Good quality data: 10 age grains 18 track lengths	No	Yes [The mean length is ~2.1 µm less than predicted on the basis of the Default Thermal History. Modelling the AFTA parameters through likely thermal history scenarios shows that the track length data in this sample cannot be explained by inheritance of shorter tracks from sediment source terrains, and must be due to the effects of higher paleotemperatures at some time after deposition.]	Yes [The pooled fission track age of this sample is significantly less than that predicted on the basis of the Default Thermal History.]	Fission track age and track length data show that this sample has been hotter in the past.

Note: Interpretation of AFTA data is based on comparison of measured AFTA parameters with values predicted from "Default Thermal History" (Section 2.1); i.e., assuming that each sample is now at its maximum temperature since deposition. The predicted values for each sample are summarised in Table 5.1, and refer only to tracks formed after deposition. Samples may also contain tracks inherited from sediment provenance areas, which must be allowed for in interpreting the data. Calculations refer to apatites with the compositional range appropriate to each sample, as explained in Appendix A.



Table 5.3: Estimates of timing and magnitude of elevated paleotemperatures from AFTA data in Irish Rockall Trough Borehole 83/24-sb02 (Geotrack Report #777)

Sample Details	Paleo-thermal episodes			Comments
	Event	Maximum paleo-temperature (°C)	Onset Of Cooling (Ma)	
GC777-6 39.9 m 6°C 130-65 Ma	-	-	-	No apatite
GC777-7 44.8 m 6°C 130-65 Ma Low quality data: 2 age grain 8 track lengths	Single	50-70	85-0	<p>AFTA data from this sample can be explained by a single episode of heating to a maximum paleotemperature between 50 and 70°C, from which cooling began some time between 85 and 0 Ma, as summarised left. This solution provides a satisfactory explanation of the available data, but is based on only two ages and 8 track lengths, and thus should probably be treated with some caution. However, the result is consistent with results from sample GC777-8&12 from this borehole, and in samples from other boreholes, and is therefore regarded as reliable. Note the wider timing constraints in this sample, compared to others where larger numbers of track lengths are available.</p> <p>Equivalent R_0max 0.33-0.42%. No VR data are available from depths adjacent to this AFTA sample, for comparison.</p>
GC777-11 44.8-45.4 m 6°C 130-65 Ma	-	-	-	No apatite
GC777-8&12 70.8-71.0 m 7°C >178 Ma Good quality data: 10 age grains 18 track lengths	Single	60-75 <i>(60-90)</i> <i>(60-125)</i> <i>(>90)</i>	50-0 <i>90-50)</i> <i>170-90)</i> <i>>170)</i>	<p>AFTA data from this sample can be explained by a single episode of heating to a maximum paleotemperature between 60 and 75°C, from which cooling began some time between 50 and 0 Ma, as summarised left. AFTA data would also allow an earlier episode of heating and cooling, within the allowed ranges shown to the left, although such an episode is not required by the data. Due to the indeterminate depositional age of this sample, events in the earlier history cannot be resolved with confidence.</p> <p>Equivalent R_0max 0.37-0.45% (assuming no earlier episodes). No VR data are available from depths adjacent to this AFTA sample, for comparison.</p>

All thermal history constraints are based on assumed heating rates of 1°C/Ma and cooling rates of 10°C/Ma.

Events shown as italics in brackets are not required by the AFTA data, though they are allowed within the limits shown.



Table 5.4: Fluid inclusion homogenisation temperatures in Irish Rockall Trough Borehole 83/24-sb02 (Geotrack Report #777)

		Quartz					Calcite			
Depth (m)	Stratigraphic age	Cement	Trail 1	Trail 2	Trail 3	Trail 4	Cement	Recryst.	Cement 2	Vein
39.9	Middle to Upper Cretaceous				146.6 (6)	193.1 (12)			<50 (5)	
40.0-40.5	Middle to Upper Cretaceous	130 (8)			162.3 (13)				<50 (4)	
44.8	Middle to Upper Cretaceous				157.7 (6)	192.6 (3)	70 (2)	157.1 (13)	<50 (6)	
45.4	Middle to Upper Cretaceous				157.3 (14)		75.6 (7)	149.8 (8)	<50 (5)	
69.25	?Middle to Upper Jurassic				146.5 (19)					
69.3	?Middle to Upper Jurassic							132 (11)		
70.75	pre-Middle Jurassic				155.6 (3)	179.3 (10)				
71.45	pre-Middle Jurassic				148.7 (1)					

Numbers shown in brackets show the numbers of inclusions in each population.

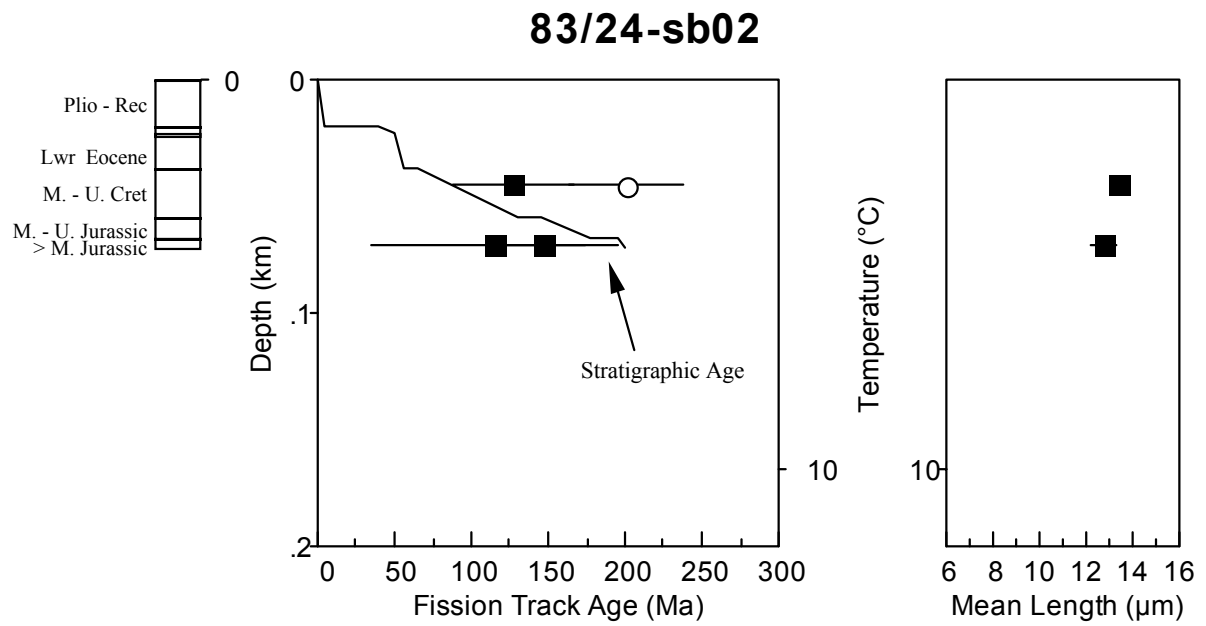


Figure 5.1: AFTA (filled squares) and ZFTA (open circles) parameters plotted against sample depth and present temperature for samples from **borehole 83/24-sb02, Irish Rockall Trough**. The variation of stratigraphic age with depth is also shown, as the solid line in the central panel.

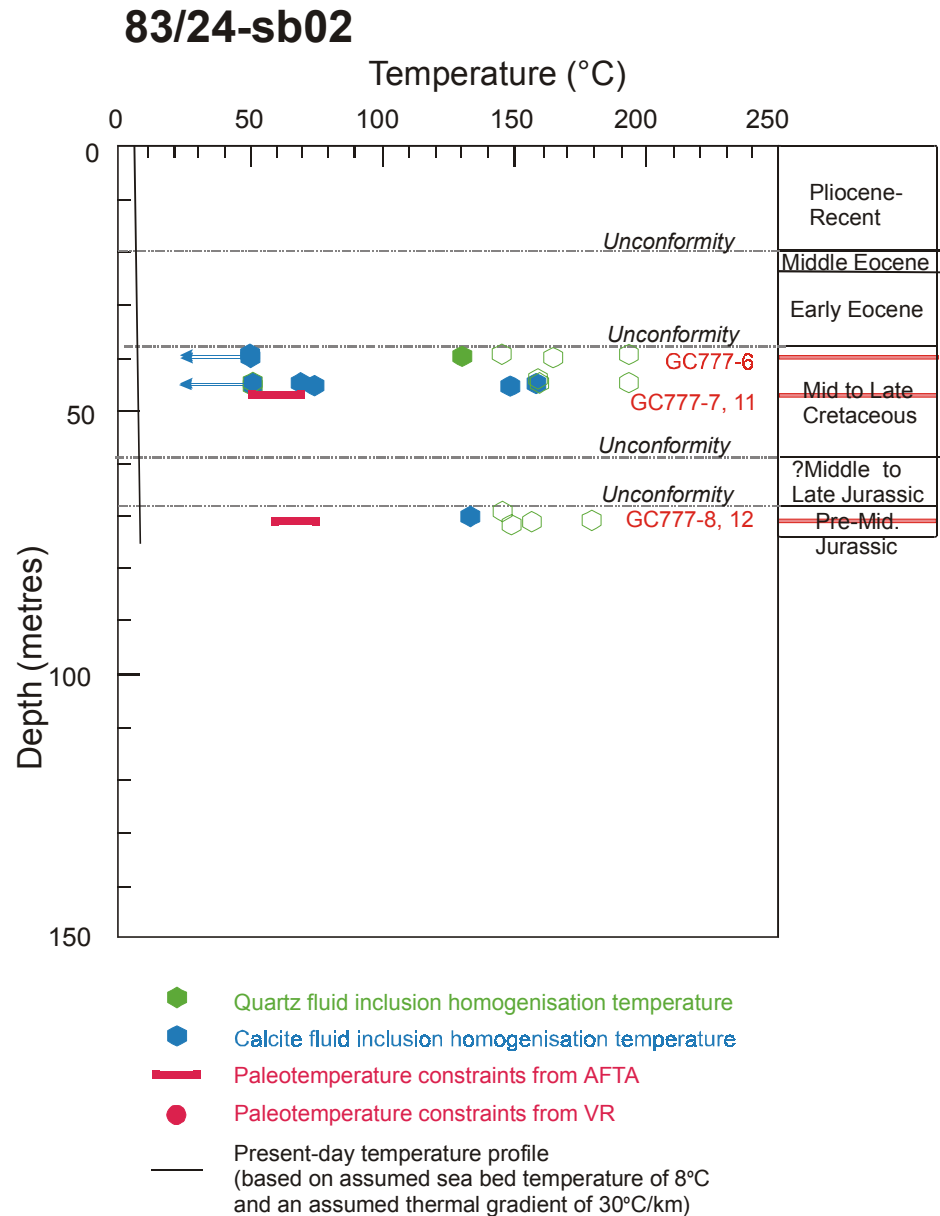


Figure 5.2: Paleotemperature constraints derived from AFTA in **borehole 83/24-sb02, Irish Rockall Trough**, plotted against depth (below sea bed). Fluid inclusion homogenisation temperatures from Dr John Parnell (summarised in Table 5.4) are also plotted against depth. Open symbols represent veins and trails, while filled symbols represent cements and recrystallised calcite. The assumed present-day temperature profile in the well is also shown. AFTA data from this well define a single paleo-thermal episode, from which cooling began some time between 50 and 0 Ma. Fluid inclusion homogenisation temperatures are generally much higher than paleotemperatures indicated by AFTA. See text for further discussion.



6. Thermal history synthesis

6.1 Mechanisms of heating and cooling

Introductory comments

Information on the nature of the processes responsible for producing paleo-thermal effects can usually be obtained from the variation of paleotemperatures with depth through a sedimentary section (Bray et al., 1992). Heating due to deeper burial, elevated heat flow, or hot fluid movement through a localised horizon (or a combination of these processes) produce different styles of variation which are diagnostic of the underlying mechanism.

With thermal history constraints from only a very narrow range of depths in each borehole studied for this report, it is not possible to obtain direct information on mechanisms of heating and cooling, and we must rely on the magnitude of observed heating effects and the timing of cooling revealed by AFTA, combined with regional geological evidence in order to obtain any insights into the processes responsible for heating and cooling.

Timing of cooling revealed by AFTA

Figure 6.1 compares the timing of cooling derived from AFTA data in individual samples in each borehole, within the context of the preserved sedimentary units in each case. Two conclusions can be drawn from this Figure. First, results from all samples which give firm constraints on the timing of cooling are consistent with cooling beginning some time between 40 and 0 Ma. Second, this interval corresponds to a prominent regional unconformity between Late Cretaceous or Early Tertiary units and Late Miocene or younger units. The interval of time from Middle Eocene to Middle Miocene, representing the interval 39 to 15 Ma, is not represented by preserved sedimentary units anywhere across the region. The coincidence between this interval of erosion/emergence across the region with the time of cooling revealed by AFTA suggests that at least a proportion of the cooling revealed by AFTA and VR in these boreholes is likely to be due to exhumation during this interval.

Integration of AFTA and VR data with fluid inclusion results

As reviewed in Sections 3, 4 and 5, homogenisation temperatures (T_{hom}) from fluid inclusions in quartz and calcite are generally much higher than the maximum paleotemperatures indicated by AFTA and VR at similar depths. In contrast, AFTA



and VR give very consistent results (albeit with VR data available from only one sample). In some cases, a population of lower T_{hom} values is present close to the range of paleotemperatures indicated by AFTA and VR.

These observations could be explained in a variety of ways, but two end-member scenarios may be defined. At one extreme, the paleotemperatures indicated by AFTA and VR data, together with the lower T_{hom} values, could represent ambient conditions reached during a period of deeper burial, while most of the T_{hom} values would represent localised, short-term pulses of hot fluids which are not expressed in the AFTA and VR data due to the short timescales of heating. In this scenario, the lowest modes in the T_{hom} values could also represent ambient conditions around maximum burial. As an alternative, the heating revealed by the AFTA and VR data may have been dominantly due to hot fluid circulation, taking place over a much shorter timescale than assumed in the interpretation of data set out in Sections 3, 4 and 5, such that some of the higher T_{hom} values actually represent the true ambient paleotemperatures reached during this event (note that in this scenario, the timing of cooling derived from AFTA would be the same as outlined in Sections 3, 4 and 5 - only the magnitude of the maximum paleotemperature would change). In this scenario, lower T_{hom} values could represent later events during cooling. Combinations of these end-member scenarios may be possible, with different mechanisms dominating in different regions.

We suggest that the coincidence between the timing of cooling and the regional mid-Tertiary unconformity in the region provides strong support for the former option, in which the pervasive paleo-thermal effects identified by AFTA and VR data, together with the lower T_{hom} values, represent the effects of heating due to deeper burial, while most of the T_{hom} values represent localised effects of hot fluid movement. Experience involving comparison of AFTA, VR and fluid inclusion measurements in a variety of geological environments (e.g. Parnell et al., 1999) provides strong support for such an interpretation. The relative uniformity of the magnitude of heating revealed by AFTA and VR in the three boreholes, compared to the considerable variability in T_{hom} values (Figures 3.2, 4.2, 5.2), provides further support for this explanation.

6.2 Amounts of removed section

Following the preferred interpretation outlined in Section 6.1 for the paleotemperatures revealed by AFTA and VR data in this study, we can evaluate the



amounts of additional burial (and subsequent exhumation) required to produce the observed paleotemperatures.

As emphasised in Section 2.5, estimation of amounts of removed section from paleotemperature data depends critically on various key assumptions, particularly in studies such as this where paleotemperature information is available from only a narrow range of depths in each borehole, and paleogeothermal gradients cannot be constrained directly. Nevertheless, given the necessary assumptions it is straightforward to estimate the amount by which the samples must have been more deeply buried in order to explain the observed paleotemperature, as explained below.

Assuming that the paleogeothermal gradient was linear throughout the entire section (i.e. preserved and removed) at the time of maximum paleotemperatures, extrapolation of the observed paleotemperature to an assumed paleo-surface temperature for any specific value of paleo-gradient and then projecting back to the depth of the appropriate unconformity provides an estimate of the amount by which that unconformity surface was more deeply buried, and hence the amount of section that has since been removed by erosion. In this report, estimates of removed section are made with respect to the Late Cretaceous or Early Tertiary to Late Tertiary unconformity in each borehole, as illustrated in Figure 6.1. In each borehole, estimates of additional burial are based on paleotemperature constraints in key samples, characterised by high quality data and taken to be representative of the section, as follows:

Table 6.1: Key samples for burial estimation: Irish Rockall Trough Boreholes (Geotrack Report #777).

Borehole	Depth of unconformity (metres below sea bed)	Sample number	Sample depth (m)	Paleotemperature (°C)
16/28-sb01	14.5	GC777-2	147.2	50-60
83/20-sb01	86.0	GC777-4	153.2	45-60
83/24-sb02	20.0	GC777-8&12	70.9	60-75

Given all the assumptions which underlie this analysis (as set out in Section 2.5), estimates of the amounts of removed section required to explain the observed paleotemperatures for a range of values of paleogeothermal gradients are summarised in Table 6.2. These are calculated using the equation:

$$\text{Additional burial} = [(T_{\text{pal}} - T_o) / dT/dz] - (z_s - z_u)$$

where: T_{pal} = maximum paleotemperature



T_o = paleo-surface temperature

dT/dz = paleogeothermal gradient

z_s = depth of sample

z_u = depth of unconformity

Since paleo-surface temperatures could well have been hotter than the present-day value in the Mid-Tertiary, estimates are also provided in Table 6.2 for a paleo-surface temperature of 20°C, representing a likely upper limit to the range of possible values.

Table 6.2: Removed section estimates: Irish Rockall Trough Boreholes (Geotrack Report #777).

Borehole	Paleogeothermal Gradient	Estimates of removed section (km)	
		<i>5°C surface temperature</i>	<i>20°C surface temperature</i>
16/28-sb01	20°C/km	2.12-2.67	1.37-1.87
	30°C/km	1.37-1.70	0.87-1.20
	40°C/km	0.99-1.24	0.62-0.87
	50°C/km	0.77-0.97	0.47-0.67
	60°C/km	0.62-0.78	0.37-0.53
83/20-sb01	20°C/km	1.93-2.68	1.18-1.93
	30°C/km	1.27-1.77	0.77-1.27
	40°C/km	0.93-1.30	0.56-0.93
	50°C/km	0.73-1.03	0.43-0.73
	60°C/km	0.60-0.85	0.35-0.60
83/24-sb02	20°C/km	2.70-3.45	1.95-2.70
	30°C/km	1.78-2.28	1.28-1.78
	40°C/km	1.32-1.70	0.92-1.32
	50°C/km	1.05-1.35	0.75-1.05
	60°C/km	0.87-1.12	0.62-0.87

The range of values for each paleo-gradient corresponds to the range of allowed maximum paleotemperatures for each key sample (Table 6.1). For likely values of paleogeothermal gradient in the range 30 to 40°C/km, results from the three boreholes suggest amounts of additional burial in the general range 0.5 to 2 km.

The magnitude of removed section required to explain the observed paleotemperatures can be easily adjusted to an alternative paleo-surface temperatures by subtracting or adding the difference in depth equivalent to the change in paleo-surface temperature, for the appropriate paleo-gradient, as described in Section 2.5.



6.3 Timescales of hot fluid pulses

We can further develop the interpretation of the paleotemperatures derived from AFTA and VR as outlined in Section 6.1 by investigating likely timescales of heating to temperatures indicated by fluid inclusion results, such that no detectable effects are produced in the AFTA data. For this exercise, we focus on sample GC777-2, from borehole 16/28-sb01, as a typical example. The starting point for discussion is the thermal history solution derived from the AFTA data as summarised in Table 3.3, to which is added a heating pulse of varying duration. By investigating the duration of heating required to produce a detectable effect in the AFTA data, limits can be placed on the maximum timescale of heating allowed by the AFTA data.

This process is illustrated in detail in Figures 6.2 and 6.3. Figure 6.2 shows the preferred thermal history interpretation derived from the AFTA data as explained in Table 3.3, involving a maximum post-depositional paleotemperature of 55°C, together with the predicted track length distribution and variation of fission track age with Cl content, each compared with the measured data. Cooling is shown as commencing at 20 Ma (although any time between 40 and 0 Ma is allowed by the data). A pre-depositional history is also included to explain the shorter track lengths within the sample. As expected for this best-fit history, the predictions show a good match to the measured data.

In contrast, Figure 6.3 shows similar plots for a history in which a short-term thermal event at 10 Ma as been added. In Figure 6.3 the duration of heating is 1 Ma (i.e. heating begins at 11 Ma, reaches the maximum value of 175°C at 10 Ma and then cools back to ambient temperature at 9 Ma. This history produces total annealing of tracks in all compositional groups at 10 Ma, and the predicted parameters show a very poor match to the measured data. This shows that if this sample reached a temperature of 175°C, as suggested by the fluid inclusion homogenisation temperatures (Table 3.4), then the timescale of heating must have been much shorter than 1 Ma, such that heating produced no detectable effect on the AFTA data.

To further assess this question, Figure 6.4 shows a comparison of measured values of summary AFTA parameters (mean track length and fission track age) for apatites containing between 0.0 and 0.1 wt % Cl in sample GC777-2 with values predicted from thermal histories of the style illustrated in Figure 6.3a), using various timescales of heating to a selection of maximum temperatures.

For each maximum temperature, the shortest durations of heating have no detectable effect (because of the kinetics of annealing), but as the duration of heating increases,



the heat pulse progressively overprints the effects of the previous history. Fission track ages are progressively reduced to a value of ~ 9 Ma (corresponding to the time of cooling) as duration increases. Track lengths are first shortened as the lengths of tracks formed prior to the event are reduced. Then as duration of heating increases further, the mean track lengths begin to rise once more as the degree of length reduction in tracks formed prior to the thermal event becomes severe, approaching total annealing, and the track length data are dominated by tracks formed after cooling, which are much longer.

The final values of fission track age and mean track length in this example are specific to the thermal history illustrated, but the general principles apply to all styles of history. Similar calculations can be made for other samples, and other compositional groups, but again, similar principles apply and this example serves to illustrate the general nature of effects.

It is clear from Figure 6.4 that the timescale of heating to temperatures around 200°C must have been less than 10 years (10^{-5} Ma), so as to produce no detectable effect. In contrast, for a maximum temperature of 125°C , a duration of 0.1 Ma is required before a detectable change in the predicted track length is produced.

In summary, if we follow our preferred interpretation of the AFTA and VR data as representing the effects of deeper burial while fluid inclusions represent transient pulses of hot fluid, then Figure 6.4 provides constraints on the likely timescales of heating.

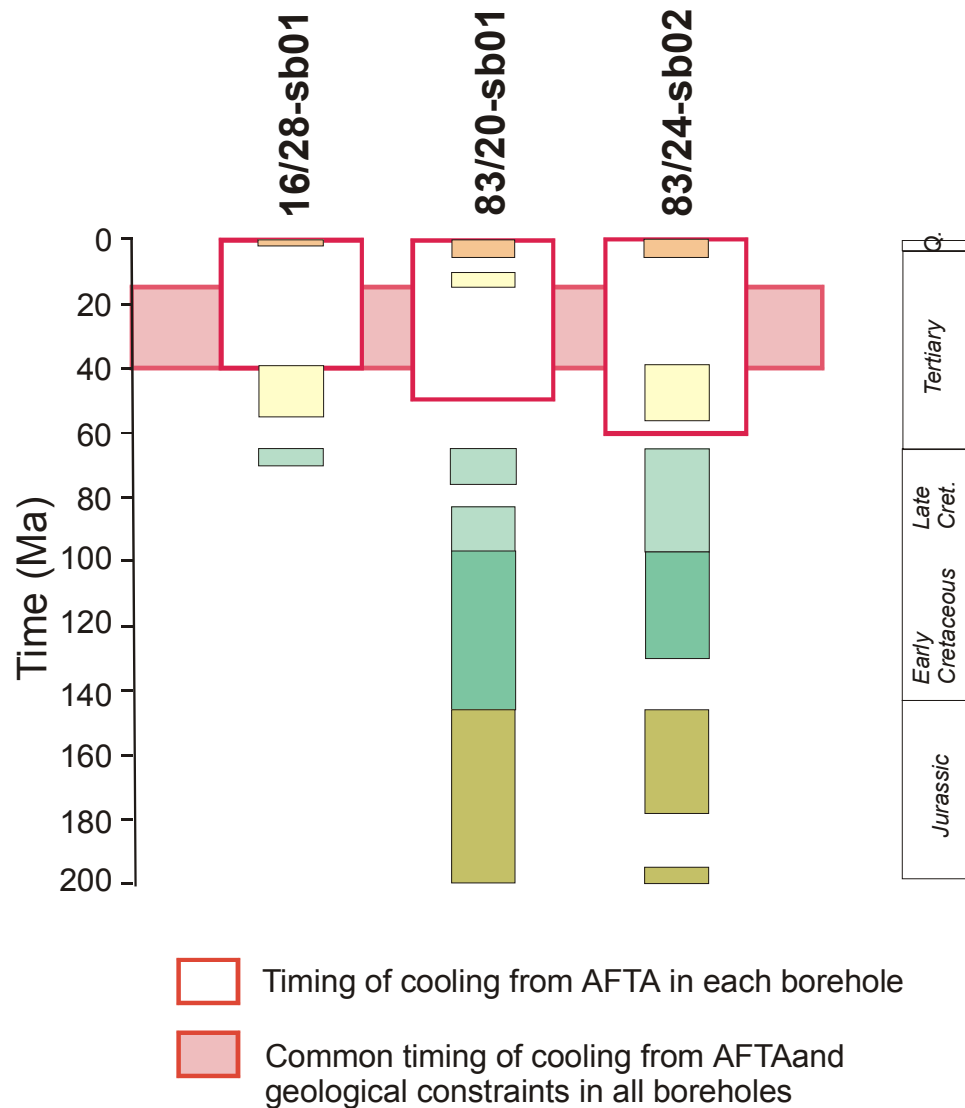


Figure 6.1:

For each borehole, the intervals of the stratigraphic column represented by preserved sediments (coloured boxes – based on information in Table A.1) are compared with the timing of cooling derived from AFTA data from the combination of all samples in that borehole. Cooling identified from AFTA overlaps in time with a prominent regional unconformity. Integration of results from all three boreholes with geological evidence suggests that an interpretation of cooling due to uplift and erosion (exhumation) in the Late Eocene to Middle Miocene (approximately 39 to 15 Ma) would be consistent with all data from the three boreholes. However, this may be an oversimplification, and it is possible that cooling was diachronous across the region.

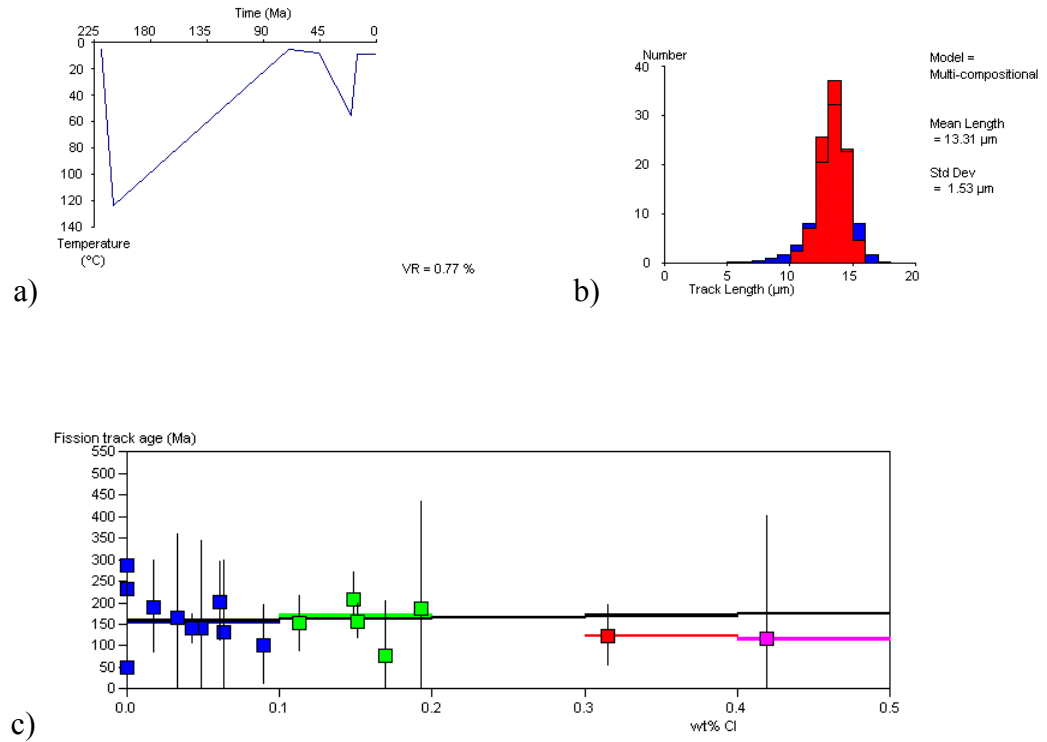


Figure 6.2: a) Preferred thermal history interpretation derived from AFTA data in sample GC777-2 as explained in Table 3.3. b) Track length distribution predicted from the thermal history in a) (blue), compared with measured track length distribution for sample GC777-2 (red). c) Pattern of fission track age variation against Cl content measured in sample GC777-2, plus variation predicted from the thermal history in a) (black horizontal lines).

The measured parameters show a good match to the predictions, as expected for this best-fit solution.

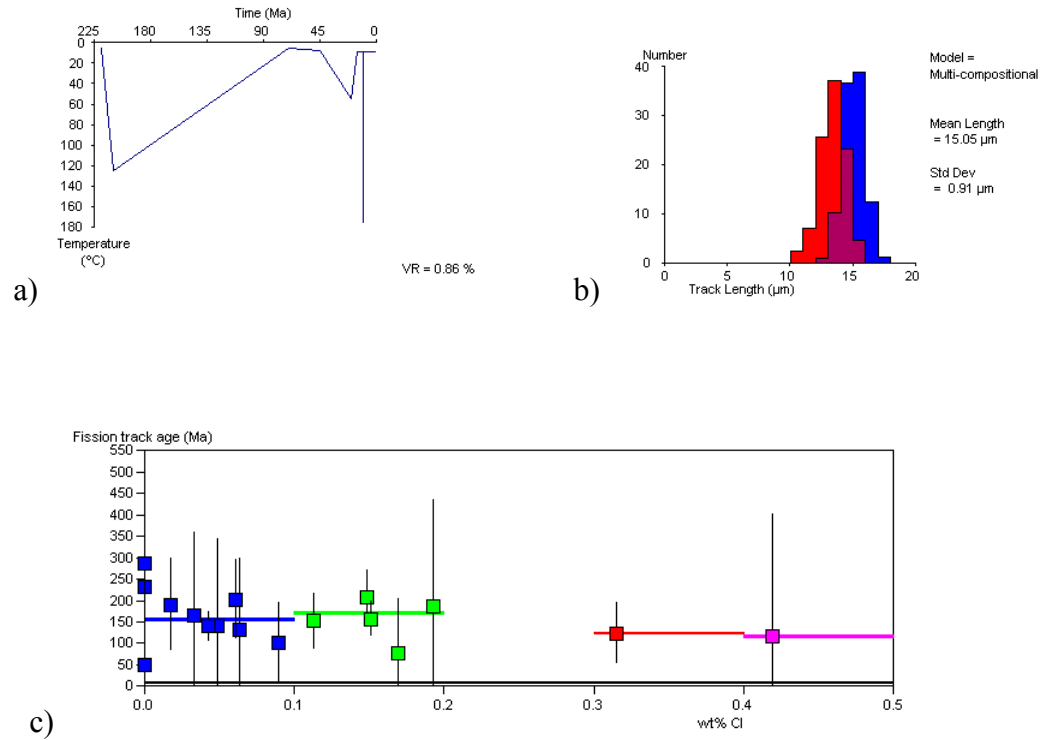


Figure 6.3:

a) Thermal history as in Figure 6.2a), but with the addition of a short-term heating pulse involving a maximum temperature of 175°C at 10 Ma. In this illustration the duration of the heating pulse (i.e. the time from the onset of heating to attainment of the maximum pulse temperature) is 1 Ma. **b)** Track length distribution predicted from the thermal history shown in a) (in blue), compared with measured track length distribution in sample GC777-2 (red). **c)** Pattern of fission track age variation against Cl content measured in sample GC777-2, plus variation predicted from the thermal history shown in a) (black horizontal lines).

In this scenario, heating to 175°C predicts a much greater degree of annealing than observed in the data, with total annealing of tracks in all Cl groups prior to cooling at 10 Ma. Thus, the measured fission track ages are much older than predicted values and the predicted length distribution is longer than the observed tracks. This shows that if this sample reached 175°C, as suggested the fluid inclusion homogenisation temperatures, the timescale of heating must have been much shorter than 1 Ma.

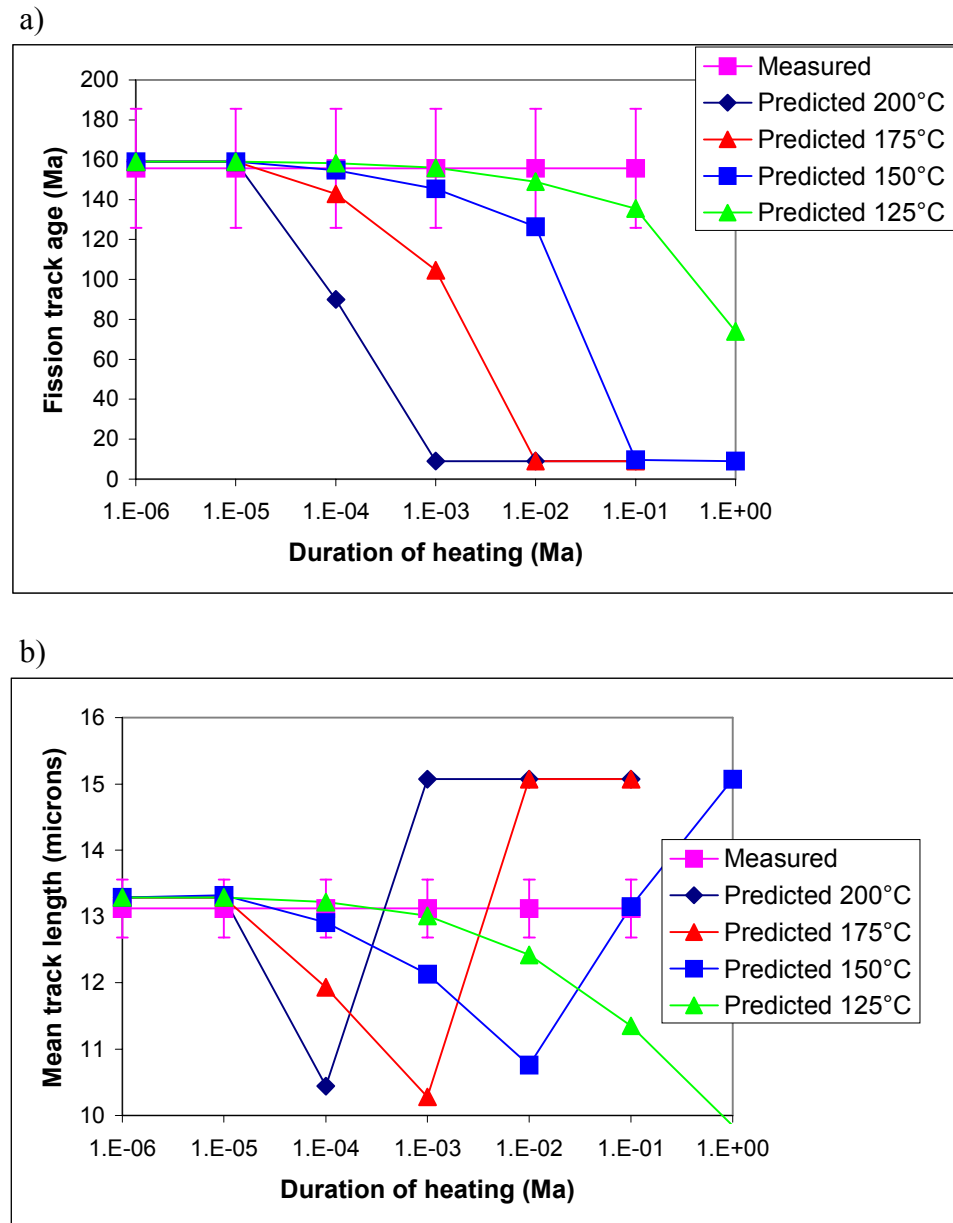


Figure 6.4:

Patterns of fission track age (a) and length (b) predicted for apatites containing between 0.0 and 0.1 wt% Cl in sample GC777-2 for thermal histories of the type illustrated in Figure 6.3a), for various durations of heating in the thermal event at 10 Ma (x-axis) and various maximum temperatures (see legends). In each case, predicted values are compared with the appropriate measured value (with analytical uncertainty also shown at 2 sigma). These plots allow us to determine the maximum duration for heating to a given temperature such that no observable effect is seen in the AFTA data. For example, for a maximum temperature of 175°C, the duration of heating must have been less than 100 years (10^{-4} Ma). Similar plots can be constructed using data from other samples, with all producing similar results, and this example serves to illustrate the overall trend.



7. ZFTA data: sediment provenance and depositional age constraints

7.1 Introduction

Fission tracks in zircon are more resistant to thermal disturbance than those in apatite, requiring paleotemperatures of around 300°C (equivalent to VR values in excess of 5%, Appendix C) to produce significant fission track age reduction. Therefore, in most sedimentary basins, zircon fission track ages can be interpreted as providing information on sediment provenance rather than post-depositional effects. In addition, due to the low likelihood of thermal disturbance, the youngest group of zircon fission track ages in a sediment can provide an upper limit to the depositional age, which can be particularly useful where other methods are equivocal or non-specific. In the following Sections, results ZFTA analyses undertaken in selected samples from the three boreholes are discussed in the context of provenance information and depositional age constraints (samples for ZFTA were selected on the basis of zircon yields). Brief discussion of provenance aspects of the AFTA data from the same or adjacent samples is also provided, where appropriate.

7.2 Borehole 16/28-sb01

Sample GC777-9

Zircons in this sample were small and showed a variety of forms including euhedral, rounded and anhedral. Eleven zircon grains analysed from this sample gave a pooled fission track age of 260.2 ± 22.6 Ma (Table B.1). This is much older than the Lower to Middle Eocene depositional age of this sample (Table A.1), suggesting derivation from a much older source terrain. Thus, the zircon data do not provide any useful constraint on the depositional age.

AFTA data from this sample also show a group of fission track ages around 200 to 300 Ma (see the radial plot of single grain age data in the Data Summary Sheet in Appendix B), while a number of apatites also give younger ages around 60 or 70 Ma (also present in adjacent sample GC777-1). These probably originate from Late Cretaceous to Early Tertiary volcanic activity, while the older ages from both apatite and zircon suggest derivation from a terrain dominated by Permian cooling, which could represent the effects of late-stage Variscan cooling or may be due to a specific episode of Permian volcanic and/or intrusive activity.



Sample GC777-2

Only a small number of zircons were obtained from this sample, most having euhedral form and larger than those in sample GC777-9. Seven zircon grains analysed from this sample showed a significant spread of fission track ages, with a central age of 245.3 ± 43.2 Ma (Table B.1). The youngest single grain age of 115.2 ± 33.2 Ma provides a broad upper limit to the depositional age of this sample. As the host sediment is attributed a ?Maastrichtian age (Table A.2), this result does not provide much in the way of additional constraint. Most of the grains give fission track ages which are much older than the likely depositional age, again suggesting derivation from a much older source terrain, as seen in sample GC777-9. Apatite fission track ages define a pooled fission track age of 161.5 ± 10.8 Ma, which suggests some degree of later thermal disturbance in the source terrain compared to that for sample GC777-9. Since sample GC777-2 is stratigraphically below sample GC777-9, this suggests that source regions have varied through time.

7.3 Borehole 83/20-sb01

Sample GC777-3

Zircons in this sample were small and mainly euhedral, with a smaller component of rounded and anhedral grains. Fifteen zircon grains analysed from this sample gave a significant spread of single grain ages. The radial plot in the Data Summary Sheet in Appendix B suggests the presence of two distinct components to the ages, with a younger group giving a pooled fission track age of 96 ± 8 Ma and an older group giving a pooled fission track age of 218 ± 14 Ma.

The younger group provides an upper limit to the depositional age of the host sediment which is assigned a Coniacian to Turonian age according to the Summary Log (Appendix A), corresponding to the interval 86.6 to 90.4 Ma, according to the timescale of Harland et al. (1989). The pooled age of the younger group is close to this interval, suggesting that the age assignment is broadly correct, and further, that some component of Late Cretaceous volcanic activity contributed zircons to the sediment. The quite large error on the age of this age component results from the small number of grains within the group.

The pooled age of the older group is much older than the depositional age of this sample, suggesting derivation from a much older source terrain. This age is slightly



younger than the older age group present in most of the other samples in which zircons have been analysed, which may result from the presence of an unresolved younger group of ages around 150 Ma, possibly representing Late Jurassic or perhaps Early Cretaceous volcanism. Note that the AFTA data also show a distinct component of ages around this value, lending further support to this possibility. Older ages in sample GC777-3, in the 200 to 300 Ma range, again suggest derivation from a terrain dominated by Permian cooling, which could represent the effects of late-stage Variscan cooling or may be due to a specific episode of Permian volcanic and/or intrusive activity.

Sample GC777-4

Zircons in this sample were again small and mainly euhedral, with a smaller component of rounded and anhedral grains. Fifteen zircon grains analysed from this sample gave a significant spread of single grain ages. The radial plot in the Data Summary Sheet in Appendix B suggests the presence of two distinct components to the ages, with a younger group giving a pooled fission track age of 152 ± 13 Ma and an older group giving a pooled fission track age of 234 ± 12 Ma.

The younger group provides an upper limit to the depositional age of the host sediment which is assigned a “undifferentiated Lower Cretaceous?” age according to the Summary Log (Appendix A). The pooled age of the younger group suggests a depositional age closer to the earlier part of the Lower Cretaceous, although strictly providing only an upper limit to the depositional age. Note that the presence of an age component of this value in this sample strengthens the possibility of an unresolved population around this value in shallower sample, GC777-3 (above).

The pooled age of the older group is again older than the depositional age of this sample, suggesting derivation from a terrain dominated by Late Permian to Early Triassic cooling.

7.4 Borehole 83/24-sb02

Sample GC777-11

Zircons in this sample were larger than in the other samples and of very high quality, dominated by euhedral or sub-euhedral forms. Twenty zircon grains analysed from this sample gave a significant spread of single grain ages. The radial plot in the Data Summary Sheet in Appendix B suggests the presence of two distinct components to



the ages, with a younger group giving a pooled fission track age of 89 ± 9 Ma and an older group giving a pooled fission track age of 233 ± 11 Ma.

The younger group provides an upper limit to the depositional age of the host sediment which is assigned a Mid to Upper Cretaceous age according to the Summary Log (Appendix A). The pooled age of the younger group suggests that the depositional age cannot be older than 107 Ma (taking the age \pm error at the $+2$ sigma limit), and further, that some component of Mid to Late Cretaceous volcanic activity contributed zircons to the sediment. The relatively large error on the age of this age component results from the small number of grains within the group.

The pooled age of the older group is again older than the depositional age of this sample, and is very similar to that seen in zircons from other samples, suggesting derivation from a terrain dominated by Late Permian to Early Triassic cooling.

Sample GC777-11 did not yield any apatites suitable for analysis. Apatites from other samples in this borehole give ages similar to the younger group of zircons, suggesting a sediment source characterised by contemporaneous igneous and/or tectonic activity.

7.5 Synthesis of ZFTA data

Zircon fission track age data in the five samples are summarised in Table ii. Samples of Late Cretaceous to Early Tertiary age from borehole 16/28-sb01 each contains a single population of zircon fission track ages while samples of older units from the other two boreholes contain two populations, the older of which is highly consistent with the single population in the younger units from borehole 16/28-sb01.

Based on a comparison of data from all samples, the older ages in the range 200 to 250 Ma are probably best interpreted in terms of derivation of these sediments from a terrain dominated by Triassic to Late Permian cooling, which probably represent the effects of late-stage Variscan cooling. The presence of reworked coals of Carboniferous age in Jurassic sediments from borehole 83/20-sb01 (see Section 4), provides support for this scenario.

The absence of zircons with ages close to depositional ages in units younger than Mid Cretaceous suggests an absence of Late Cretaceous to Early Tertiary volcanism in the region, possibly due to migration of igneous activity to the northeast, or alternatively may reflect a switch to basaltic volcanism producing no detrital zircons.



References

- Burnham, A.K. and Sweeney, J.J., 1989, A chemical kinetic model of vitrinite reflectance maturation. *Geochimica et Cosmochimica Acta*, 53, 2649-2657.
- Bray, R.J., Green, P.F. and Duddy, I.R. 1992. Thermal history reconstruction using apatite fission track analysis and vitrinite reflectance: a case study from the UK East Midlands and the Southern North Sea. In: Hardman, R.F.P. (ed.), *Exploration Britain: Into the next decade*. Geological Society Special Publication, 67, 3-25.
- Harland, W.B., Armstrong, R.L., Cox, A.V., Craig, L.E., Smith, A.G. and Smith, D.G. (1989). *A geologic time scale 1989*, Cambridge University Press.
- Parnell, J., Carey, P.F., Green, P.F. and Duncan, W. 1999. Hydrocarbon migration history, West of Shetland: Integrated fluid inclusion and fission track studies. In: Fleet, A.J. and Boldy, S.A.R. (eds): *Petroleum Geology of North West Europe*, Proceedings of the 5th Conference. Geological Society, London, 613-625.
- Sweeney, J.J. and Burnham, A.K., 1990, Evaluation of a simple model of vitrinite reflectance based on chemical kinetics. *AAPG Bulletin*, 74, 1559-1570.



APPENDIX A

Sample Details, Geological Data and Apatite Compositions

A.1 Sample details

Core samples from **Irish Rockall Trough Boreholes 16/28-sb01, 83/20-sb01, 83/24-sb02** were submitted for AFTA and ZFTA by Dr John Parnell, University of Aberdeen, on behalf of the **Irish Petroleum Infrastructure Programme**. Three samples were also provided for vitrinite reflectance (VR) determinations.

Details of all AFTA samples, including sample depths, stratigraphic ages and estimates of present temperature, are summarised in Table A.1. Details of present temperature estimation are discussed in Section A.3 (below). Apatite and zircon yields are summarised and discussed in Section 1.3, together with discussion of overall AFTA and ZFTA data quality. VR data, together with sample details, are summarised in Table D.2 (Appendix D).

A.2 Stratigraphic details

Details of the stratigraphic breakdown of the preserved section in each borehole were provided by the client. The chronostratic (relative succession) assignment of each unit was converted to a chronometric (numerical) scale using Harland et al. (1989), as summarised in Table A.2. The stratigraphic age of the AFTA sample, derived from this information, is summarised in Table A.1.

Any slight errors in the estimated chronometric ages of each sample are not expected to affect the thermal history interpretation of the AFTA to any significant degree.

A.3 Present temperatures

No information was available on present-day geothermal gradients in the vicinity of the boreholes. Present-day temperatures were assigned on the basis of an assumed sea-bed temperature of 5°C and an assumed thermal gradient of 30°C/km. As the samples were



taken from shallow depths close to sea bed, any slight uncertainty in the magnitude of present-day temperatures does not significantly affect the interpretation of the data, and should not affect the conclusions of this report to any significant degree.

A.4 Grain morphologies

Apatite and zircon grains obtained from samples analysed for this study were dominated by euhedral or sub-euhedral forms. No differences or trends between samples were evident which may reflect different sediment sources.

A.5 Apatite compositions

The annealing kinetics of fission tracks in apatite are affected by chemical composition, specifically the Cl content, as explained in more detail in Appendix C. In all samples collected for this study, Cl contents were measured in all apatite grains analysed (i.e. for both fission track age determination and track length measurement), and the measured compositions in individual grains have been employed in interpreting the AFTA data, using methods outlined in Appendix C.

Chlorine contents were measured using a fully automated Jeol JXA-5A electron microprobe equipped with a computer controlled X-Y-Z stage and three computer controlled wavelength dispersive crystal spectrometers, with an accelerating voltage of 15kV and beam current of 25nA. The beam was defocussed to 20 μm diameter to avoid problems associated with apatite decomposition, which occur under a fully focussed 1 - 2 μm beam. The X-Y co-ordinates of dated grains within the grain mount were transferred from the Autoscan Fission Track Stage to a file suitable for direct input into the electron microprobe. The identification of each grain was verified optically prior to analysis. Cl count rates from the analysed grains were converted to wt% Cl by reference to those from a Durango apatite standard (Melbourne University Standard APT151), analysed at regular intervals. This approach implicitly takes into account atomic number absorption and fluorescence matrix effects, which are normally calculated explicitly when analysing for all elements. A value of 0.43 wt% Cl was used for the Durango standard, based on repeated measurements on the same single fragment using pure rock salt (NaCl) as a standard for chlorine. This approach gives essentially identical results to Cl contents determined from full compositional measurements, but has the advantage of reducing analytical time by a factor of ten or more.



Chlorine contents in individual grains are listed in the fission track age summary data sheet for the sample in Appendix B. Table B.3 contains fission track age and length data grouped into 0.1 wt% Cl intervals on the basis of chlorine contents of the grains from which the data are derived. A plot of fission track age against Cl content is also shown in the data sheet for the sample, together with a histogram of Cl contents in all individual apatite grains analysed from the sample (i.e. grains analysed for both age and length measurements).

Lower limits of detection for chlorine content have been calculated for typical analytical conditions (beam current, counting time, etc.) and are listed in Table A.3. Errors in wt% composition are given as a percentage and quoted at 1σ for chlorine determinations. A generalised summary of errors for various wt% chlorine values is presented in Table A.4.

In all of the samples analysed using AFTA, the histogram of Cl contents shows a familiar pattern, typical of the distribution of Cl contents found in detrital apatites from common sandstone samples. The majority of grains have Cl contents between 0 and 0.1 wt%, while a smaller number of grains give values up to ~0.5 wt%, close to the value found in the Durango apatite, on which our original kinetic model of fission track behaviour was based (Appendix C).

The measured distribution of compositions in each sample has been employed in interpreting the AFTA data, using methods outlined in Appendix C.

References

- Harland, W.B., Armstrong, R.L., Cox, A.V., Craig, L.E., Smith, A.G. and Smith, D.G. (1989). A geologic time scale 1989. Cambridge University Press.

Table A.1: Details of fission track samples and apatite and zircon yields - samples from Irish Rockall Trough boreholes (Geotrack Report #777)

Sample number	Depth (m)	Sample type	Stratigraphic Subdivision	Stratigraphic age (Ma)	Present temperature* ¹ (°C)	Raw weight (g)	Washed weight (g)	Apatite yield* ²	Zircon yield* ³
16/28-sb01									
GC777-1	41	core	Middle Eocene	50-39	6	30		very poor	-
GC777-9	41-80	core	Lower to Mid Eocene	55-39	7	330		excellent	excellent
GC777-2	147	core	Maastrichtian	70-65	9	80		good	good
83/20-sb01									
GC777-3	118	core	Coniacian? - Turonian	89-87	9	110		excellent	excellent
GC777-4	151-156	core	Undifferentiated Lower Cretaceous?	146-112	10	190		good	excellent
GC777-5	177-177	core	Jurassic?	208-146	10	190		very poor	-
GC777-10	177	core	Jurassic?	208-146	10	200		none	-
83/24-sb02									
GC777-6	40	core	Mid to Upper Cretaceous	130-65	6	130		none	-
GC777-7	45	core	Mid to Upper Cretaceous	130-65	6	140		very poor	-
GC777-11	45-45	core	Mid to Upper Cretaceous	130-65	6	200		none	excellent
GC777-8	71	core	Age Indeterminate Pre Mid Jurassic	200-195	7	100		very poor	-
GC777-12	71-71	core	Age Indeterminate Pre Mid Jurassic	200-195	7	150		poor	-

*¹ See Appendix A for discussion of present temperature data.

*² Yield based on quantity of mineral suitable for age determination. Excellent: >20 grains; Good: 15-19 grains; Fair: 10-14 grains; Poor: 5-9 grains; Very Poor: <5 grains.

*³ Yield based on quantity of mineral suitable for age determination. Excellent: >10 grains; Good: 7-9 grains; Fair: 3-6 grains; Poor: <3 grains.



Table A.2: Summary of stratigraphy - Irish Rockall Trough boreholes (Geotrack Report #777)

	KB elevation (mAMSL)	Ground level (m)	Stratigraphic Interval	Depth of Top TVD rKB (m)	Age of Top (Ma)
16/28-sb01	0	0	Quaternary	0	0
			<i>Unconformity</i>	14.5	2
			Middle Eocene	14.5	39
			Lower Eocene	45	50
			Upper Paleocene - Lowest Eocene	138	55
			<i>Unconformity</i>	146	60
			?Maastrichtian	146	65
			<i>Unconformity</i>	147.3	70
			post Maastrichtian sill	147.3	
			TD	148.3	70
83/20-sb01	0	0	Pliocene - Recent	0	0
			<i>Unconformity</i>	72	5
			Middle Miocene	72	10
			<i>Unconformity</i>	86	15
			Upper Campanian - Maastrichtian	86	65
			<i>Unconformity</i>	103	76
			Santonian	103	83
			Coniacian? - Turonian	107	87
			Turonian	122	89
			Albian - Cenomanian	129	90
			Undifferentiated Lower Cretaceous?	145	112
			Jurassic?	167	146
			TD	177	208
83/24-sb02	0	0	Pliocene - Recent	0	0
			<i>Unconformity</i>	20	5
			Middle Eocene	20	39
			Lower Eocene	23.5	50
			<i>Unconformity</i>	38.1	56
			Middle to Upper Cretaceous	38.1	65
			<i>Unconformity</i>	59	130
			?Middle to Upper Jurassic	59	146
			<i>Unconformity</i>	68	178
			Age Indeterminate (Pre Middle Jurassic)	68	195
			TD	72	200

All depths quoted are with respect to KB, except where otherwise stated.

**Table A.3: Lower Limits of Detection for Apatite Analyses (Geotrack Report #776)**

Element	LLD (95% c.l.)		LLD (99% c.l.)	
	(wt%)	(ppm)	(wt%)	(ppm)
Cl	0.01	126	0.02	182

Table A.4 Per cent errors in chlorine content (Geotrack Report #776)

Chlorine content (wt%)	Error (%)
0.01	9.3
0.02	8.7
0.05	7.3
0.10	6.1
0.20	4.7
0.50	3.2
1.00	2.3
1.50	1.9
2.00	1.7
2.50	1.5
3.00	1.4

Errors quoted are at 1σ . See Appendix A for more details.



APPENDIX B

Sample Preparation, Analytical Details and Data Presentation

B.1 Sample Preparation

Core and outcrop samples are crushed in a jaw crusher and then ground to sand grade in a rotary disc mill. Cuttings samples are washed and dried before grinding to sand grade. The ground material is then washed to remove dust, dried and processed by conventional heavy liquid and magnetic separation techniques to recover heavy minerals.

Apatite grains are mounted in epoxy resin on glass slides, polished and etched for 20 sec in 5M HNO₃ at 20°C to reveal the fossil fission tracks. Zircon grains were embedded in FEP Teflon between heated microscope slides on a hot plate, then polished and etched in a molten KOH:NaOH eutectic mixture at ~220°C (Gleadow et al., 1976), for an appropriate time (typically between 10 and 100 hours) to reveal properly etched fission tracks in a high proportion of the grains present.

After etching, all mounts are cut down to 1.5 X 1 cm, and cleaned in detergent, alcohol and distilled water. The mounts are then sealed in intimate contact with low-uranium muscovite detectors within heat-shrink plastic film. Each batch of mounts is stacked between two pieces of uranium standard glass, which has been prepared in similar fashion. The stack is then inserted into an aluminium can for irradiation.

After irradiation, the mica detectors are removed from the grain mounts and standard glasses and etched in hydrofluoric acid to reveal the fission tracks produced by induced fission of ²³⁵U in the apatite and standard glass.

B.2 Analytical Details

Fission track ages

Fission track ages are determined by the external detector method or EDM (Gleadow, 1981). The EDM has the advantage of allowing fission track ages to be determined on single grains. In apatite, tracks are counted in 20 grains from each mount wherever



possible. In zircon, 10 grains are normally analysed. In those samples where the desired number is not present, all available grains are counted, the actual number depending on the availability of suitably etched and oriented grains. Only grains oriented with surfaces parallel to the crystallographic c-axis are analysed. Such grains can be identified on the basis of the etching characteristics, as well as from morphological evidence in euhedral grains. The grain mount is scanned sequentially, and for apatite the first 20 suitably oriented grains identified are analysed, while for zircon the first 10 suitable grains are used.

Fission track ages are calculated using the standard fission track age equation using the zeta calibration method (equation five of Hurford and Green, 1983), viz:

$$\text{F.T. AGE} = \frac{1}{\lambda_D} \ln \left[1 + \left(\frac{\zeta \lambda_D \rho_s g \rho_D}{\rho_i} \right) \right] \quad \text{B.1}$$

where: λ_D = Total decay constant of ^{238}U ($= 1.55125 \times 10^{-10}$)
 ζ = Zeta calibration factor
 ρ_s = Spontaneous track density
 ρ_i = Induced track density
 ρ_D = Track density from uranium standard glass
 g = A geometry factor ($= 0.5$)

Tracks are counted within an eyepiece graticule divided into 100 grid squares. In each grain, the number of spontaneous tracks (N_s) within a certain number of grid squares (N_a) is recorded. The number of induced tracks (N_i) in the corresponding location within the mica external detector is then counted. Spontaneous and induced track densities (ρ_s and ρ_i , respectively) are calculated by dividing the track counts by the total area counted, given by the product of N_a and the area of each grid square (determined by calibration against a ruled stage graticule or diffraction grating). Fission track ages may be calculated by substituting track counts (N_s and N_i) for track densities (ρ_s and ρ_i) in equation B.1, since the areas cancel in the ratio.

Translation between apatite grains in the grain mount and external detector locations corresponding to each grain is carried out using Autoscan™ microcomputer-controlled automatic stages (Smith and Leigh Jones, 1985). This system allows repeated movement between grain and detector, and all grain locations are stored for later reference if required.

Neutron irradiations are carried out in a well-thermalised flux (X-7 facility; Cd ratio for Au ~98) in the Australian Atomic Energy Commission's HIFAR research reactor. Total



neutron fluence is monitored by counting tracks in mica external detectors attached to two pieces of Corning Glass Works standard glass (CN5 containing ~11 ppm uranium for apatite, and U3 containing ~55 ppm uranium for zircon) included in the irradiation canister at each end of the sample stack. In determining track densities in external detectors irradiated adjacent to uranium standard glasses, 25 fields are normally counted in each detector. The total track count (N_D) is divided by the total area counted to obtain the track density (ρ_D). The positions of the counted fields are arranged in a 5 x 5 grid covering the whole area of the detector. For typical track densities of between $\sim 5 \times 10^5$ and 5×10^6 , this is a convenient arrangement to sample across the detector while gathering sufficient counts to achieve a precision of $\sim \pm 2\%$ in a reasonable time.

A small flux gradient is often present in the irradiation facility over the length of the sample package. If a detectable gradient is present, the track count in the external detector adjacent to each standard glass is converted to a track density ρ_D and a value for each mount in the stack is calculated by linear interpolation. When no detectable gradient is present, the track counts in the two external detectors are pooled to give a single value of ρ_D which is used to calculate fission track ages for each sample.

A Zeta calibration factor (ζ) has been determined empirically for each observer by analysing a set of carefully chosen age standards with independently known K-Ar ages, following the methods outlined by Hurford and Green (1983) and Green (1985).

All track counting is carried out using Zeiss^(R) Axioplan microscopes, with an overall linear magnification of 1068 x using dry objectives.

For further details and background information on practical aspects of fission track age determination, see e.g. Fleischer, Price and Walker (1975), Naeser (1979) and Hurford (1986).

Track length measurements

For track length studies in apatite, the full lengths of "confined" fission tracks are measured. Confined tracks are those which do not intersect the polished surface but have been etched from other tracks or fractures, so that the whole length of the track is etched. Confined track lengths are measured using a digitising tablet connected to a microcomputer, superimposed on the microscope field of view via a projection tube. With this system, calibrated against a stage graticule ruled in 2 μm divisions, individual tracks can be measured to a precision of $\pm 0.2 \mu\text{m}$. Tracks are measured only in prismatic grains, characterised by sharp polishing scratches with well-etched tracks of narrow cone angle in all orientations, because of the anisotropy of annealing of fission tracks in apatite (as discussed by Green et al. 1986). Tracks are also measured



following the recommendations of Laslett et al. (1982), the most important of which is that only horizontal tracks should be measured. One hundred tracks are measured whenever possible. In apatite samples with low track density, or in those samples in which only a small number of apatite grains are obtained, fewer confined tracks may be available. In such cases, the whole mount is scanned to measure as many confined tracks as possible.

Integrated fission track age and length measurement

Fission track age determination and length measurement are now made in a single pass of the grain mount, in an integrated approach. The location of each grain in which tracks are either counted or measured is recorded for future reference. Thus, track length measurements can be tied to age determination in individual grains. As a routine procedure we do not measure the age of every grain in which lengths are determined, as this would be much too time-consuming. Likewise we do not only measure ages in grain in which lengths are measured, as this would bias the age data against low track density grains. Nevertheless, the ability to determine the fission track age of certain grains from which length data originate can be a particularly useful aid to interpretation in some cases. Grain location data are not provided in this report, but are available on request.

B.3 Data Presentation

Fission track age data

Data sheets summarising the fission track age data for both apatite and zircon, including full details of fission track age data for individual grains in each sample, together with the primary counting results and statistical data, are given in the following pages. Individual grain fission track ages are calculated from the ratio of spontaneous to induced fission track counts for each grain using equation B.1, and errors in the single grain ages are calculated using Poissonian statistics, as explained in more detail by Galbraith (1981) and Green (1981). All errors are quoted as $\pm 1\sigma$ throughout this report, unless otherwise stated.

The variability of fission track ages between individual apatite grains within each sample can be assessed using a chi-squared (χ^2) statistic (Galbraith, 1981), the results of which are summarised for each sample in the data sheets. If all the grains counted belong to a single age population, the probability of obtaining the observed χ^2 value, for



ν degrees of freedom (where ν = number of crystals -1), is listed in the data sheets as $P(\chi^2)$ or $P(\text{chi squared})$.

A $P(\chi^2)$ value greater than 5% can be taken as evidence that all grains are consistent with a single population of fission track age. In this case, the best estimate of the fission track age of the sample is given by the "pooled age", calculated from the ratio of the total spontaneous and induced track counts in all grains analysed. Errors for the pooled age are calculated using the "conventional" technique outlined by Green (1981), based on the total number of tracks counted for each track density measurement (see also Galbraith, 1981).

A $P(\chi^2)$ value of less than 5% denotes a significant spread of single grain ages, suggesting real differences exist between the fission track ages of individual apatite grains. A significant spread in grain ages can result either from inheritance of detrital grains from mixed source areas (in sedimentary rocks), or from differential annealing in apatite grains of different composition, within a narrow range of temperature.

Calculation of the pooled age inherently assumes that only a single population of ages is present, and is thus not appropriate to samples containing a significant spread of fission track ages. In such cases, Galbraith has recently devised a means of estimating the modal age of a distribution of single grain fission track ages which is referred to as the "central age". Calculation of the central age assumes that all single grain ages belong to a Normal distribution of ages, with a standard deviation (σ) known as the "age dispersion". An iterative algorithm (Galbraith and Laslett, 1993) is used to provide estimates of the central age with its associated error, and the age dispersion, which are all quoted in the data sheets. Note that this treatment replaces use of the "mean age", which has been used in the past for those samples in which $P(\chi^2) < 5\%$. For samples in which $P(\chi^2) > 5\%$, the central age and the pooled age should be equal, and the age dispersion should be less than $\sim 10\%$.

Table B.1 summarises the fission track age data in apatite from each sample analysed, while Table B.3 summarises similar data for zircon in each sample analysed.

Construction of radial plots of single grain age data

Single grain age data are best represented in the form of radial plot diagrams (Galbraith, 1988, 1990). As illustrated in Figure B.1, these plots display the variation of individual grain ages in a plot of y against x , where:

$$y = (z_j - z_0) / \sigma_i \qquad x = 1 / \sigma_j \qquad \text{B.2}$$



and; z_j = Fission track age of grain j
 z_o = A reference age
 σ_j = Error in age for grain j

In this plot, all points on a straight line from the origin define a single value of fission track age, and, at any point, the value of x is a measure of the precision of each individual grain age. Therefore, precise individual grain ages fall to the right of the plot (small error, high x), which is useful, for example, in enabling precise, young grains to be identified. The age scale is shown radially around the perimeter of the plot (in Ma). If all grains belong to a single age population, all data should scatter between $y = +2$ and $y = -2$, equivalent to scatter within $\pm 2\sigma$. Scatter outside these boundaries shows a significant spread of individual grain ages, as also reflected in the values of $P(\chi^2)$ and age dispersion.

In detail, rather than using the fission track age for each grain as in equation B.2, we use:

$$z_j = \frac{N_{sj}}{N_{ij}} \quad s_j = \{1/N_{sj} + 1/N_{ij}\} \quad B.3$$

as we are interested in displaying the scatter within the data from each sample in comparison with that allowed by the Poissonian uncertainty in track counts, without the additional terms which are involved in determination of the fission track age (ρ_D , ζ , etc).

Zero ages cannot be displayed in such a plot. This can be achieved using a modified plot, (Galbraith, 1990) with:

$$z_j = \arcsin \sqrt{\left\{ \frac{N_{sj} + 3/8}{N_{sj} + N_{ij} + 3/4} \right\}} \quad \sigma_j = \frac{1}{2} \sqrt{\left\{ \frac{1}{N_{sj} + N_{ij}} \right\}} \quad B.4$$

Note that the numerical terms in the equation for z_j are standard terms, introduced for statistical reasons. Using this arc-sin transformation, zero ages plot on a diagonal line which slopes from upper left to lower right. Note that this line does not go through the origin. Figure B.2 illustrates this difference between conventional and arc-sin radial plots, and also provides a simple guide to the structure of radial plots.

Use of arc-sin radial plots is particularly useful in assessing the relative importance of zero ages. For instance, grains with $N_s = 0$, $N_i = 1$ are compatible with ages up to ~900 Ma (at the 95% confidence level), whereas grains with $N_s = 0$, $N_i = 50$ are only compatible with ages up to ~14 Ma. The two data would readily be distinguishable on



the radial plot as the 0,50 datum would plot well to the right (high x) compared to the 0,1 datum.

In this report the value of z corresponding to the stratigraphic age of each sample (or the midpoint of the range where appropriate) is adopted as the reference value, z_0 . This allows rapid assessment of the fission track age of individual grains in relation to the stratigraphic age, which is a key component in the interpretation of AFTA data, as explained in more detail in Appendix C.

Note that the x axis of the radial plot is normally not labelled, as this would obscure the age scale around the plot. In general labelling is not considered necessary, as we are concerned only with relative variation within the data, rather than absolute values of precision.

Radial plots of the single grain age data in apatite and zircon from each sample analysed in this report are shown on the fission track age data summary sheets at the end of this Appendix. Use of radial plots to provide thermal history information is explained in Appendix C and Figure C.7.

Track length data

Distributions of confined track lengths in apatite from each sample are shown as simple histograms on the fission track age data summary sheets at the end of this Appendix. For every track length measurement, the length is recorded to the nearest 0.1 μm , but the measurements have been grouped into 1 μm intervals for construction of these histograms. Each distribution has been normalised to 100 tracks for each sample to facilitate comparison. A summary of the length distribution in each sample is presented in Table B.2, which also shows the mean track length in each sample and its associated error, the standard deviation of each distribution and the number of tracks (N) measured in each sample. The angle which each confined track makes with the crystallographic c -axis is also routinely recorded, as is the width of each fracture within which tracks are revealed. These data are not provided in this report, but can be supplied on request. Track length data is not routinely collected in zircon.

Breakdown of data into compositional groups

In Table B.4, AFTA data are grouped into compositional intervals of 0.1 wt% Cl width. Parameters for each interval represent the data from all grains with Cl contents within each interval. Also shown are the parameters for each compositional interval predicted from the Default Thermal History (see Section 2.1). These data form the basis of interpretation of the AFTA data, which takes full account of the influence of Cl content



on annealing kinetics, as described in Appendix C. Distributions of Cl contents in all apatites analysed from each sample (i.e. for both age and length determinations) are shown on the fission track age data summary sheets at the end of this Appendix.

Plots of fission track age against Cl content for individual apatite grains

Fission track ages of single apatite grains within individual samples are plotted against the Cl content of each grain on the fission track age data summary sheets at the end of this Appendix. These plots are useful in assessing the degree of annealing, as expressed by the fission track age data. For example, if grains with a range of Cl contents from zero to some upper limit all give similar fission track ages which are significantly less than the stratigraphic age, then grains with these compositions must have been totally annealed. Alternatively, if fission track age falls rapidly with decreasing Cl content, the sample displays a high degree of partial annealing.

B.4 A note on terminology

Note that throughout this report, the term "fission track age" is understood to denote the parameter calculated from the fission track age equation, using the observed spontaneous and induced track counts (either pooled for all grains or for individual grains). The resulting number (with units of Ma) should not be taken as possessing any significance in terms of events taking place at the time indicated by the measured fission track age, but should rather be regarded as a measure of the integrated thermal history of the sample, and should be interpreted in that light using the principles outlined in Appendix C. Use of the term "apparent age" is not considered to be useful in this regard, as almost every fission track age should be regarded as an apparent age, in the classic sense, and repeated use becomes cumbersome.



References

- Fleischer, R.L., Price, P.B., and Walker, R.M. (1975) Nuclear tracks in solids, University of California Press, Berkeley.
- Galbraith, R.F. (1981) On statistical models for fission-track counts. *Mathematical Geology*, 13, 471-488.
- Galbraith, R.F. (1988) Graphical display of estimates having differing standard errors. *Technometrics*, 30, 271-281.
- Galbraith, R.F. (1990) The radial plot: graphical assessment of spread in ages. *Nuclear tracks*, 17, 207-214.
- Galbraith R.F. & Laslett G.M. (1993) Statistical methods for mixed fission track ages. *Nuclear Tracks* 21, 459-470.
- Gleadow, A.J.W. (1981) Fission track dating methods; what are the real alternatives? *Nuclear Tracks*, 5, 3-14.
- Green, P.F. (1981) A new look at statistics in fission track dating. *Nuclear Tracks* 5, 77-86.
- Green, P.F. (1985) A comparison of zeta calibration baselines in zircon, sphene and apatite. *Chem. Geol. (Isot. Geol. Sect.)*, 58, 1-22.
- Green, P.F., Duddy, I.R., Gleadow, A.J.W., Tingate, P.R. and Laslett, G.M. (1986) Thermal annealing of fission tracks in apatite 1. A qualitative description. *Chem. Geol. (Isot. Geosci. Sect.)*, 59, 237-253.
- Hurford, A.J. (1986) Application of the fission track dating method to young sediments: Principles, methodology and Examples. In: Hurford, A.J., Jäger, E. and Ten Cate, J.A.M. (eds), Dating young sediments, CCOP Technical Publication 16, CCOP Technical Secretariat, Bangkok, Thailand.
- Hurford, A.J. and Green, P.F. (1982) A user's guide to fission track dating calibration. *Earth. Planet. Sci Lett.* 59, 343-354.
- Hurford, A.J. and Green, P.F. (1983) The zeta age calibration of fission track dating. *Isotope Geoscience* 1, 285-317.
- Laslett, G.M., Kendall, W.S., Gleadow, A.J.W. and Duddy, I.R. (1982) Bias in measurement of fission track length distributions. *Nuclear Tracks*, 6, 79-85.
- Naeser, C.W. (1979) Fission track dating and geologic annealing of fission tracks. In: Jäger, E. and Hunziker, J.C. (eds), Lectures in Isotope Geology, Springer Verlag, Berlin.
- Smith, M.J. and Leigh-Jones, P. (1985) An automated microscope scanning stage for fission-track dating. *Nuclear Tracks*, 10, 395-400.

**Table B.1: Apatite fission track analytical results - samples from Irish Rockall Trough boreholes (Geotrack Report #777)**

Sample number	Number of grains	ρ_D (Nd) x10 ⁶ /cm ²	ρ_s (Ns) x10 ⁶ /cm ²	ρ_i (Ni) x10 ⁶ /cm ²	Uranium content (ppm)	P(χ^2) (%)	Age dispersion (%)	Fission track age (Ma)
16/28-sb01								
GC777-1	2	1.213 (2004)	0.101 (4)	0.404 (16)	4	14	17	58.2 ± 32.6
GC777-2	17	1.221 (2004)	1.633 (445)	2.351 (640)	22	51	6	161.5 ± 10.8
GC777-9	20	1.139 (1865)	1.134 (366)	1.307 (422)	13	<1	34	187.7 ± 14.2 180.6 ± 21.1*
83/20-sb01								
GC777-3	20	1.239 (2004)	0.823 (316)	1.120 (430)	10	<1	37	173.1 ± 13.5 142.2 ± 18.5*
GC777-4	18	1.256 (2004)	1.194 (659)	1.132 (625)	10	<1	72	250.4 ± 15.3 216.6 ± 41.6*
GC777-5	2	1.274 (2004)	0.162 (6)	0.215 (8)	2	40	<1	182.0 ± 98.5
GC777-10		No apatite						
83/24-sb02								
GC777-6		No apatite						
GC777-7	2	1.291 (2004)	0.678 (64)	1.309 (124)	12	11	12	127.6 ± 19.9
GC777-8	4	1.309 (2004)	0.261 (12)	0.566 (26)	5	92	<1	115.4 ± 40.4
GC777-11		No apatite						
GC777-12	6	1.145 (1865)	2.992 (209)	4.438 (310)	44	33	<1	147.1 ± 13.7

ρ_s = spontaneous track density; ρ_i = induced track density; ρ_D = track density in glass standard external detector. Brackets show number of tracks counted. ρ_D and ρ_i measured in mica external detectors; ρ_s measured in internal surfaces.

*Central age, used where sample contains a significant spread of single grain ages ($P(\chi^2) < 5\%$). Errors quoted at 1σ .

Ages calculated using dosimeter glass CN5, with a zeta of 385.5 ± 4.3 (Analyst: P. F. Green) for samples; 1 - 12



Table B.2: Length distribution summary data - samples from Irish Rockall Trough boreholes (Geotrack Report #777)

Sample number	Mean track length (μm)	Standard deviation (μm)	Number of tracks (N)	Number of tracks in Length Intervals (μm)																			
				1	2	3	4	5	6	7	8	9	10	11	12	13	14	15	16	17	18	19	20
16/28-sb01																							
GC777-1	12.16 ± 0.11	0.16	2	-	-	-	-	-	-	-	-	-	-	-	-	2	-	-	-	-	-	-	-
GC777-2	13.31 ± 0.16	1.06	43	-	-	-	-	-	-	-	-	-	-	1	3	11	16	10	2	-	-	-	-
GC777-9	13.68 ± 0.17	1.51	82	-	-	-	-	-	-	-	1	-	1	2	5	11	24	24	12	2	-	-	-
83/20-sb01																							
GC777-3	13.11 ± 0.25	1.21	23	-	-	-	-	-	-	-	-	-	-	1	2	7	7	5	1	-	-	-	-
GC777-4	12.59 ± 0.30	2.23	57	-	-	-	-	1	-	2	-	1	1	5	6	10	16	12	3	-	-	-	-
GC777-5	13.84	-	1	-	-	-	-	-	-	-	-	-	-	-	-	-	1	-	-	-	-	-	-
GC777-10	No apatite	-	-	-	-	-	-	-	-	-	-	-	-	-	-	-	-	-	-	-	-	-	-
83/24-sb02																							
GC777-6	No apatite	-	-	-	-	-	-	-	-	-	-	-	-	-	-	-	-	-	-	-	-	-	-
GC777-7	13.44 ± 0.36	1.01	8	-	-	-	-	-	-	-	-	-	-	-	1	2	4	-	1	-	-	-	-
GC777-8	12.80 ± 0.99	1.40	2	-	-	-	-	-	-	-	-	-	-	-	1	-	1	-	-	-	-	-	-
GC777-11	No apatite	-	-	-	-	-	-	-	-	-	-	-	-	-	-	-	-	-	-	-	-	-	-
GC777-12	12.76 ± 0.29	1.16	16	-	-	-	-	-	-	-	-	-	-	2	2	5	6	-	1	-	-	-	-

Track length measurements by: P. F. Green for samples;

1 - 12

Table B.3: AFTA Data in Compositional Groups - (Geotrack Report #777)

Cl	Default fission track age* (Ma)	Measured fission track age (Ma)	Error in age (Ma)	P (c2)	Number of grains	Default fission track length* (µm)	Mean track length (µm)	Error in length (µm)	Std deviation (µm)	Number of lengths	Number of grains	Number of tracks in length interval																			
												1	2	3	4	5	6	7	8	9	10	11	12	13	14	15	16	17	18	19	20
Wt %	(Ma)	(Ma)	(Ma)			(µm)	(µm)	(µm)	(µm)			(µm)																			
16/28-sb01																															
†777-1	51.2	58.2	32.5	14.0	2	15.0	12.2	0.1	0.2	2	1	0	0	0	0	0	0	0	0	0	0	0	0	2	0	0	0	0	0	0	0
0.0-0.1	-	-	-	-	-	-	-	-	-	-	-	-	-	-	-	-	-	-	-	-	-	-	-	-	-	-	-	-	-	-	-
0.1-0.2	51.0	92.8	55.0	100.0	1	15.0	12.2	0.1	0.2	2	1	0	0	0	0	0	0	0	0	0	0	0	0	2	0	0	0	0	0	0	0
0.2-0.3	-	-	-	-	-	-	-	-	-	-	-	-	-	-	-	-	-	-	-	-	-	-	-	-	-	-	-	-	-	-	-
0.3-0.4	-	-	-	-	-	-	-	-	-	-	-	-	-	-	-	-	-	-	-	-	-	-	-	-	-	-	-	-	-	-	-
0.4-0.5	-	-	-	-	-	-	-	-	-	-	-	-	-	-	-	-	-	-	-	-	-	-	-	-	-	-	-	-	-	-	-
0.5-0.6	-	-	-	-	-	-	-	-	-	-	-	-	-	-	-	-	-	-	-	-	-	-	-	-	-	-	-	-	-	-	-
0.6-0.7	51.4	0.0	0.0	110.0	1	15.2	0.0	0.0	0.0	0	0	0	0	0	0	0	0	0	0	0	0	0	0	0	0	0	0	0	0	0	0
†777-2	70.8	160.7	10.5	49.0	17	14.9	13.3	0.2	1.1	43	12	0	0	0	0	0	0	0	0	0	0	1	3	11	16	10	2	0	0	0	0
0.0-0.1	70.7	154.8	14.5	33.0	10	14.9	13.1	0.2	1.0	22	7	0	0	0	0	0	0	0	0	0	0	1	2	6	9	3	1	0	0	0	0
0.1-0.2	70.9	170.8	15.5	46.0	5	14.9	13.5	0.2	1.1	21	5	0	0	0	0	0	0	0	0	0	0	1	5	7	7	1	0	0	0	0	0
0.2-0.3	-	-	-	-	-	-	-	-	-	-	-	-	-	-	-	-	-	-	-	-	-	-	-	-	-	-	-	-	-	-	-
0.3-0.4	71.1	123.5	36.1	100.0	1	15.0	0.0	0.0	0.0	0	0	0	0	0	0	0	0	0	0	0	0	0	0	0	0	0	0	0	0	0	0
0.4-0.5	71.3	116.7	142.9	100.0	1	15.0	0.0	0.0	0.0	0	0	0	0	0	0	0	0	0	0	0	0	0	0	0	0	0	0	0	0	0	0
†777-9	50.9	180.6	20.6	0.0	20	15.0	13.7	0.2	1.5	82	33	0	0	0	0	0	0	1	0	1	2	5	11	24	24	12	2	0	0	0	0
0.0-0.1	50.9	170.4	18.1	4.0	19	15.0	13.6	0.2	1.5	71	28	0	0	0	0	0	0	1	0	1	2	5	11	21	19	10	1	0	0	0	0
0.1-0.2	51.0	450.4	136.9	100.0	1	15.0	14.1	0.3	0.9	8	4	0	0	0	0	0	0	0	0	0	0	0	0	3	4	1	0	0	0	0	0
0.2-0.3	-	-	-	-	-	-	-	-	-	-	-	-	-	-	-	-	-	-	-	-	-	-	-	-	-	-	-	-	-	-	-
0.3-0.4	51.2	0.0	0.0	0.0	0	15.1	15.2	0.6	1.1	3	1	0	0	0	0	0	0	0	0	0	0	0	0	0	0	1	1	1	0	0	0
†777-1 & 9	50.9	171.2	19.8	0.0	22	15.0	13.6	0.2	1.5	84	34	0	0	0	0	0	0	1	0	1	2	5	13	24	24	12	2	0	0	0	0
0.0-0.1	50.9	170.4	18.1	4.0	19	15.0	13.6	0.2	1.5	71	28	0	0	0	0	0	0	1	0	1	2	5	11	21	19	10	1	0	0	0	0
0.1-0.2	51.0	226.7	123.7	1.0	2	15.0	13.7	0.4	1.1	10	5	0	0	0	0	0	0	0	0	0	0	0	2	3	4	1	0	0	0	0	0
0.2-0.3	-	-	-	-	-	-	-	-	-	-	-	-	-	-	-	-	-	-	-	-	-	-	-	-	-	-	-	-	-	-	-
0.3-0.4	51.2	0.0	0.0	0.0	0	15.1	15.2	0.6	1.1	3	1	0	0	0	0	0	0	0	0	0	0	0	0	0	0	1	1	1	0	0	0
0.4-0.5	-	-	-	-	-	-	-	-	-	-	-	-	-	-	-	-	-	-	-	-	-	-	-	-	-	-	-	-	-	-	-
0.5-0.6	-	-	-	-	-	-	-	-	-	-	-	-	-	-	-	-	-	-	-	-	-	-	-	-	-	-	-	-	-	-	-
0.6-0.7	51.4	0.0	0.0	110.0	1	15.2	0.0	0.0	0.0	0	0	0	0	0	0	0	0	0	0	0	0	0	0	0	0	0	0	0	0	0	0

* Fission Track Age and Mean Track Length predicted from the Default Thermal History (i.e. if the sample has not been hotter in the past)

† Combined data for all compositional groups

Table B.3: Continued - (Geotrack Report #777)

Cl	Default fission track age*	Measured fission track age	Error in age	P (c2)	Number of grains	Default fission track length*	Mean track length	Error in length	Std deviation	Number of lengths	Number of grains	Number of tracks in length interval																				
												1	2	3	4	5	6	7	8	9	10	11	12	13	14	15	16	17	18	19	20	
Wt %	(Ma)	(Ma)	(Ma)			(µm)	(µm)	(µm)	(µm)			(µm)																				
83/20-sb01																																
†777-3	91.4	141.7	18.1	0.0	20	15.0	13.1	0.3	1.2	23	10	0	0	0	0	0	0	0	0	0	0	1	2	7	7	5	1	0	0	0	0	
0.0-0.1	91.1	153.7	26.3	0.0	9	14.9	13.2	0.2	0.9	18	7	0	0	0	0	0	0	0	0	0	0	0	1	6	7	4	0	0	0	0	0	
0.1-0.2	91.3	160.0	33.8	57.0	4	15.0	12.1	0.9	1.2	2	1	0	0	0	0	0	0	0	0	0	0	0	1	1	0	0	0	0	0	0	0	
0.2-0.3	91.5	183.1	92.4	70.0	2	15.0	12.5	2.1	2.9	2	1	0	0	0	0	0	0	0	0	0	0	1	0	0	0	1	0	0	0	0	0	
0.3-0.4	91.6	42.0	26.3	43.0	2	15.0	0.0	0.0	0.0	0	0	0	0	0	0	0	0	0	0	0	0	0	0	0	0	0	0	0	0	0	0	
0.4-0.5	91.8	104.2	37.8	37.0	2	15.0	0.0	0.0	0.0	0	0	0	0	0	0	0	0	0	0	0	0	0	0	0	0	0	0	0	0	0	0	
0.5-0.6	-	-	-	-	-	-	-	-	-	-	-	-	-	-	-	-	-	-	-	-	-	-	-	-	-	-	-	-	-	-	-	
0.6-0.7	-	-	-	-	-	-	-	-	-	-	-	-	-	-	-	-	-	-	-	-	-	-	-	-	-	-	-	-	-	-	-	
0.7-0.8	-	-	-	-	-	-	-	-	-	-	-	-	-	-	-	-	-	-	-	-	-	-	-	-	-	-	-	-	-	-	-	
0.8-0.9	92.4	135.0	84.7	100.0	1	15.1	15.2	0.0	0.0	1	1	0	0	0	0	0	0	0	0	0	0	0	0	0	0	0	0	1	0	0	0	0
†777-4	121.0	215.9	41.1	0.0	18	14.9	12.6	0.3	2.2	57	13	0	0	0	0	1	0	2	0	1	1	5	6	10	16	12	3	0	0	0	0	
0.0-0.1	121.0	194.9	40.6	0.0	16	14.9	12.8	0.3	2.1	37	11	0	0	0	0	0	2	0	0	1	4	3	4	11	10	2	0	0	0	0	0	
0.1-0.2	121.2	463.4	72.9	100.0	1	14.9	12.6	0.3	0.9	8	1	0	0	0	0	0	0	0	0	0	0	0	2	3	3	0	0	0	0	0	0	
0.2-0.3	-	-	-	-	-	-	-	-	-	-	-	-	-	-	-	-	-	-	-	-	-	-	-	-	-	-	-	-	-	-	-	
0.3-0.4	121.7	373.1	51.8	100.0	1	15.0	12.1	0.9	3.1	12	1	0	0	0	0	1	0	0	0	1	0	1	1	3	2	2	1	0	0	0	0	0
†777-5	163.0	181.6	98.1	39.0	2	14.8	13.8	0.0	0.0	1	1	0	0	0	0	0	0	0	0	0	0	0	0	0	1	0	0	0	0	0	0	
0.0-0.1	-	-	-	-	-	-	-	-	-	-	-	-	-	-	-	-	-	-	-	-	-	-	-	-	-	-	-	-	-	-	-	
0.1-0.2	161.1	0.0	0.0	0.0	0	14.8	13.8	0.0	0.0	1	1	0	0	0	0	0	0	0	0	0	0	0	0	0	1	0	0	0	0	0	0	
0.2-0.3	-	-	-	-	-	-	-	-	-	-	-	-	-	-	-	-	-	-	-	-	-	-	-	-	-	-	-	-	-	-	-	
0.3-0.4	-	-	-	-	-	-	-	-	-	-	-	-	-	-	-	-	-	-	-	-	-	-	-	-	-	-	-	-	-	-	-	
0.4-0.5	-	-	-	-	-	-	-	-	-	-	-	-	-	-	-	-	-	-	-	-	-	-	-	-	-	-	-	-	-	-	-	
0.5-0.6	-	-	-	-	-	-	-	-	-	-	-	-	-	-	-	-	-	-	-	-	-	-	-	-	-	-	-	-	-	-	-	
0.6-0.7	-	-	-	-	-	-	-	-	-	-	-	-	-	-	-	-	-	-	-	-	-	-	-	-	-	-	-	-	-	-	-	
0.7-0.8	162.9	241.0	152.5	100.0	1	15.0	0.0	0.0	0.0	0	0	0	0	0	0	0	0	0	0	0	0	0	0	0	0	0	0	0	0	0	0	
0.8-0.9	-	-	-	-	-	-	-	-	-	-	-	-	-	-	-	-	-	-	-	-	-	-	-	-	-	-	-	-	-	-	-	
0.9-1.0	163.2	81.3	93.9	100.0	1	15.0	0.0	0.0	0.0	0	0	0	0	0	0	0	0	0	0	0	0	0	0	0	0	0	0	0	0	0	0	

* Fission Track Age and Mean Track Length predicted from the Default Thermal History (i.e. if the sample has not been hotter in the past)

† Combined data for all compositional groups

Table B.3: Continued - (Geotrack Report #777)

Cl	Default fission track age*	Measured fission track age	Error in age	P (c2)	Number of grains	Default fission track length*	Mean track length	Error in length	Std deviation	Number of lengths	Number of grains	Number of tracks in length interval																				
												1	2	3	4	5	6	7	8	9	10	11	12	13	14	15	16	17	18	19	20	
Wt %	(Ma)	(Ma)	(Ma)			(μm)	(μm)	(μm)	(μm)			(μm)																				
83/24-sb02																																
†777-7 0.0-0.1	111.3 111.3	127.2 127.2	19.8 19.8	10.0 10.0	2 2	14.9 14.9	13.4 13.4	0.4 0.4	1.0 1.0	8 8	2 2	0 0	0 0	0 0	0 0	0 0	0 0	0 0	0 0	0 0	0 0	0 0	1 1	2 2	4 4	0 0	1 1	0 0	0 0	0 0	0 0	
†777-8 0.0-0.1	160.4 160.0	115.4 109.4	40.3 49.6	92.0 55.0	4 2	14.8 14.8	12.8 12.8	1.0 1.0	1.4 1.4	2 2	1 1	0 0	0 0	0 0	0 0	0 0	0 0	0 0	0 0	0 0	0 0	0 0	1 1	0 0	1 1	0 0	0 0	0 0	0 0	0 0	0 0	
0.1-0.2	160.5	149.6	109.3	100.0	1	14.8	0.0	0.0	0.0	0	0	0	0	0	0	0	0	0	0	0	0	0	0	0	0	0	0	0	0	0	0	0
0.2-0.3	-	-	-	-	-	-	-	-	-	-	-	-	-	-	-	-	-	-	-	-	-	-	-	-	-	-	-	-	-	-	-	
0.3-0.4	161.2	100.1	83.8	100.0	1	14.9	0.0	0.0	0.0	0	0	0	0	0	0	0	0	0	0	0	0	0	0	0	0	0	0	0	0	0	0	0
†777-12 0.0-0.1	196.9 196.3	147.1 139.6	13.6 14.0	33.0 21.0	6 3	14.9 14.8	12.8 12.8	0.3 0.3	1.2 1.2	16 15	4 3	0 0	0 0	0 0	0 0	0 0	0 0	0 0	0 0	0 0	0 0	2 2	2 2	5 4	6 6	0 0	1 1	0 0	0 0	0 0	0 0	
0.1-0.2	196.8	217.0	62.8	56.0	2	14.9	12.4	0.0	0.0	1	1	0	0	0	0	0	0	0	0	0	0	0	0	1	0	0	0	0	0	0	0	0
0.2-0.3	-	-	-	-	-	-	-	-	-	-	-	-	-	-	-	-	-	-	-	-	-	-	-	-	-	-	-	-	-	-	-	
0.3-0.4	-	-	-	-	-	-	-	-	-	-	-	-	-	-	-	-	-	-	-	-	-	-	-	-	-	-	-	-	-	-	-	
0.4-0.5	-	-	-	-	-	-	-	-	-	-	-	-	-	-	-	-	-	-	-	-	-	-	-	-	-	-	-	-	-	-	-	
0.5-0.6	-	-	-	-	-	-	-	-	-	-	-	-	-	-	-	-	-	-	-	-	-	-	-	-	-	-	-	-	-	-	-	
0.6-0.7	-	-	-	-	-	-	-	-	-	-	-	-	-	-	-	-	-	-	-	-	-	-	-	-	-	-	-	-	-	-	-	
0.7-0.8	-	-	-	-	-	-	-	-	-	-	-	-	-	-	-	-	-	-	-	-	-	-	-	-	-	-	-	-	-	-	-	
0.8-0.9	199.3	166.6	61.5	100.0	1	15.1	0.0	0.0	0.0	0	0	0	0	0	0	0	0	0	0	0	0	0	0	0	0	0	0	0	0	0	0	0
†777-8 & 12 0.0-0.1	196.9 196.3	145.3 138.1	13.0 13.5	67.0 44.0	10 5	14.9 14.8	12.8 12.8	0.3 0.3	1.1 1.2	18 17	5 4	0 0	0 0	0 0	0 0	0 0	0 0	0 0	0 0	0 0	0 0	2 2	3 3	5 4	7 7	0 0	1 1	0 0	0 0	0 0	0 0	
0.1-0.2	196.8	209.4	56.7	79.0	3	14.9	12.4	0.0	0.0	1	1	0	0	0	0	0	0	0	0	0	0	0	0	1	0	0	0	0	0	0	0	0
0.2-0.3	-	-	-	-	-	-	-	-	-	-	-	-	-	-	-	-	-	-	-	-	-	-	-	-	-	-	-	-	-	-	-	
0.3-0.4	197.6	109.4	94.8	100.0	1	14.9	0.0	0.0	0.0	0	0	0	0	0	0	0	0	0	0	0	0	0	0	0	0	0	0	0	0	0	0	0
0.4-0.5	-	-	-	-	-	-	-	-	-	-	-	-	-	-	-	-	-	-	-	-	-	-	-	-	-	-	-	-	-	-	-	
0.5-0.6	-	-	-	-	-	-	-	-	-	-	-	-	-	-	-	-	-	-	-	-	-	-	-	-	-	-	-	-	-	-	-	
0.6-0.7	-	-	-	-	-	-	-	-	-	-	-	-	-	-	-	-	-	-	-	-	-	-	-	-	-	-	-	-	-	-	-	
0.7-0.8	-	-	-	-	-	-	-	-	-	-	-	-	-	-	-	-	-	-	-	-	-	-	-	-	-	-	-	-	-	-	-	
0.8-0.9	199.3	166.6	61.5	100.0	1	15.1	0.0	0.0	0.0	0	0	0	0	0	0	0	0	0	0	0	0	0	0	0	0	0	0	0	0	0	0	0

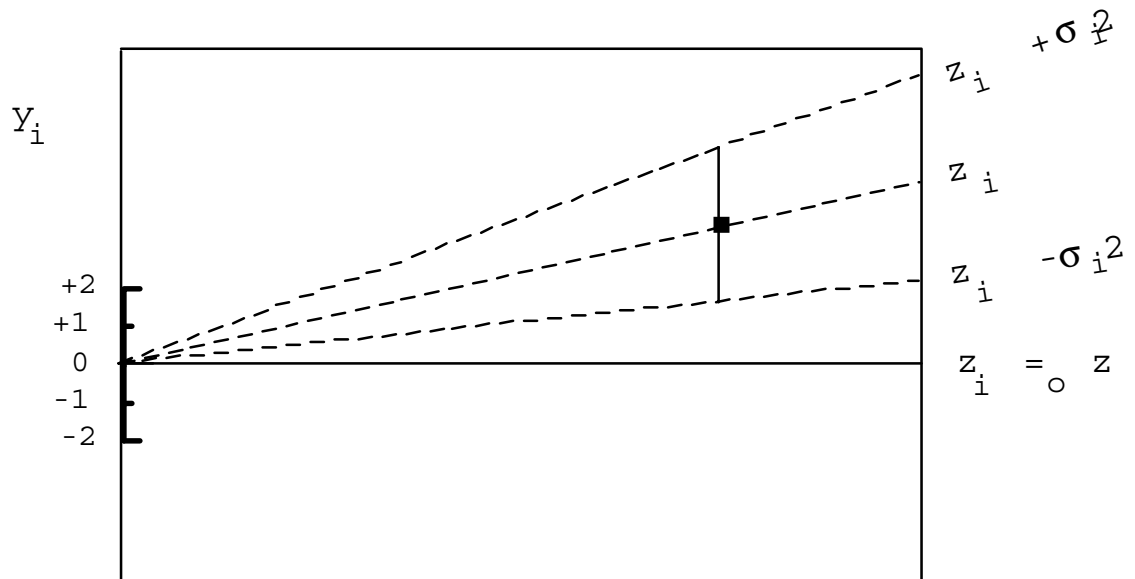
* Fission Track Age and Mean Track Length predicted from the Default Thermal History (i.e. if the sample has not been hotter in the past)

† Combined data for all compositional groups



Estimates	z_i
Standard errors	σ_i
Reference value	z_o
Standardised estimates	$y_i = (z_i - z_o) / \sigma_i$
Precision	$x_i = 1 / \sigma_i$

PLOT y_i against x_i



Slope of line from origin through data point

$$\begin{aligned}
 x_i &= y_i / x_i \\
 &= \{(z_i - z_o) / \sigma_i\} / \{1 / \sigma_i\} \\
 &= z_i - z_o
 \end{aligned}$$

Key Points:

Radial lines emanating from the origin correspond to fixed values of z

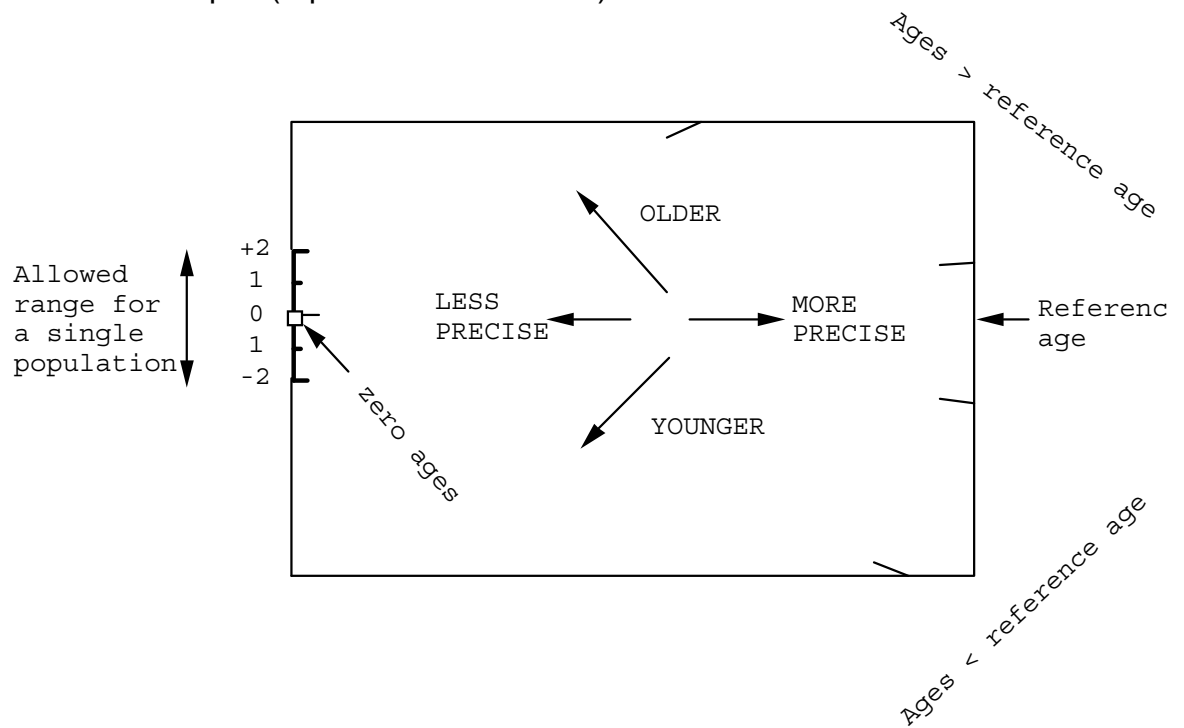
Data points with higher values of x_i have greater precision.

Error bars on all points are the same size in this plot.

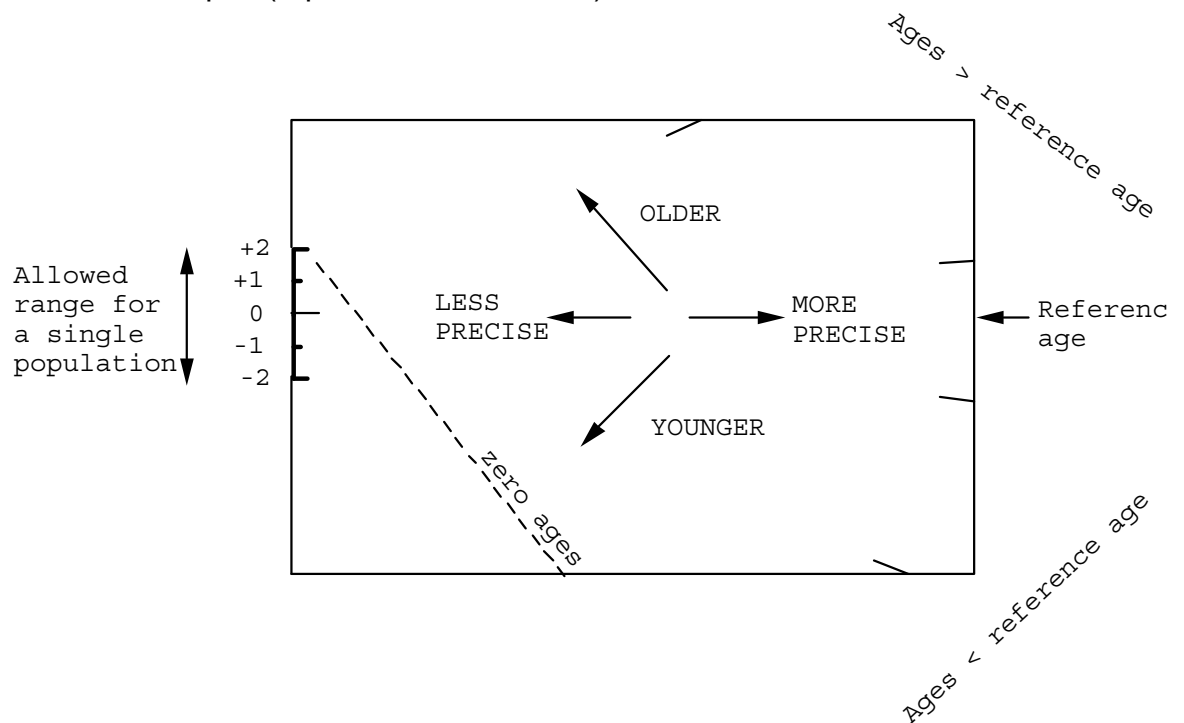
Figure B.1 Basic construction of a radial plot. In AFTA, the estimates z_i correspond to the fission track age values for individual apatite grains. Any convenient value of age can be chosen as the reference value corresponding to the horizontal in the radial plot. Radial lines emanating from the origin with positive slopes correspond to fission track ages greater than the reference value. Lines with negative slopes correspond to fission track ages less than the reference value.



Normal radial plot (equations B.2 and B.3)



Arc-sin radial plot (equations B.2 and B.4)

**Figure B.2** Simplified structure of Normal and Arc-sin radial plots.



Fission Track Age Data Sheets - Glossary

N_s	=	Number of spontaneous tracks in N_a grid squares
N_i	=	Number of induced tracks in N_a grid squares
N_a	=	Number of grid squares counted in each grain
RATIO	=	N_s/N_i
U (ppm)	=	Uranium content of each grain (= U content of standard glass * ρ_i/ρ_D)
Cl (wt%)	=	Weight percent chlorine content of each grain
ρ_s	=	Spontaneous track density (ρ_s) = $N_s/(N_a \cdot \text{area of basic unit})$
ρ_i	=	Induced track density (ρ_i) = $N_i/(N_a \cdot \text{area of basic unit})$
F.T. AGE	=	Fission track age, calculated using equation B.1
Area of basic unit	=	Area of one grid square
Chi squared	=	χ^2 parameter, used to assess variation of single grain ages within the sample
P(chi squared)	=	Probability of obtaining observed χ^2 value for the relevant number of degrees of freedom, if all grains belong to a single population
Age Dispersion	=	% variation in single grain ages - see discussion in text re "Central age"
N_s/N_i	=	Pooled ratio, total spontaneous tracks divided by total induced tracks for all grains
Mean ratio	=	Mean of (N_s/N_i) for individual grains
Zeta	=	Calibration constant, determined empirically for each observer
ρ_D	=	Track density (ρ_D) from uranium standard glass (interpolated from values at each end of stack)
ND	=	Total number of tracks counted for determining ρ_D
POOLED AGE	=	Fission track age calculated from pooled ratio N_s/N_i . Valid only when $P(\chi^2) > 5\%$
CENTRAL AGE	=	Alternative to pooled age when $P(\chi^2) < 5\%$

Key to Figures:

A: Radial plot of single grain ages <i>(See Figures B.1 and B.2 for details of radial plot construction)</i>	B: Distribution of Cl contents in apatite grains
C: Single grain age vs weight % Cl for individual apatite grains.	D: Distribution of confined track lengths



GC777-1 Apatite
Counted by: PFG

16/28-sb01 40.87-m

Slide ref	Current grain no	N _s	N _i	N _a	ρ _s	ρ _i	RATIO	U (ppm)	Cl (wt%)	F.T. AGE (Ma)
G839-1	3	0	6	12	0.000E+00	7.945E+05	0.000	7.5	0.64	0.0 ± 74.8
G839-1	5	4	10	51	1.246E+05	3.116E+05	0.400	2.9	0.15	92.8 ± 55.0
		4	16		1.009E+05	4.036E+05		3.8		

Area of basic unit = 6.293E-07 cm²

$\chi^2 = 2.143$ with 1 degrees of freedom

P(χ^2) = 14.3%

Age Dispersion = 17.109% (did not converge)

N_s / N_i = 0.250 ± 0.140

Mean Ratio = 0.200 ± 0.200

Ages calculated using a zeta of 385.5 ± 4.3 for CN5 glass

ρ_D = 1.213E+06cm⁻² ND = 2004

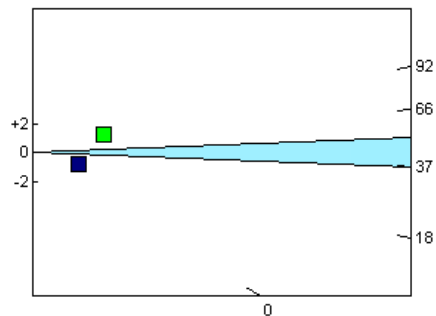
ρ_D interpolated between top of can; ρ_D = 1.213E+06cm⁻² ND = 954

bottom of can; ρ_D = 1.335E+06cm⁻² ND = 1050

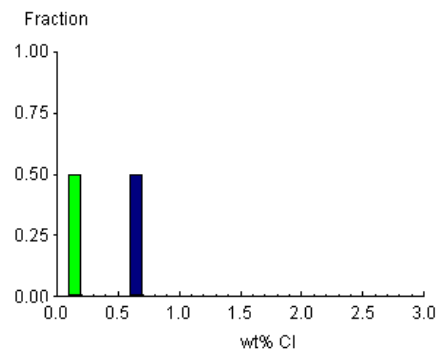
POOLED AGE = 58.2 ± 32.6 Ma

CENTRAL AGE = 57.3 ± 33.1 Ma

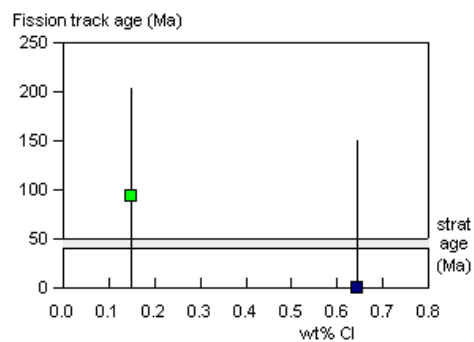
A:



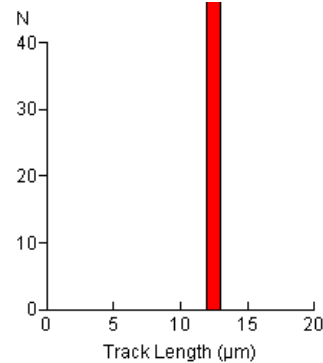
B:



C:



D:



Mean track length 12.16 ± 0.11 μm Std. Dev. 0.16 μm 2 tracks



GC777-2 Apatite
Counted by: PFG

16/28-sb01 147.2-m

Slide ref	Current grain no	N _s	N _i	N _a	ρ _s	ρ _i	RATIO	U (ppm)	Cl (wt%)	F.T. AGE (Ma)
G839-2	3	5	5	25	3.178E+05	3.178E+05	1.000	3.0	0.00	231.2 ± 146.4
G839-2	4	15	12	25	9.534E+05	7.628E+05	1.250	7.1	0.00	287.8 ± 111.7
G839-2	6	4	7	30	2.119E+05	3.708E+05	0.571	3.5	0.06	133.2 ± 83.5
G839-2	7	4	5	12	5.297E+05	6.621E+05	0.800	6.2	0.19	185.7 ± 124.6
G839-2	9	84	93	30	4.449E+06	4.926E+06	0.903	46.0	0.15	209.2 ± 31.9
G839-2	10	23	28	18	2.030E+06	2.472E+06	0.821	23.1	0.02	190.6 ± 53.8
G839-3	3	3	5	12	3.973E+05	6.621E+05	0.600	6.1	0.05	140.7 ± 102.8
G839-3	5	2	6	20	1.589E+05	4.767E+05	0.333	4.4	0.17	78.6 ± 64.2
G839-3	6	7	16	30	3.708E+05	8.475E+05	0.438	7.9	0.09	102.9 ± 46.7
G839-3	7	3	14	20	2.384E+05	1.112E+06	0.214	10.3	0.00	50.6 ± 32.2
G839-3	8	35	40	16	3.476E+06	3.973E+06	0.875	36.8	0.06	204.2 ± 47.5
G839-3	9	99	147	45	3.496E+06	5.191E+06	0.673	48.1	0.15	157.7 ± 20.9
G839-3	10	101	168	30	5.350E+06	8.899E+06	0.601	82.5	0.04	141.0 ± 18.1
G839-3	14	36	55	40	1.430E+06	2.185E+06	0.655	20.2	0.11	153.4 ± 33.1
G839-3	15	5	7	20	3.973E+05	5.562E+05	0.714	5.2	0.03	167.2 ± 98.0
G839-3	17	1	2	20	7.945E+04	1.589E+05	0.500	1.5	0.42	117.5 ± 143.9
G839-3	18	18	34	40	7.151E+05	1.351E+06	0.529	12.5	0.32	124.3 ± 36.4
		445	640		1.633E+06	2.351E+06		21.9		

Area of basic unit = 6.293E-07 cm⁻²

$\chi^2 = 15.160$ with 16 degrees of freedom

P(χ^2) = 51.3%

Age Dispersion = 5.532% (did not converge)

Ns / Ni = 0.695 ± 0.043

Mean Ratio = 0.678 ± 0.061

Ages calculated using a zeta of 385.5 ± 4.3 for CN5 glass

ρ_D = 1.221E+06cm⁻² ND = 2004

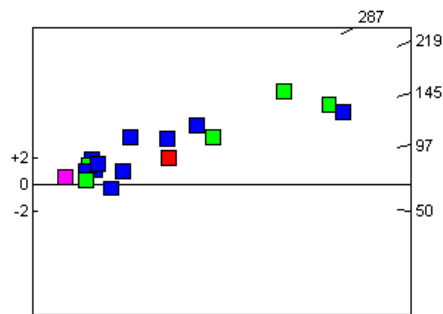
ρ_D interpolated between top of can; ρ_D = 1.213E+06cm⁻² ND = 954

bottom of can; ρ_D = 1.335E+06cm⁻² ND = 1050

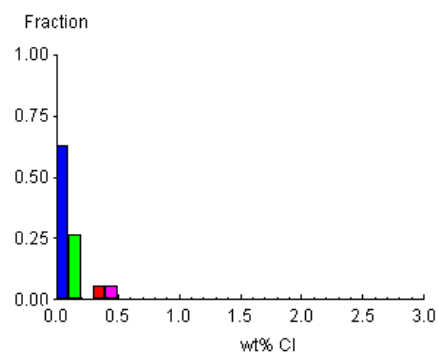
POOLED AGE = 161.5 ± 10.8 Ma

CENTRAL AGE = 161.7 ± 11.3 Ma

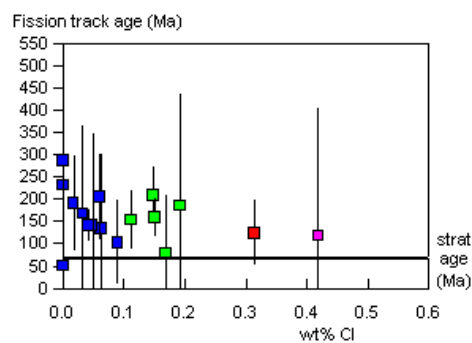
A:



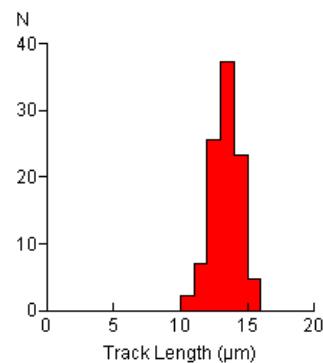
B:



C:



D:



Mean track length 13.31 ± 0.16 μm Std. Dev. 1.06 μm 43 tracks



GC777-3 Apatite
Counted by: PFG

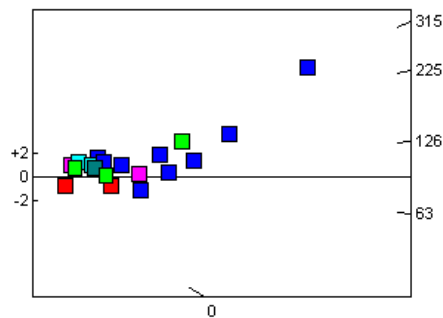
83/20-sb01 117.8-m

Slide ref	Current grain no	N _s	N _i	N _a	ρ _s	ρ _i	RATIO	U (ppm)	Cl (wt%)	F.T. AGE (Ma)
G839-4	8	15	37	20	1.192E+06	2.940E+06	0.405	27.1	0.00	96.1 ± 29.5
G839-4	9	4	8	24	2.648E+05	5.297E+05	0.500	4.9	0.16	118.3 ± 72.5
G839-4	11	2	2	30	1.059E+05	1.059E+05	1.000	1.0	0.48	234.5 ± 234.6
G839-4	13	3	3	24	1.986E+05	1.986E+05	1.000	1.8	0.26	234.5 ± 191.5
G839-4	14	6	6	25	3.814E+05	3.814E+05	1.000	3.5	0.10	234.5 ± 135.5
G839-4	17	25	48	50	7.945E+05	1.526E+06	0.521	14.0	0.03	123.2 ± 30.5
G839-4	18	8	14	25	5.085E+05	8.899E+05	0.571	8.2	0.00	135.0 ± 59.9
G839-4	20	0	3	36	0.000E+00	1.324E+05	0.000	1.2	0.39	0.0 ± 198.5
G839-4	21	9	23	50	2.860E+05	7.310E+05	0.391	6.7	0.46	92.8 ± 36.6
G839-4	23	4	6	25	2.543E+05	3.814E+05	0.667	3.5	0.26	157.3 ± 101.6
G839-5	4	18	27	12	2.384E+06	3.575E+06	0.667	32.7	0.00	158.4 ± 48.3
G839-5	5	6	8	25	3.814E+05	5.085E+05	0.750	4.6	0.03	177.9 ± 96.2
G839-5	6	4	7	40	1.589E+05	2.781E+05	0.571	2.5	0.80	136.0 ± 85.3
G839-5	11	47	61	24	3.112E+06	4.039E+06	0.770	36.9	0.07	182.7 ± 35.7
G839-5	22	3	14	40	1.192E+05	5.562E+05	0.214	5.1	0.37	51.3 ± 32.7
G839-5	28	4	11	25	2.543E+05	6.992E+05	0.364	6.4	0.19	86.9 ± 50.8
G839-5	30	28	34	24	1.854E+06	2.251E+06	0.824	20.6	0.13	195.1 ± 50.0
G839-5	31	2	3	16	1.986E+05	2.980E+05	0.667	2.7	0.14	158.4 ± 144.6
G839-5	40	122	90	70	2.770E+06	2.043E+06	1.356	18.7	0.04	318.0 ± 44.9
G839-5	42	6	27	25	3.814E+05	1.716E+06	0.222	15.7	0.00	53.2 ± 24.1
		316	430		8.232E+05	1.120E+06		10.3		

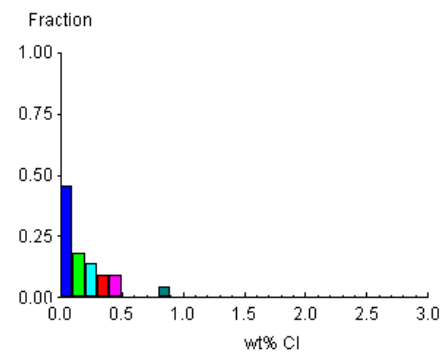
Area of basic unit = 6.293E-07 cm⁻²
 $\chi^2 = 46.426$ with 19 degrees of freedom
 $P(\chi^2) = 0.0\%$
 Age Dispersion = 36.832%
 $N_s / N_i = 0.735 \pm 0.054$
 Mean Ratio = 0.625 ± 0.072

Ages calculated using a zeta of 385.5 ± 4.3 for CN5 glass
 $\rho_D = 1.239E+06 \text{ cm}^{-2}$ ND = 2004
 ρ_D interpolated between top of can; $\rho_D = 1.213E+06 \text{ cm}^{-2}$ ND = 954
 bottom of can; $\rho_D = 1.335E+06 \text{ cm}^{-2}$ ND = 1050
 POOLED AGE = 173.1 ± 13.5 Ma
CENTRAL AGE = 142.2 ± 18.5 Ma

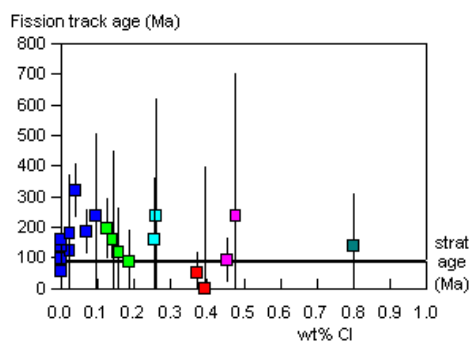
A:



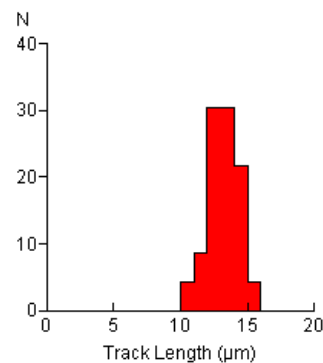
B:



C:



D:



Mean track length 13.11 ± 0.25 μm Std. Dev. 1.21 μm 23 tracks



GC777-4 Apatite
Counted by: PFG

83/20-sb01 150.8-155.6m

Slide ref	Current grain no	N _s	N _i	N _a	ρ _s	ρ _i	RATIO	U (ppm)	Cl (wt%)	F.T. AGE (Ma)
G839-6	3	10	14	12	1.324E+06	1.854E+06	0.714	16.8	0.00	170.7 ± 70.8
G839-6	12	123	62	49	3.989E+06	2.011E+06	1.984	18.2	0.17	463.4 ± 73.1
G839-6	13	138	87	60	3.655E+06	2.304E+06	1.586	20.9	0.40	373.1 ± 51.9
G839-6	14	5	5	100	7.945E+04	7.945E+04	1.000	0.7	0.09	237.7 ± 150.5
G839-6	16	49	110	90	8.652E+05	1.942E+06	0.445	17.6	0.00	107.0 ± 18.6
G839-6	17	0	1	50	0.000E+00	3.178E+04	0.000	0.3	0.08	0.0 ± 1736.3
G839-6	18	40	27	30	2.119E+06	1.430E+06	1.481	13.0	0.09	349.1 ± 87.4
G839-6	19	7	5	85	1.309E+05	9.347E+04	1.400	0.8	0.08	330.4 ± 193.6
G839-6	20	3	15	15	3.178E+05	1.589E+06	0.200	14.4	0.04	48.3 ± 30.5
G839-7	8	4	40	20	3.178E+05	3.178E+06	0.100	28.6	0.00	24.3 ± 12.8
G839-7	15	3	12	30	1.589E+05	6.356E+05	0.250	5.7	0.01	60.7 ± 39.2
G839-7	18	54	72	90	9.534E+05	1.271E+06	0.750	11.5	0.00	180.3 ± 32.8
G839-7	20	42	19	42	1.589E+06	7.189E+05	2.211	6.5	0.01	517.7 ± 143.7
G839-7	23	6	4	40	2.384E+05	1.589E+05	1.500	1.4	0.09	355.8 ± 229.8
G839-7	24	42	91	58	1.151E+06	2.493E+06	0.462	22.5	0.04	111.6 ± 21.0
G839-7	29	58	21	15	6.144E+06	2.225E+06	2.762	20.0	0.10	640.6 ± 163.9
G839-7	30	63	29	41	2.442E+06	1.124E+06	2.172	10.1	0.02	509.1 ± 114.9
G839-7	31	12	13	50	3.814E+05	4.132E+05	0.923	3.7	0.04	221.2 ± 88.7

659

625

1.194E+06

1.132E+06

10.3

Area of basic unit = 6.293E-07 cm²

$\chi^2 = 160.917$ with 17 degrees of freedom

P(χ^2) = 0.0%

Age Dispersion = 72.001%

N_s / N_i = 1.055 ± 0.059

Mean Ratio = 1.112 ± 0.194

Ages calculated using a zeta of 385.5 ± 4.3 for CN5 glass

ρ_D = 1.256E+06cm⁻² ND = 2004

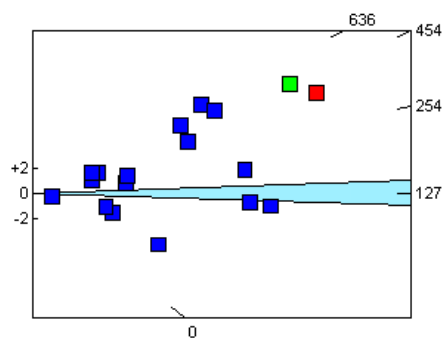
ρ_D interpolated between top of can; ρ_D = 1.213E+06cm⁻² ND = 954

bottom of can; ρ_D = 1.335E+06cm⁻² ND = 1050

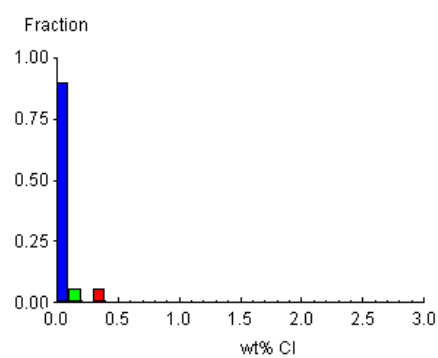
POOLED AGE = 250.4 ± 15.3 Ma

CENTRAL AGE = 216.6 ± 41.6 Ma

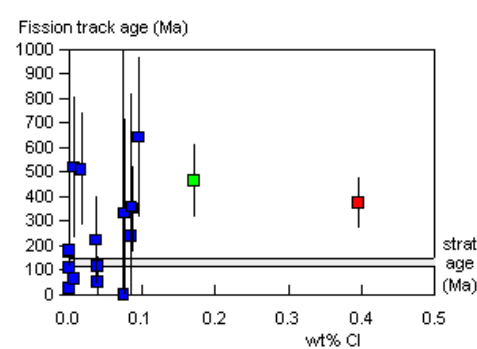
A:



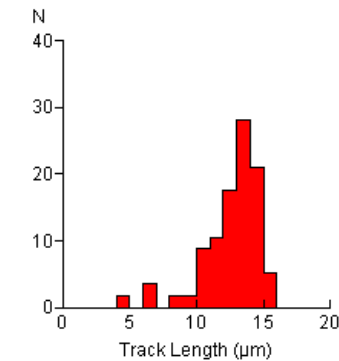
B:



C:



D:



Mean track length 12.59 ± 0.30 μm Std. Dev. 2.23 μm 57 tracks



GC777-5 Apatite
Counted by: PFG

83/20-sb01 176.7-177.3m

Slide ref	Current grain no	N _s	N _i	N _a	ρ _s	ρ _i	RATIO	U (ppm)	Cl (wt%)	F.T. AGE (Ma)
G839-8	6	5	5	50	1.589E+05	1.589E+05	1.000	1.4	0.74	241.0 ± 152.5
G839-9	4	1	3	9	1.766E+05	5.297E+05	0.333	4.7	0.96	81.9 ± 94.6
		6	8		1.616E+05	2.149E+05		1.9		

Area of basic unit = 6.293E-07 cm²

$\chi^2 = 0.719$ with 1 degrees of freedom

P(χ^2) = 39.6%

Age Dispersion = 0.000% (did not converge)

N_s / N_i = 0.752 ± 0.406

Mean Ratio = 0.668 ± 0.332

Ages calculated using a zeta of 385.5 ± 4.3 for CN5 glass

ρ_D = 1.274E+06cm⁻² ND = 2004

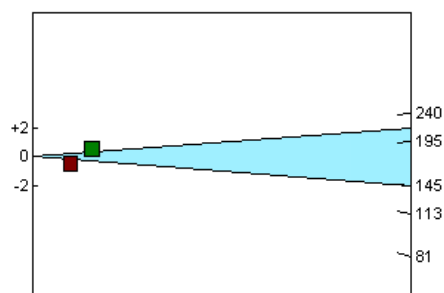
ρ_D interpolated between top of can; ρ_D = 1.213E+06cm⁻² ND = 954

bottom of can; ρ_D = 1.335E+06cm⁻² ND = 1050

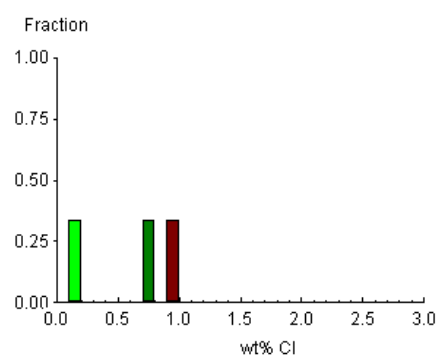
POOLED AGE = 182.0 ± 98.5 Ma

CENTRAL AGE = 182.0 ± 98.5 Ma

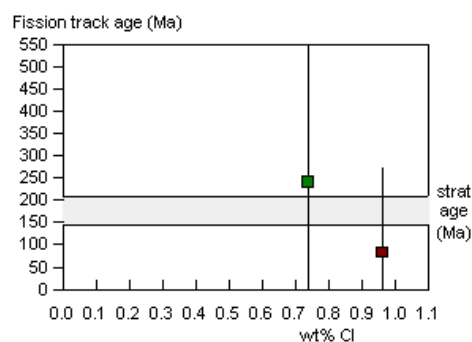
A:



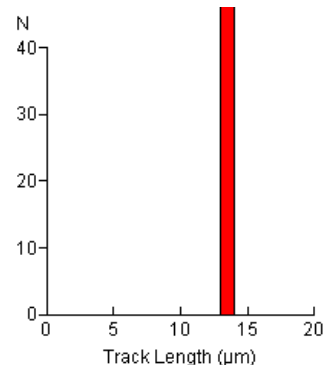
B:



C:



D:



Mean track length 13.84 ± 0.00 μm Std. Dev. μm 1 tracks



GC777-7 Apatite
Counted by: PFG

83/24-sb02 44.8-m

Slide ref	Current grain no	N _s	N _i	N _a	ρ _s	ρ _i	RATIO	U (ppm)	Cl (wt%)	F.T. AGE (Ma)
G839-10	3	39	60	60	1.033E+06	1.589E+06	0.650	14.0	0.00	159.8 ± 33.1
G839-11	4	25	64	90	4.414E+05	1.130E+06	0.391	9.9	0.00	97.1 ± 23.0
		64	124		6.780E+05	1.309E+06		11.6		

Area of basic unit = 6.293E-07 cm²

$\chi^2 = 2.597$ with 1 degrees of freedom

P(χ^2) = 10.7%

Age Dispersion = 11.970% (did not converge)

N_s / N_i = 0.518 ± 0.080

Mean Ratio = 0.522 ± 0.128

Ages calculated using a zeta of 385.5 ± 4.3 for CN5 glass

ρ_D = 1.291E+06cm⁻² ND = 2004

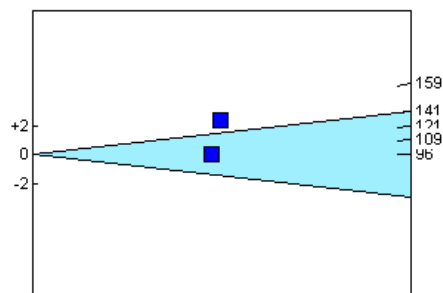
ρ_D interpolated between top of can; ρ_D = 1.213E+06cm⁻² ND = 954

bottom of can; ρ_D = 1.335E+06cm⁻² ND = 1050

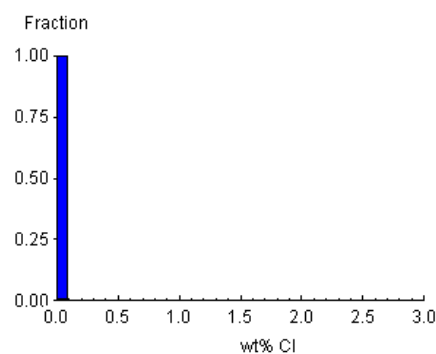
POOLED AGE = 127.6 ± 19.9 Ma

CENTRAL AGE = 127.2 ± 22.6 Ma

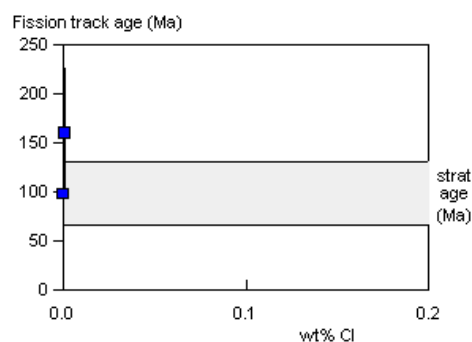
A:



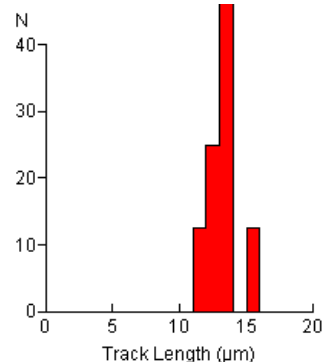
B:



C:



D:



Mean track length 13.44 ± 0.36 μm Std. Dev. 1.01 μm 8 tracks



GC777-8 Apatite
Counted by: PFG

83/24-sb02 70.75-m

Slide ref	Current grain no	N _s	N _i	N _a	ρ _s	ρ _i	RATIO	U (ppm)	Cl (wt%)	F.T. AGE (Ma)
G839-12	1	3	9	24	1.986E+05	5.959E+05	0.333	5.2	0.07	83.5 ± 55.7
G839-12	5	3	5	24	1.986E+05	3.311E+05	0.600	2.9	0.10	149.6 ± 109.3
G839-12	9	4	7	10	6.356E+05	1.112E+06	0.571	9.7	0.10	142.6 ± 89.4
G839-12	10	2	5	15	2.119E+05	5.297E+05	0.400	4.6	0.35	100.1 ± 83.8
		12	26		2.612E+05	5.660E+05		4.9		

Area of basic unit = 6.293E-07 cm²

$\chi^2 = 0.516$ with 3 degrees of freedom

P(χ^2) = 91.5%

Age Dispersion = 0.000% (did not converge)

N_s / N_i = 0.462 ± 0.161

Mean Ratio = 0.476 ± 0.065

Ages calculated using a zeta of 385.5 ± 4.3 for CN5 glass

ρ_D = 1.309E+06cm⁻² ND = 2004

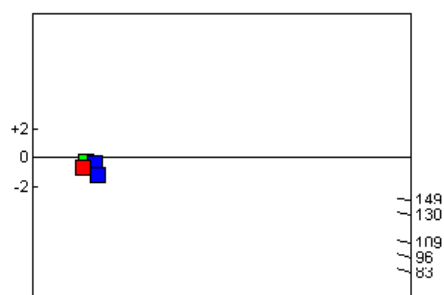
ρ_D interpolated between top of can; ρ_D = 1.213E+06cm⁻² ND = 954

bottom of can; ρ_D = 1.335E+06cm⁻² ND = 1050

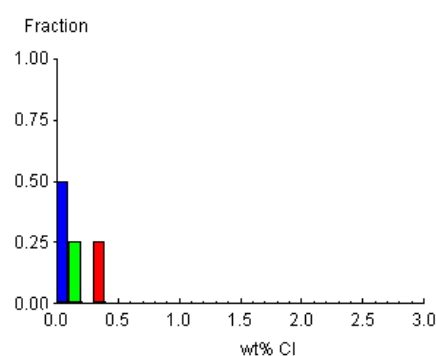
POOLED AGE = 115.4 ± 40.4 Ma

CENTRAL AGE = 115.4 ± 40.4 Ma

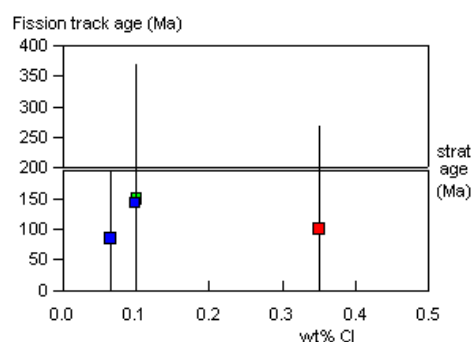
A:



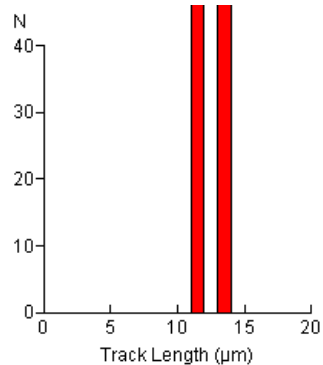
B:



C:



D:



Mean track length 12.80 ± 0.99 μm Std. Dev. 1.40 μm 2 tracks



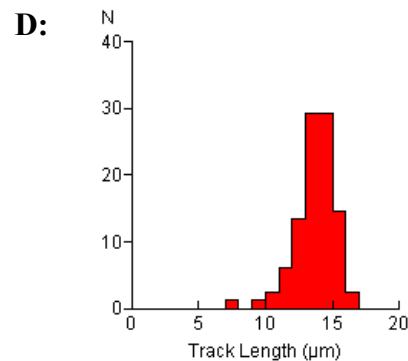
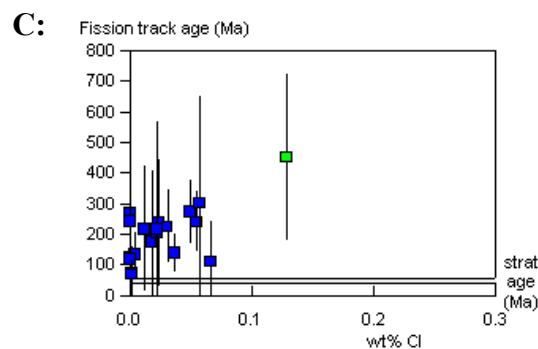
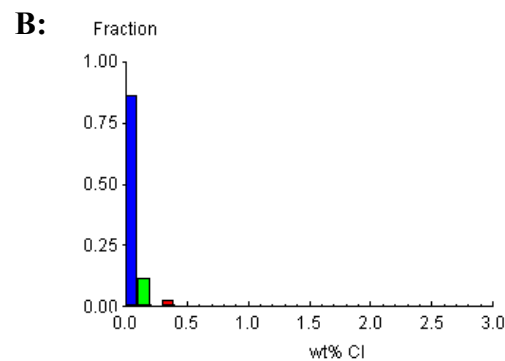
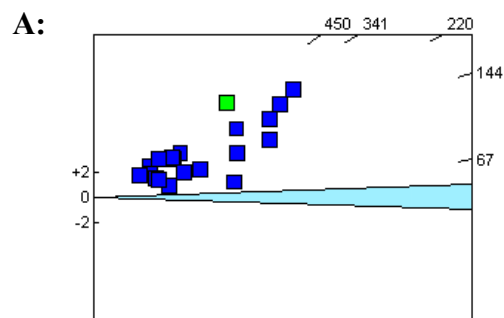
GC777-9 Apatite
Counted by: PFG

16/28-sb01 40.87-80m

Slide ref	Current grain no	N _s	N _i	N _a	ρ _s	ρ _i	RATIO	U (ppm)	Cl (wt%)	F.T. AGE (Ma)
G845-1	6	5	4	24	3.311E+05	2.648E+05	1.250	2.7	0.00	268.8 ± 180.4
G845-1	9	4	5	8	7.945E+05	9.932E+05	0.800	9.9	0.02	173.3 ± 116.3
G845-1	13	11	10	26	6.723E+05	6.112E+05	1.100	6.1	0.02	237.1 ± 103.8
G845-1	16	4	12	30	2.119E+05	6.356E+05	0.333	6.4	0.00	72.8 ± 42.1
G845-1	18	4	7	21	3.027E+05	5.297E+05	0.571	5.3	0.00	124.3 ± 77.9
G845-1	19	9	9	20	7.151E+05	7.151E+05	1.000	7.2	0.01	215.9 ± 101.9
G845-1	20	8	15	16	7.945E+05	1.490E+06	0.533	14.9	0.00	116.0 ± 50.9
G845-1	22	9	8	40	3.575E+05	3.178E+05	1.125	3.2	0.00	242.4 ± 117.9
G845-1	23	42	45	16	4.171E+06	4.469E+06	0.933	44.7	0.02	201.7 ± 43.6
G845-1	24	4	8	24	2.648E+05	5.297E+05	0.500	5.3	0.07	108.9 ± 66.7
G845-1	26	51	46	45	1.801E+06	1.624E+06	1.109	16.3	0.06	238.9 ± 49.0
G845-1	27	34	16	30	1.801E+06	8.475E+05	2.125	8.5	0.13	450.4 ± 137.0
G845-1	28	34	53	40	1.351E+06	2.106E+06	0.642	21.1	0.04	139.3 ± 30.8
G845-1	33	22	36	15	2.331E+06	3.814E+06	0.611	38.2	0.00	132.8 ± 36.1
G845-1	34	11	21	28	6.243E+05	1.192E+06	0.524	11.9	0.00	114.0 ± 42.5
G845-1	38	62	49	21	4.692E+06	3.708E+06	1.265	37.1	0.05	272.0 ± 52.5
G845-1	39	3	3	49	9.729E+04	9.729E+04	1.000	1.0	0.02	215.9 ± 176.4
G845-1	43	13	42	24	8.607E+05	2.781E+06	0.310	27.8	0.00	67.6 ± 21.5
G845-1	47	7	5	15	7.416E+05	5.297E+05	1.400	5.3	0.06	300.3 ± 176.0
G845-1	51	29	28	21	2.194E+06	2.119E+06	1.036	21.2	0.03	223.5 ± 59.5
		366	422		1.134E+06	1.307E+06		13.1		

Area of basic unit = 6.293E-07 cm⁻²
 $\chi^2 = 39.490$ with 19 degrees of freedom
 $P(\chi^2) = 0.4\%$
 Age Dispersion = 34.399%
 $N_s / N_i = 0.867 \pm 0.062$
 Mean Ratio = 0.908 ± 0.097

Ages calculated using a zeta of 385.5 ± 4.3 for CN5 glass
 $\rho_D = 1.139E+06 \text{ cm}^{-2}$ ND = 1865
 ρ_D interpolated between top of can; $\rho_D = 1.213E+06 \text{ cm}^{-2}$ ND = 954
 bottom of can; $\rho_D = 1.335E+06 \text{ cm}^{-2}$ ND = 1050
 POOLED AGE = 187.7 ± 14.2 Ma
CENTRAL AGE = 180.6 ± 21.1 Ma



Mean track length 13.68 ± 0.17 μm Std. Dev. 1.51 μm 82 tracks



GC777-12 Apatite
Counted by: PFG

83/24-sb02 70.75-71m

Slide ref	Current grain no	N _s	N _i	N _a	ρ _s	ρ _i	RATIO	U (ppm)	Cl (wt%)	F.T. AGE (Ma)
G845-2	4	23	45	10	3.655E+06	7.151E+06	0.511	71.2	0.07	111.8 ± 28.8
G845-2	5	11	9	12	1.457E+06	1.192E+06	1.222	11.9	0.20	264.3 ± 119.0
G845-2	6	19	18	20	1.510E+06	1.430E+06	1.056	14.2	0.00	228.9 ± 75.5
G845-2	8	13	17	8	2.582E+06	3.377E+06	0.765	33.6	0.81	166.6 ± 61.5
G845-2	9	13	15	25	8.263E+05	9.534E+05	0.867	9.5	0.16	188.5 ± 71.6
G845-2	10	130	206	36	5.738E+06	9.093E+06	0.631	90.5	0.00	137.8 ± 15.8
		209	310		2.992E+06	4.438E+06		44.2		

Area of basic unit = 6.293E-07 cm²

$\chi^2 = 5.775$ with 5 degrees of freedom

P(χ^2) = 32.9%

Age Dispersion = 0.319% (did not converge)

N_s / N_i = 0.674 ± 0.060

Mean Ratio = 0.842 ± 0.108

Ages calculated using a zeta of 385.5 ± 4.3 for CN5 glass

ρ_D = 1.145E+06cm⁻² ND = 1865

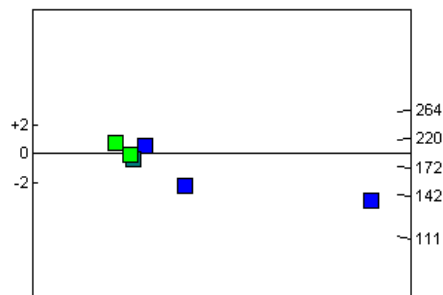
ρ_D interpolated between top of can; ρ_D = 1.213E+06cm⁻² ND = 954

bottom of can; ρ_D = 1.335E+06cm⁻² ND = 1050

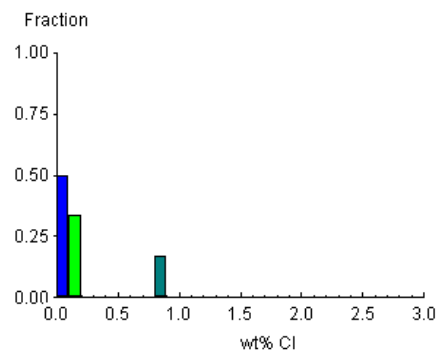
POOLED AGE = 147.1 ± 13.7 Ma

CENTRAL AGE = 147.1 ± 13.7 Ma

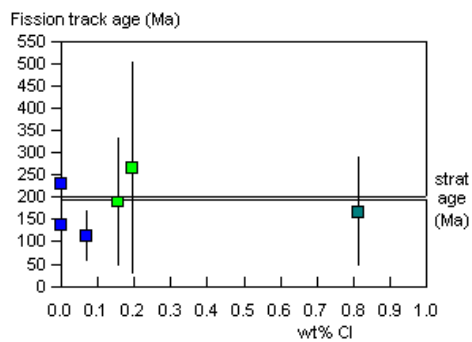
A:



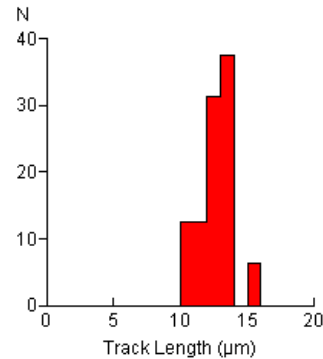
B:



C:



D:



Mean track length 12.76 ± 0.29 μm Std. Dev. 1.16 μm 16 tracks



GC777-2 Zircon
Counted by: PFG

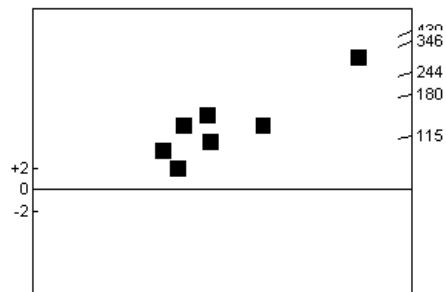
16/28-sb01 147.2-m

Slide ref	Current grain no	N _s	N _i	N _a	ρ _s	ρ _i	RATIO	U (ppm)	F.T. AGE (Ma)	
G847-1	6	42	17	7	9.534E+06	3.859E+06	2.471	191.7	115.2 ±	33.2
G847-1	8	120	28	10	1.907E+07	4.449E+06	4.286	221.0	198.5 ±	42.0
G847-1	11	71	17	5	2.256E+07	5.403E+06	4.176	268.4	193.6 ±	52.5
G847-1	12	264	32	20	2.098E+07	2.543E+06	8.250	126.3	376.9 ±	71.2
G847-1	13	58	6	4	2.304E+07	2.384E+06	9.667	118.4	439.5 ±	188.8
G847-1	14	77	8	9	1.360E+07	1.413E+06	9.625	70.2	437.6 ±	163.0
G847-1	15	39	8	9	6.886E+06	1.413E+06	4.875	70.2	225.4 ±	87.7
		671	116		1.666E+07	2.880E+06		143.1		

Area of basic unit = 6.293E-07 cm⁻²
 $\chi^2 = 20.040$ with 6 degrees of freedom
 $P(\chi^2) = 0.3\%$
Age Dispersion = 35.879%
Ns / Ni = 5.784 ± 0.582
Mean Ratio = 6.193 ± 1.106

Ages calculated using a zeta of 87.7 ± 0.8 for U3 glass
 $\rho_D = 1.073E+06\text{cm}^{-2}$ ND = 1743
 ρ_D interpolated between top of can; $\rho_D = 1.073E+06\text{cm}^{-2}$ ND = 844
bottom of can; $\rho_D = 1.143E+06\text{cm}^{-2}$ ND = 899
POOLED AGE = 266.6 ± 27.7 Ma
CENTRAL AGE = 245.3 ± 43.2 Ma

A:





GC777-3 Zircon
Counted by: PFG

83/20-sb01 117.8-m

Slide ref	Current grain no	N _s	N _i	N _a	ρ _s	ρ _i	RATIO	U (ppm)	F.T. AGE (Ma)
G847-2	3	76	23	8	1.510E+07	4.569E+06	3.304	224.0	155.6 ± 37.2
G847-2	4	134	75	20	1.065E+07	5.959E+06	1.787	292.2	84.6 ± 12.4
G847-2	7	111	35	12	1.470E+07	4.635E+06	3.171	227.3	149.4 ± 29.2
G847-2	13	215	53	25	1.367E+07	3.369E+06	4.057	165.2	190.5 ± 29.6
G847-2	21	218	96	40	8.660E+06	3.814E+06	2.271	187.0	107.3 ± 13.4
G847-2	29	209	55	20	1.661E+07	4.370E+06	3.800	214.3	178.6 ± 27.5
G847-2	32	60	12	6	1.589E+07	3.178E+06	5.000	155.8	234.0 ± 74.2
G847-2	36	132	24	10	2.098E+07	3.814E+06	5.500	187.0	256.9 ± 57.4
G847-2	51	161	25	18	1.421E+07	2.207E+06	6.440	108.2	299.9 ± 64.9
G847-2	53	101	18	16	1.003E+07	1.788E+06	5.611	87.7	262.0 ± 67.4
G847-2	62	137	29	12	1.814E+07	3.840E+06	4.724	188.3	221.3 ± 45.6
G847-2	64	110	23	6	2.913E+07	6.091E+06	4.783	298.7	224.0 ± 51.7
G847-2	71	147	28	18	1.298E+07	2.472E+06	5.250	121.2	245.5 ± 51.0
G847-2	84	143	20	15	1.515E+07	2.119E+06	7.150	103.9	332.1 ± 79.7
G847-2	89	97	51	16	9.634E+06	5.065E+06	1.902	248.4	90.0 ± 15.7
		2051	567		1.347E+07	3.723E+06		182.6	

Area of basic unit = 6.293E-07 cm⁻²

$\chi^2 = 85.256$ with 14 degrees of freedom

P(χ^2) = 0.0%

Age Dispersion = 39.982%

Ns / Ni = 3.617 ± 0.172

Mean Ratio = 4.317 ± 0.416

Ages calculated using a zeta of 87.7 ± 0.8 for U3 glass

ρ_D = 1.087E+06cm⁻² ND = 1743

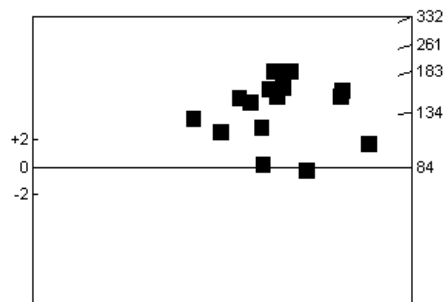
ρ_D interpolated between top of can; ρ_D = 1.073E+06cm⁻² ND = 844

bottom of can; ρ_D = 1.143E+06cm⁻² ND = 899

POOLED AGE = 170.1 ± 9.2 Ma

CENTRAL AGE = 177.3 ± 20.8 Ma

A:





GC777-4 Zircon

83/20-sb01 150.8-155.6m

Counted by: PFG

Slide ref	Current grain no	N _s	N _i	N _a	ρ _s	ρ _i	RATIO	U (ppm)	F.T. AGE (Ma)
G847-3	7	192	52	15	2.034E+07	5.509E+06	3.692	266.7	175.8 ± 27.9
G847-3	23	208	41	24	1.377E+07	2.715E+06	5.073	131.4	240.4 ± 41.5
G847-3	30	665	130	50	2.113E+07	4.132E+06	5.115	200.0	242.3 ± 24.1
G847-3	32	192	43	16	1.907E+07	4.271E+06	4.465	206.8	212.0 ± 36.2
G847-3	34	343	73	40	1.363E+07	2.900E+06	4.699	140.4	222.9 ± 29.3
G847-3	40	226	83	30	1.197E+07	4.396E+06	2.723	212.9	130.1 ± 17.0
G847-3	52	337	76	40	1.339E+07	3.019E+06	4.434	146.2	210.6 ± 27.3
G847-3	53	102	23	8	2.026E+07	4.569E+06	4.435	221.2	210.6 ± 48.9
G847-3	60	325	54	30	1.721E+07	2.860E+06	6.019	138.5	284.2 ± 42.4
G847-3	73	245	73	30	1.298E+07	3.867E+06	3.356	187.2	160.0 ± 21.7
G847-3	75	210	45	18	1.854E+07	3.973E+06	4.667	192.3	221.4 ± 36.8
G847-3	81	171	28	16	1.698E+07	2.781E+06	6.107	134.6	288.3 ± 59.2
G847-3	82	315	56	20	2.503E+07	4.449E+06	5.625	215.4	266.0 ± 39.2
G847-3	95	153	36	25	9.725E+06	2.288E+06	4.250	110.8	202.0 ± 37.8
G847-3	116	197	47	20	1.565E+07	3.734E+06	4.191	180.8	199.2 ± 32.7
		3881	860		1.614E+07	3.577E+06		173.2	

Area of basic unit = 6.293E-07 cm² $\chi^2 = 33.511$ with 14 degrees of freedomP(χ^2) = 0.2%

Age Dispersion = 16.467%

Ns / Ni = 4.513 ± 0.170

Mean Ratio = 4.590 ± 0.240

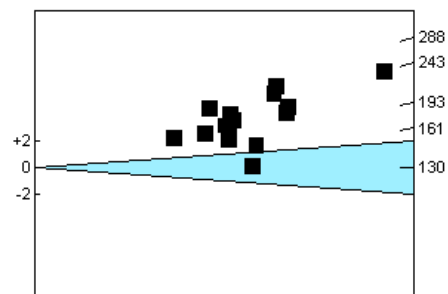
Ages calculated using a zeta of 87.7 ± 0.8 for U3 glass

ρ_D = 1.101E+06cm⁻² ND = 1743ρ_D interpolated between top of can; ρ_D = 1.073E+06cm⁻² ND = 844bottom of can; ρ_D = 1.143E+06cm⁻² ND = 899

POOLED AGE = 214.3 ± 9.8 Ma

CENTRAL AGE = 211.5 ± 13.4 Ma

A:





GC777-9 Zircon

16/28-sb01 40.87-80m

Counted by: PFG

Slide ref	Current grain no	N _s	N _i	N _a	ρ _s	ρ _i	RATIO	U (ppm)	F.T. AGE (Ma)	
G847-4	4	62	11	4	2.463E+07	4.370E+06	5.636	208.9	269.8 ±	88.5
G847-4	9	29	9	4	1.152E+07	3.575E+06	3.222	170.9	155.6 ±	59.5
G847-4	10	52	11	4	2.066E+07	4.370E+06	4.727	208.9	227.1 ±	75.6
G847-4	14	120	11	9	2.119E+07	1.942E+06	10.909	92.9	512.4 ±	162.0
G847-4	20	67	13	10	1.065E+07	2.066E+06	5.154	98.8	247.2 ±	75.2
G847-4	24	72	12	8	1.430E+07	2.384E+06	6.000	114.0	286.8 ±	89.7
G847-4	26	78	21	6	2.066E+07	5.562E+06	3.714	265.9	179.1 ±	44.3
G847-4	32	45	6	8	8.939E+06	1.192E+06	7.500	57.0	356.6 ±	155.3
G847-4	33	173	41	14	1.964E+07	4.654E+06	4.220	222.5	203.1 ±	35.7
G847-4	36	82	14	9	1.448E+07	2.472E+06	5.857	118.2	280.2 ±	81.3
G847-4	37	154	23	12	2.039E+07	3.046E+06	6.696	145.6	319.3 ±	71.8
		934	172		1.687E+07	3.106E+06		148.5		

Area of basic unit = 6.293E-07 cm⁻² $\chi^2 = 13.382$ with 10 degrees of freedomP(χ^2) = 20.3%

Age Dispersion = 15.393%

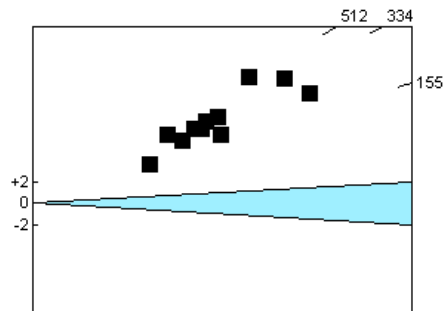
Ns / Ni = 5.430 ± 0.451

Mean Ratio = 5.785 ± 0.639

Ages calculated using a zeta of 87.7 ± 0.8 for U3 glass

ρ_D = 1.115E+06cm⁻² ND = 1743ρ_D interpolated between top of can; ρ_D = 1.073E+06cm⁻² ND = 844bottom of can; ρ_D = 1.143E+06cm⁻² ND = 899**POOLED AGE = 260.2 ± 22.6 Ma****CENTRAL AGE = 260.0 ± 26.1 Ma**

A:





GC777-11 Zircon

83/24-sb02 44.8-45.4m

Counted by: PFG

Slide ref	Current grain no	N _s	N _i	N _a	ρ _s	ρ _i	RATIO	U (ppm)	F.T. AGE (Ma)	
G847-5	9	391	76	30	2.071E+07	4.026E+06	5.145	190.1	249.8 ±	32.0
G847-5	17	132	31	16	1.311E+07	3.079E+06	4.258	145.4	207.4 ±	41.7
G847-5	22	121	29	16	1.202E+07	2.880E+06	4.172	136.0	203.3 ±	42.4
G847-5	26	206	46	20	1.637E+07	3.655E+06	4.478	172.6	218.0 ±	36.0
G847-5	46	239	121	40	9.495E+06	4.807E+06	1.975	227.0	97.0 ±	11.1
G847-5	50	272	51	24	1.801E+07	3.377E+06	5.333	159.4	258.7 ±	40.0
G847-5	58	101	19	50	3.210E+06	6.038E+05	5.316	28.5	257.9 ±	64.8
G847-5	62	81	55	30	4.290E+06	2.913E+06	1.473	137.6	72.5 ±	12.8
G847-5	63	302	54	30	1.600E+07	2.860E+06	5.593	135.1	271.1 ±	40.6
G847-5	74	203	37	14	2.304E+07	4.200E+06	5.486	198.3	266.0 ±	48.0
G847-5	78	102	24	15	1.081E+07	2.543E+06	4.250	120.0	207.0 ±	47.3
G847-5	79	157	47	20	1.247E+07	3.734E+06	3.340	176.3	163.3 ±	27.5
G847-5	81	245	59	30	1.298E+07	3.125E+06	4.153	147.6	202.3 ±	29.8
G847-5	88	137	35	20	1.089E+07	2.781E+06	3.914	131.3	190.9 ±	36.5
G847-5	90	486	93	50	1.545E+07	2.956E+06	5.226	139.6	253.6 ±	29.4
G847-5	93	104	21	15	1.102E+07	2.225E+06	4.952	105.0	240.6 ±	57.9
G847-5	98	154	30	15	1.631E+07	3.178E+06	5.133	150.1	249.2 ±	50.1
G847-5	108	130	36	18	1.148E+07	3.178E+06	3.611	150.1	176.3 ±	33.5
G847-5	117	217	35	20	1.724E+07	2.781E+06	6.200	131.3	299.8 ±	55.2
G847-5	119	210	43	20	1.669E+07	3.416E+06	4.884	161.3	237.3 ±	40.2
		3990	942		1.286E+07	3.036E+06		143.4		

Area of basic unit = 6.293E-07 cm⁻² $\chi^2 = 113.401$ with 19 degrees of freedomP(χ^2) = 0.0%

Age Dispersion = 35.339%

Ns / Ni = 4.236 ± 0.153

Mean Ratio = 4.445 ± 0.264

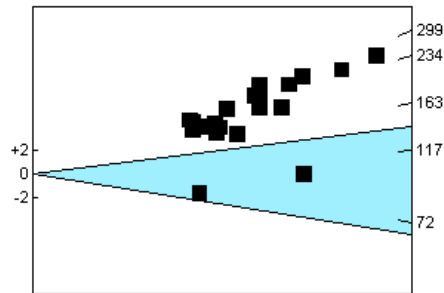
Ages calculated using a zeta of 87.7 ± 0.8 for U3 glass

 $\rho_D = 1.129E+06\text{cm}^{-2}$ ND = 1743 ρ_D interpolated between top of can; $\rho_D = 1.073E+06\text{cm}^{-2}$ ND = 844
bottom of can; $\rho_D = 1.143E+06\text{cm}^{-2}$ ND = 899

POOLED AGE = 206.3 ± 9.2 Ma

CENTRAL AGE = 200.7 ± 18.4 Ma

A:





APPENDIX C

Principles of Interpretation of AFTA and ZFTA Data in Sedimentary Basins

C.1 Introduction

In this Appendix, we set out some basic aspects of the processes underlying the AFTA and ZFTA techniques, and explain the principles involved in determining thermal history parameters from AFTA and ZFTA data. As the processes involved in AFTA are understood in considerably more detail than for ZFTA, the discussion is centred on AFTA, with some additional comments on ZFTA provided at the end of the Appendix.

Detrital apatite grains are incorporated into sedimentary rocks from three dominant sources - crystalline basement rocks, older sediments and contemporaneous volcanism. Apatites derived from the first two sources will, in general, contain fission tracks when they are deposited, with AFTA parameters characteristic of the source regions. However, apatites derived from contemporaneous volcanism, or from rapidly uplifted basement, will contain no tracks when they are deposited. For now, we will restrict discussion to this situation, and generalise at a later point to cover the case of apatites which contain tracks that have been inherited from source regions.

C.2 Basic principles of Apatite Fission Track Analysis

Fission tracks are trails of radiation damage, which are produced within apatite grains at a more or less constant rate through geological time, as a result of the spontaneous fission of ^{238}U impurity atoms. Therefore, the number of fission events which occur within an apatite grain during a fixed time interval depends on the magnitude of the time interval and the uranium content of the grain. Each fission event leads to the formation of a single fission track, and the proportion of tracks which can intersect a polished surface of an apatite grain depends on the length of the tracks. Therefore, the number of tracks which are etched in unit area of the surface of an apatite grain (the "spontaneous track density") depends on three factors - (i) The time over which tracks have been accumulating; (ii) The uranium content of the apatite grain; and, (iii) The



distribution of track lengths in the grain. In sedimentary rocks which have not been subjected to temperatures greater than $\sim 50^{\circ}\text{C}$ since deposition, spontaneous fission tracks have a characteristic distribution of confined track lengths, with a mean length in the range 14-15 μm and a standard deviation of $\sim 1 \mu\text{m}$. In such samples, by measuring the spontaneous track density and the uranium content of a collection of apatite grains, a "fission track age" can be calculated which will be equal to the time over which tracks have been accumulating. The technique is calibrated against other isotopic systems using age standards which also have this type of length distribution (see Appendix B).

In samples which have been subjected to temperatures greater than $\sim 50^{\circ}\text{C}$ after deposition, fission tracks are shortened because of the gradual repair of the radiation damage which constitutes the unetched tracks. In effect, the tracks shrink from each end, in a process which is known as fission track "annealing". The final length of each individual track is essentially determined by the maximum temperature which that track has experienced. A time difference of an order of magnitude produces a change in fission track parameters which is equivalent to a temperature change of only $\sim 10^{\circ}\text{C}$, so temperature is by far the dominant factor in determining the final fission track parameters. As temperature increases, all existing tracks shorten to a length determined by the prevailing temperature, regardless of when they were formed. After the temperature has subsequently decreased, all tracks formed prior to the thermal maximum are "frozen" at the degree of length reduction they attained at that time. Thus, the length of each track can be thought of as a maximum-reading thermometer, recording the maximum temperature to which it has been subjected.

Therefore, in samples for which the present temperature is maximum, all tracks have much the same length, resulting in a narrow, symmetric distribution. The degree of shortening will depend on the temperature, with the mean track length falling progressively from $\sim 14 \mu\text{m}$ at 50°C , to zero at around $110^{\circ}\text{--}120^{\circ}\text{C}$ - the precise temperature depending on the timescale of heating and the composition of the apatites present in the sample (see below). Values quoted here relate to times of the order of 10^7 years (heating rates around 1 to $10^{\circ}\text{C}/\text{Ma}$) and average apatite composition. If the effective timescale of heating is shorter than 10^7 years, the temperature responsible for a given degree of track shortening will be higher, depending in detail on the kinetics of the annealing process (Green et al., 1986; Laslett et al., 1987; Duddy et al., 1988; Green et al., 1989b). Shortening of tracks produces an accompanying reduction in the fission track age, because of the reduced proportion of tracks which can intersect the polished surface. Therefore, the fission track age is also highly temperature dependent, falling to zero at around 120°C due to total erasure of all tracks.



Samples which have been heated to a maximum paleotemperature less than $\sim 120^{\circ}\text{C}$ at some time in the past and subsequently cooled will contain two populations of tracks, and will show a more complex distribution of lengths and ages. If the maximum paleotemperature was less than $\sim 50^{\circ}\text{C}$ then the two components will not be resolvable, but for maximum paleotemperatures between $\sim 50^{\circ}$ and 120°C the presence of two components can readily be identified. Tracks formed prior to the thermal maximum will all be shortened to approximately the same degree (the precise value depending on the maximum paleotemperature), while those formed during and after cooling will be longer, due to the lower prevailing temperatures. The length distribution in such samples will be broader than in the simple case, consisting of a shorter and a longer component, and the fission track age will reflect the amount of length reduction shown by the shorter component (determined by the maximum paleotemperature).

If the maximum paleotemperature was sufficient to shorten tracks to between 9 and 11 μm , and cooling to temperatures of $\sim 50^{\circ}\text{C}$ or less was sufficiently rapid, tracks formed after cooling will have lengths of 14-15 μm and the resulting track length distribution will show a characteristic bimodal form. If the maximum paleotemperature was greater than ~ 110 to 120°C , all pre-existing tracks will be erased, and all tracks now present will have formed after the onset of cooling. The fission track age in such samples relates directly to the time of cooling.

In thermal history scenarios in which a heating episode is followed by cooling and then temperature increases again, the tracks formed during the second heating phase will undergo progressive shortening. The tracks formed prior to the initial cooling, which were shortened in the first heating episode, will not undergo further shortening until the temperature exceeds the maximum temperature reached in the earlier heating episode. (In practice, differences in timescale of heating can complicate this simple description. In detail, it is the integrated time-temperature effect of the two heating episodes which should be considered.) If the maximum and peak paleotemperatures in the two episodes are sufficiently different ($>\sim 10^{\circ}\text{C}$), and the later peak paleotemperature is less than the earlier maximum value, then the AFTA parameters allow determination of both episodes. As the peak paleotemperature in the later episode approaches the earlier maximum, the two generations of tracks become increasingly more difficult to resolve, and when the two paleotemperatures are the same, both components are shortened to an identical degree and all information on the earlier heating phase will be lost.

No information is preserved on the approach to maximum paleotemperature because the great majority of tracks formed up to that time have the same mean track length. Only those tracks formed in the last few per cent of the history prior to the onset of cooling



are not shortened to the same degree (because temperature dominates over time in the annealing kinetics). These form a very small proportion of the total number of tracks and therefore cannot be resolved within the length distribution because of the inherent spread of several μm in the length distribution.

To summarise, AFTA allows determination of the magnitude of the maximum temperature and the time at which cooling from that maximum began. In some circumstances, determination of a subsequent peak paleotemperature and the time of cooling is also possible.

C.3 Quantitative understanding of fission track annealing in apatite

Annealing kinetics and modelling the development of AFTA parameters

Our understanding of the behaviour of fission tracks in apatite during geological thermal histories is based on study of the response of fission tracks to elevated temperatures in the laboratory (Green et al., 1986; Laslett et al., 1987; Duddy et al., 1988; Green et al., 1989b), in geological situations (Green et al. 1989a), observations of the lengths of spontaneous tracks in apatites from a wide variety of geological environments (Gleadow et al. 1986), and the relationship between track length reduction and reduction in fission track age observed in controlled laboratory experiments (Green, 1988).

These studies resulted in the capability to simulate the development of AFTA parameters resulting from geological thermal histories for an apatite of average composition (Durango apatite, ~ 0.43 wt% Cl). Full details of this modelling procedure have been explained in Green et al. (1989b). The following discussion presents a brief explanation of the approach.

Geological thermal histories involving temperatures varying through time are broken down into a series of isothermal steps. The progressive shortening of track length through sequential intervals is calculated using the extrapolated predictions of an empirical kinetic model fitted to laboratory annealing data. Contributions from tracks generated throughout the history (remembering that new tracks are continuously generated through time as new fissions occur) are summed to produce the final distribution of track lengths expected to result from the input history. In summing these components, care is taken to allow for various biases which affect revelation of confined tracks (Laslett et al. 1982). The final length reduction of each component of



tracks is converted to a contribution of fission track age, using the relationship between track length and density reduction determined by Green (1988). These age contributions are summed to generate the final predicted fission track age.

This approach depends critically on the assumption that extrapolation of the laboratory-based kinetic model to geological timescales, over many orders of magnitude in time, is valid. This was assessed critically by Green et al. (1989b), who showed that predictions from this approach agree well with observed AFTA parameters in apatites of the appropriate composition in samples from a series of reference wells in the Otway Basin of south-east Australia (Gleadow and Duddy, 1981; Gleadow et al., 1983; Green et al., 1989a). This point is illustrated in Figure C.1. Green et al. (1989b) also quantitatively assessed the errors associated with extrapolation of the Laslett et al. (1987) model from laboratory to geological timescales (i.e. precision, as opposed to accuracy). Typical levels of precision are $\sim 0.5 \mu\text{m}$ for mean lengths $< \sim 10 \mu\text{m}$, and $\sim 0.3 \mu\text{m}$ for lengths $> \sim 10 \mu\text{m}$. These figures are equivalent to an uncertainty in estimates of maximum paleotemperature derived using this approach of $\sim 10^\circ\text{C}$. Precision is largely independent of thermal history for any reasonable geological history. Accuracy of prediction from this model is limited principally by the effect of apatite composition on annealing kinetics, as explained in the next section.

Compositional effects

Natural apatites essentially have the composition $\text{Ca}_5(\text{PO}_4)_3(\text{F}, \text{OH}, \text{Cl})$. Most common detrital and accessory apatites are predominantly Fluor-apatites, but may contain appreciable amounts of chlorine. The amount of chlorine in the apatite lattice exerts a subtle compositional control on the degree of annealing, with apatites richer in fluorine being more easily annealed than those richer in chlorine. The result of this effect is that in a single sample, individual apatite grains may show a spread in the degree of annealing (i.e. length reduction and fission track age reduction). This effect becomes most pronounced in the temperature range $90 - 120^\circ\text{C}$ (assuming a heating timescale of $\sim 10 \text{ Ma}$), and can be useful in identifying samples exposed to paleotemperatures in this range. At temperatures below $\sim 80^\circ\text{C}$, the difference in annealing sensitivity is less marked, and compositional effects can largely be ignored.

Our original quantitative understanding of the kinetics of fission track annealing, as described above, relates to a single apatite (Durango apatite) with $\sim 0.43 \text{ wt\% Cl}$, on which most of our original experimental studies were carried out. Recently, we have extended this quantitative understanding to apatites with Cl contents up to $\sim 3 \text{ wt\%}$. This new, multi-compositional kinetic model is based both on new laboratory annealing



studies on a range of apatites with different F-Cl compositions (Figure C.2), and on observations of geological annealing in apatites from a series of samples from exploration wells in which the section is currently at maximum temperature since deposition. A composite model for Durango apatite composition was first created by fitting a common model to the old laboratory data (from Green et al., 1986) and the new geological data for a similar composition. This was then extended to other compositions on the basis of the multi-compositional laboratory and geological data sets. Details of the multi-compositional model are contained in a Technical Note, available from Geotrack in Melbourne.

The multi-compositional model allows prediction of AFTA parameters for any Cl content between 0 and 3 wt%, using a similar approach to that used in our original single composition modelling, as outlined above. Then, for an assumed or measured distribution of Cl contents within a sample, the composite parameters for the sample can be predicted. The range of Cl contents from 0 to 3 wt% spans the range of compositions commonly encountered, as discussed in the next section.

Predictions of the new multi-compositional model are in good agreement with the geological constraints on annealing rates provided by the Otway Basin reference wells, as shown in Figure C.3. However, note that the AFTA data from these Otway Basin wells were among those used in construction of the new model, so this should not be viewed as independent verification, but rather as a demonstration of the overall consistency of the model.

Distributions of Cl content in common AFTA samples

Figure C.4a shows a histogram of Cl contents, measured by electron microprobe, in apatite grains from more than 100 samples of various types. Most grains have Cl contents less than ~0.5 wt%. The majority of grains with Cl contents greater than this come from volcanic sources and basic intrusives, and contain up to ~2 wt% Cl. Figure C.4b shows the distribution of Cl contents measured in randomly selected apatite grains from 61 samples of "typical" quartzo-feldspathic sandstone. This distribution is similar to that in Figure C.4a, except for a more rapid fall-off as Cl content increases. Apatites from most common sandstones give distributions of Cl content which are very similar to that in Figure C.4b. Volcanogenic sandstones typically contain apatites with higher Cl contents, with a much flatter distribution for Cl contents up to ~1.5%, falling to zero at ~2.5 to 3 wt%, as shown in Figure C.4c. Cl contents in granitic basement samples and high-level intrusives are typically much more dominated by compositions close to end-member Fluorapatite, although many exceptions occur to this general rule.



Information about the spread of Cl contents in samples analysed in this report can be found in Appendix A.

Alternative kinetic models

Recently, both Carlson (1990) and Crowley et al. (1991) have published alternative kinetic models for fission track annealing in apatite. Carlson's model is based on our laboratory annealing data for Durango apatite (Green et al., 1986) and other (unpublished) data. In his abstract, Carlson claims that because his model is "based on explicit physical mechanisms, extrapolations of annealing rates to the lower temperatures and longer timescales required for the interpretation of natural fission track length distributions can be made with greater confidence than is the case for purely empirical relationships fitted to the experimental annealing data". As explained in detail by Green et al. (1993), all aspects of Carlson's model are in fact purely empirical, and his model is inherently no "better" for the interpretation of data than any other. In fact, detailed inspection shows that Carlson's model does not fit the laboratory data set at all well. Therefore, we recommend against use of this model to interpret AFTA data.

The approach taken by Crowley et al. (1991) is very similar to that taken by Laslett et al., (1987). They have fitted models to new annealing data in two apatites of different composition - one close to end-member Fluorapatite (B-5) and one having a relatively high Sr content (113855). The model developed by Crowley et al. (1991) from their own annealing data for the B-5 apatite gives predictions in geological conditions which are consistently higher than measured values, as shown in Figure C.5. Corrigan (1992) reported a similar observation in volcanogenic apatites in samples from a series of West Texas wells. Since the B-5 apatite is close to end-member Fluor-apatite, while the Otway Group apatites contain apatites with Cl contents from zero up to ~3 wt% (and the West Texas apatites have up to 1 wt%), the fluorapatites should have mean lengths rather less than the measured values, which should represent a mean over the range of Cl contents present. Therefore, the predictions of the Crowley et al. (1991) B-5 model appear to be consistently high.

We attribute this to the rather restricted temperature-time conditions covered by the experiments of Crowley et al. (1991), with annealing times between one and 1000 hours, in contrast to times between 20 minutes and 500 days in the experiments of Green et al. (1986). In addition, few of the measured length values in Crowley et al.'s study fall below 11 μm (in only five out of 60 runs in which lengths were measured in apatite B-5) and their model is particularly poorly defined in this region.



Crowley et al. (1991) also fitted a new model to the annealing data for Durango apatite published by Green et al. (1986). Predictions of their fit to our data are not very much different to those from the Laslett et al. (1987) model (Figure C.6). We have not pursued the differences between their model and ours in detail because the advent of our multi-compositional model has rendered the single compositional approach obsolete.

C.4 Evidence for elevated paleotemperatures from AFTA

The basic principle involved in the interpretation of AFTA data in sedimentary basins is to determine whether the degree of annealing shown by tracks in apatite from a particular sample could have been produced if the sample has never been hotter than its present temperature at any time since deposition. To do this, the burial history derived from the stratigraphy of the preserved sedimentary section is used to calculate a thermal history for each sample using the present geothermal gradient and surface temperature (i.e. assuming these have not changed through time). This is termed the "Default Thermal History". For each sample, the AFTA parameters predicted as a result of the Default Thermal History are then compared to the measured data. If the data show a greater degree of annealing than calculated on the basis of this history, the sample must have been hotter at some time in the past. In this case, the AFTA data are analysed to provide estimates of the magnitude of the maximum paleotemperature in that sample, and the time at which cooling commenced from the thermal maximum.

The degree of annealing is assessed in two ways - from fission track age and track length data. The stratigraphic age provides a basic reference point for the interpretation of fission track age, because reduction of the fission track age below the stratigraphic age unequivocally reveals that appreciable annealing has taken place after deposition of the host sediment. Large degrees of fission track age reduction, with the pooled or central fission track age very much less than the stratigraphic age, indicate severe annealing, which requires paleotemperatures of at least $\sim 100^{\circ}\text{C}$ for any reasonable geological time-scale of heating ($> \sim 1$ Ma). Note that this applies even when apatites contain tracks inherited from source areas. More moderate degrees of annealing can be detected by inspection of the single grain age data, as the most sensitive (fluorine-rich) grains will begin to give fission track ages significantly less than the stratigraphic age before the central or pooled age has been reduced sufficiently to give a noticeable signal. Note that this aspect of the single grain age data can also be used for apatites which have tracks inherited from source areas. If signs of moderate annealing (from single grain age reduction) or severe annealing (from the reduction in pooled or central



age) are seen in samples in which the Default Thermal History predicts little or no effect, the sample must have been subjected to elevated paleotemperatures at some time in the past. Figure C.7 shows how increasing degrees of annealing are observable in radial plots of the single grain fission track age data.

Similarly, the present temperature from which a sample is taken, and the way in which this has been approached (as inferred from the preserved sedimentary section), forms a basic point of reference for track length data. The observed mean track length is compared with the mean length predicted from the Default Thermal History. If the observed degree of track shortening in a sample is greater than that expected from the Default Thermal History (i.e. the mean length is significantly less than the predicted value), either the sample must have been subjected to higher paleotemperatures at some time after deposition, or the sample contains shorter tracks which were inherited from sediment source areas at the time the sediment was deposited. If shorter tracks were inherited from source areas, the sample should still contain a component of longer tracks corresponding to the tracks formed after deposition. In general, the fission track age should be greater than the stratigraphic age. This can be assessed quantitatively using the computer models for the development of AFTA parameters described in an earlier section. If the presence of shorter tracks cannot be explained by their inheritance from source areas, the sample must have been hotter in the past.

C.5 Quantitative determination of the magnitude of maximum paleotemperature and the timing of cooling using AFTA

Values of maximum paleotemperature and timing of cooling in each sample are determined using a forward modelling approach based on the quantitative description of fission track annealing described in earlier sections. The Default Thermal History described above is used as the basis for this forward modelling, but with the addition of episodes of elevated paleotemperatures as required to explain the data. AFTA parameters are modelled iteratively through successive thermal history scenarios in order to identify thermal histories that can account for observed parameters. The range of values of maximum paleotemperature and timing of cooling which can account for the measured AFTA parameters (fission track age and track length distribution) are defined using a maximum likelihood-based approach. In this way, best estimates ("maximum likelihood values") can be defined together with $\pm 95\%$ confidence limits.

In samples in which all tracks have been totally annealed at some time in the past, only a minimum estimate of maximum paleotemperature is possible. In such cases, AFTA



data provide most control on the time at which the sample cooled to temperatures at which tracks could be retained. The time at which cooling began could be earlier than this time, and therefore the timing also constitutes a minimum estimate.

Comparison of the AFTA parameters predicted by the multi-compositional model with measured values in samples which are currently at their maximum temperatures since deposition shows a good degree of consistency, suggesting the uncertainty in application of the model should be less than $\pm 10^\circ\text{C}$. This constitutes a significant improvement over earlier approaches, since the kinetic models used are constrained in both laboratory and geological conditions. It should be appreciated that relative differences in maximum paleotemperature can be identified with greater precision than absolute paleotemperatures, and it is only the estimation of absolute paleotemperature values to which the $\pm 10^\circ\text{C}$ uncertainty relates.

Cooling history

If the data are of high quality and provided that cooling from maximum paleotemperatures began sufficiently long ago (so that the history after this time is represented by a significant proportion of the total tracks in the sample), determination of the magnitude of a subsequent peak paleotemperature and the timing of cooling from that peak may also be possible (as explained in Section C.2). A similar approach to that outlined above provides best estimates and corresponding $\pm 95\%$ confidence limits for this episode. Such estimates may simply represent part of a protracted cooling history, and evidence for a later discrete cooling episode can only be accepted if this scenario provides a significantly improved fit to the data. Geological evidence and consistency of estimates between a series of samples can also be used to verify evidence for a second episode.

In practise, most typical AFTA datasets are only sufficient to resolve two discrete episodes of heating and cooling. One notable exception to this is when a sample has been totally annealed in an early episode, and has then undergone two (or more) subsequent episodes with progressively lower peak paleotemperatures in each. But in general, complex cooling histories involving a series of episodes of heating and cooling will allow resolution of only two episodes, and the results will depend on which episodes dominate the data. Typically this will be the earliest and latest episodes, but if multiple cooling episodes occur within a narrow time interval the result will represent an approximation to the actual history.



C.6 Qualitative assessment of AFTA parameters

Various aspects of thermal history can often be assessed by qualitative assessment of AFTA parameters. For example, samples which have reached maximum paleotemperatures sufficient to produce total annealing, and which only contain tracks formed after the onset of cooling, can be identified from a number of lines of evidence. In a vertical sequence of samples showing increasing degrees of annealing, the transition from rapidly decreasing fission track age with increasing depth to more or less the same age over a range of depth denotes the transition from partial to total annealing of all tracks formed prior to the thermal maximum. In samples in which all tracks have been totally annealed, the single grain age data should show that none of the individual grain fission track ages are significantly older than the time of cooling, and grains in all compositional groups should give the same fission track age unless the sample has been further disturbed by a later episode. If the sample cooled rapidly to sufficiently low temperatures, little annealing will have taken place since cooling, and all grains will give ages which are compatible with a single population around the time of cooling, as shown in Figure C.7.

Inspection of the distribution of single grain ages in partially annealed samples can often yield useful information on the time of cooling, as the most easily annealed grains (those richest in fluorine) may have been totally annealed prior to cooling, while more retentive (Cl-rich) compositions were only partially annealed (as in Figure C.7, centre). The form of the track length distribution can also provide information, from the relative proportions of tracks with different lengths. All of these aspects of the data can be used to reach a preliminary thermal history interpretation.

C.7 Allowing for tracks inherited from source areas

The effect of tracks inherited from source areas, and present at the time the apatite is deposited in the host sediment, is often posed as a potential problem for AFTA. However, this can readily be allowed for in analysing both the fission track age and length data.

In assessing fission track age data to determine the degree of annealing, the only criterion used is the comparison of fission track age with the value expected on the basis of the Default Thermal History. From this point of view, inherited tracks do not affect the conclusion: if a grain or a sample gives a fission track age which is significantly less than expected, the grain or sample has clearly undergone a higher degree of annealing



than can be accounted for by the Default Thermal History, and therefore must have been hotter in the past, whether the sample contained tracks when it was deposited or not.

The presence of inherited tracks does impose a limit on our ability to detect post-depositional annealing from age data alone, as in samples which contain a fair proportion of inherited tracks, moderate degrees of annealing may reduce the fission track age from the original value, but not to a value which is significantly less than the stratigraphic age. This is particularly noticeable in the case of Tertiary samples containing apatites derived from Paleozoic basement. In such cases, although fission track age data may show no evidence of post-depositional annealing, track length data may well show such evidence quite clearly.

The influence of track lengths inherited from source areas can be allowed for by comparison of the fission track age with the value predicted by the Default Thermal History combined with inspection of the track length distribution. If the mean length is much less than the length predicted by the Default Thermal History, either the sample has been subjected to elevated paleotemperatures, sufficient to produce the observed degree of length reduction, or else the sample contains a large proportion of shorter tracks inherited from source areas. However, in the latter case, the sample should give a pooled or central fission track age correspondingly older than the stratigraphic age, while the length distribution should contain a component of longer track lengths corresponding to the value predicted by the Default Thermal History. It is important in this regard that the length of a track depends primarily on the maximum temperature to which it has been subjected, whether in the source regions or after deposition in the sedimentary basin. Thus, any tracks retaining a provenance signature will have lengths towards the shorter end of the distribution where track lengths will not have "equilibrated" with the temperatures attained since deposition.

In general, it is only in extreme cases that inherited tracks render track length data insensitive to post-depositional annealing. For example, if practically all the tracks in a particular sample were formed prior to deposition, perhaps in a Pliocene sediment in which apatites were derived from a stable Paleozoic shield with fission track ages of ~300 Ma or more, the track length distribution will, in general, be dominated by inheritance, as only ~2% of tracks would have formed after deposition. Post-depositional heating will not be detectable as long as the maximum paleotemperature is insufficient to cause greater shortening than that which occurred in the source terrain. Even in such extreme cases, once a sample is exposed to temperatures sufficient to produce greater shortening than that inherited from source areas, the inherited tracks and those formed after deposition will all undergo the same degree of shortening, and



the effects of post-depositional annealing can be recognised. In such cases, the presence of tracks inherited from source areas is actually very useful, because the number of tracks formed after deposition is so small that little or no information would be available without the inherited tracks.

C.8 Plots of fission track age and mean track length vs depth and temperature

AFTA data from well sequences are usually plotted as shown in Figure C.8. This figure shows AFTA data for two scenarios: one in which deposition has been essentially continuous from the Carboniferous to the present and all samples are presently at their maximum paleotemperature since deposition (Figure C.8a); and, one in which the section was exposed to elevated paleotemperatures prior to cooling in the Early Tertiary (Figure C.8b).

In both figures, fission track age and mean track length are plotted against depth and present temperature. Presentation of AFTA data in this way often provides insight into the thermal history interpretation, following principles outlined earlier in this Appendix.

In Figure C.8a, for samples at temperatures below $\sim 70^{\circ}\text{C}$, the fission track age is either greater than or close to the stratigraphic age, and little fission track age reduction has affected these samples. Track lengths in these samples are all greater than $\sim 13\ \mu\text{m}$. In progressively deeper samples, both the fission track age and mean track length are progressively reduced to zero at a present temperature of around 110°C , with the precise value depending on the spread of apatite compositions present in the sample. Track length distributions in the shallowest samples would be a mixture of tracks retaining information on the thermal history of source regions, while in deeper samples, all tracks would be shortened to a length determined by the prevailing temperature. This pattern of AFTA parameters is characteristic of a sequence which is currently at maximum temperatures.

The data in Figure C.8b show a very different pattern. The fission track age data show a rapid decrease in age, with values significantly less than the stratigraphic age at temperatures of ~ 40 to 50°C , at which such a degree of age reduction could not be produced in any geological timescale. Below this rapid fall, the fission track ages do not change much over $\sim 1\ \text{km}$ (30°C). This transition from rapid fall to consistent ages is diagnostic of the transition from partial to total annealing. Samples above the "break-in slope" contain two generations of tracks: those formed prior to the thermal maximum, which have been partially annealed (shortened) to a degree which depends



on the maximum paleotemperature; and, those formed after cooling, which will be longer. Samples below the break-in slope contain only one generation of tracks, formed after cooling to lower temperatures at which tracks can be retained. At greater depths, where temperatures increase to $\sim 90^{\circ}\text{C}$ and above, the effect of present temperatures begins to reduce the fission track ages towards zero, as in the "maximum temperatures now" case.

The track length data also reflect the changes seen in the fission track age data. At shallow depths, the presence of the partially annealed tracks shortened prior to cooling causes the mean track length to decrease progressively as the fission track age decreases. However, at depths below the break in slope in the age profile, the track length increases again as the shorter component is totally annealed and so does not contribute to the measured distribution of track lengths. At greater depths, the mean track lengths decrease progressively to zero once more due to the effects of the present temperature regime.

Examples of such data have been presented, e.g. by Green (1989) and Kamp and Green (1990).

C.9 Determining paleogeothermal gradients and amount of section removed on unconformities

Estimates of maximum paleotemperatures in samples over a range of depths in a vertical sequence provides the capability of determining the paleogeothermal gradient immediately prior to the onset of cooling from those maximum paleotemperatures. The degree to which the paleogeothermal gradient can be constrained depends on a number of factors, particularly the depth range over which samples are analysed. If samples are only analysed over ~ 1 km, then the paleotemperature difference over that range may be only ~ 20 to 30°C . Since maximum paleotemperatures can often only be determined within a $\sim 10^{\circ}\text{C}$ range, this introduces considerable uncertainty into the final estimate of paleogeothermal gradient (see Figure C.9)

Another important factor is the difference between maximum paleotemperatures and present temperatures ("net cooling"). If this is only $\sim 10^{\circ}\text{C}$, which is similar to the uncertainty in absolute paleotemperature determination, only broad limits can be established on the paleogeothermal gradient. In general, the control on the paleogeothermal gradient improves as the amount of net cooling increases. However, if the net cooling becomes so great that many samples were totally annealed prior to the



onset of cooling - so that only minimum estimates of maximum paleotemperatures are possible - constraints on the paleogeothermal gradient from AFTA come only from that part of the section in which samples were not totally annealed. In this case, integration of AFTA data with VR measurements can be particularly useful in constraining the paleo-gradient.

Having constrained the paleogeothermal gradient at the time cooling from maximum paleotemperatures began, if we assume a value for surface temperature at that time, the amount of section subsequently removed by uplift and erosion can be calculated as shown in Figure C.10. The *net* amount of section removed is obtained by dividing the difference between the paleo-surface temperature (T_s) and the intercept of the paleotemperature profile at the present ground surface (T_i) by the estimated paleogeothermal gradient. The *total* amount of section removed is obtained by adding the thickness of section subsequently redeposited above the unconformity to the *net* amount estimated as in Figure C.10. If the analysis is performed using depths from the appropriate unconformity, then the analysis will directly yield the *total* amount of section removed.

Geotrack have developed a method of deriving estimates of both the paleogeothermal gradient and the net amount of section removed using estimated paleotemperatures derived from AFTA and VR. Perhaps more importantly, this method also provides rigorous values for upper and lower 95% confidence limits on each parameter. The method is based on maximum likelihood estimation of the paleogeothermal gradient and the surface intercept, from a table of paleotemperature and depth values. The method is able to accept ranges for paleotemperature estimates (e.g. where the maximum paleotemperature can only be constrained to between, for example, 60 and 90°C), as well as upper and lower limits (e.g. <60°C for samples which show no detectable annealing; >110°C in samples which were totally annealed). Estimates of paleotemperature from AFTA and VR may be combined or analysed separately. Some results from this method have been reported by Bray et al. (1992). Full details of the methods employed are presented in a confidential, in-house, Geotrack research report, copies of which are available on request from the Melbourne office.

Results are presented in two forms. Likelihood profiles, plotting the log-likelihood as a function of either gradient or section removed, portray the probability of a given value of gradient or section removed. The best estimate is given by the value of gradient or section removed for which the log-likelihood is maximised. Ideally, the likelihood profiles should show a quadratic form, and values of gradient or section removed at which the log-likelihood has fallen by two from the maximum value define the upper



and lower 95% confidence limits on the estimates. An alternative method of portraying this information is a crossplot of gradient against section removed, in which values which fall within 95% confidence limits (in two dimensions) are contoured. Note that the confidence limits defined by this method are rather tighter than those from the likelihood profiles, as the latter only reflect variation in one parameter, whereas the contoured crossplot takes variation of both parameters into account.

It must be emphasised that this method relies on the assumption that the paleotemperature profile was linear both throughout the section analysed and through the overlying section which has been removed. While the second part of this assumption can never be confirmed independently, visual inspection of the paleotemperature estimates as a function of depth should be sufficient to verify or deny the linearity of the paleotemperature profile through the preserved section.

Results of this procedure are shown in this report if the data allow sufficiently well-defined paleotemperature estimates to justify use of the method. Where the AFTA data suggest that the section is currently at maximum temperature since deposition, or that the paleotemperature profile was non-linear, or where data are of insufficient quality to allow rigorous paleotemperature estimation, the method is not used.

C.10 Thermal history interpretation of Zircon Fission Track Age data

The understanding of the annealing characteristics of fission tracks in zircon is not as well developed as for apatite. From both laboratory and geological evidence, fission tracks in zircon are known to be less sensitive to annealing than fission tracks in apatite. Zircon fission track ages are conventionally interpreted in terms of a closure temperature, defined as the nominal temperature below which a radiogenic product, in this case fission tracks, is effectively retained. Although the closure temperature in zircon is not well constrained, geological evidence suggests values between 175° and 300°C. Based on comparison of zircon fission track ages with ages from other radiometric systems, Hurford (1986) proposed a closure temperature for fission track retention in zircon of $240^{\circ} \pm 50^{\circ}\text{C}$. A value around 240°C or possibly higher is broadly consistent with all available evidence, although the $\pm 50^{\circ}\text{C}$ quoted uncertainty would allow unrealistically low values, and our experience suggests a value between 220 and 300°C would be most appropriate.

In contrast, tracks in apatite begin to be retained when the mineral cools below a temperature of the order of $\sim 110^{\circ}\text{-}120^{\circ}\text{C}$ (depending on apatite composition). Where



fission track ages are available for apatite and zircon, the cooling history of a sample can be assessed because of the differing thermal sensitivities of the tracks in the minerals. In samples which have cooled rapidly from high temperatures of $>240^{\circ}\text{C}$ to less than $\sim 50^{\circ}\text{C}$, the apatite and zircon fission track ages are usually concordant, as tracks in both minerals began to be retained at roughly the same time.

The type of analysis presented for apatite data is not possible in zircon, because it is not usually possible to measure track lengths in zircon due to the etching properties of the mineral. This makes it difficult to determine whether a thermally affected zircon fission track age represents partial or total annealing, and, thus, whether the fission track age can be interpreted in terms of a specific "event". Another problem with the interpretation of zircon data is posed by the lack of constraint on the temperatures required for a given degree of partial annealing. Therefore, unlike the situation with apatite, it is not possible to rigorously estimate maximum paleotemperatures on the basis of zircon data alone. On the basis of experience in a small number of sedimentary basins, it appears that significant age reduction in zircon does not normally occur below temperatures of $\sim 200^{\circ}\text{C}$. However, the effects of composition on annealing rates in zircon are not well understood, and it is possible that some particularly sensitive zircons may exist which undergo annealing at lower temperatures.

Investigation of zircon data in samples with different levels of vitrinite reflectance suggests that no significant age reduction occurs in zircon at VR levels below $\sim 4\%$. VR values in excess of 5% are required in order to produce any significant age reduction. Some evidence suggests that the rock needs to reach the stage of incipient recrystallisation in order to produce observable effects in zircon.

Based on all evidence currently available, we define the following broad paleotemperature ranges which may be defined on the basis of ZFTA data:

Some age reduction	$200\text{-}300^{\circ}\text{C}$
Appreciable age reduction	$\geq 240^{\circ}\text{C}$
Total annealing of most grains	$>300^{\circ}\text{C}$

It should be borne in mind that these paleotemperatures are only very loosely constrained, and any conclusions based thereon should be treated with caution.



References

- Carlson, W.D. (1990) Mechanisms and kinetics of apatite fission-track annealing. *American Mineralogist*, 75, 1120 - 1139.
- Corrigan, J. (1992) Annealing models under the microscope, *On Track*, 2, 9-11.
- Crowley, K.D., Cameron, M. and Schaefer, R.L. (1991) Experimental studies of annealing of etched fission tracks in apatite. *Geochimica et Cosmochimica Acta*, 55, 1449-1465.
- Duddy, I.R., Green, P.F. and Laslett G.M. (1988) Thermal annealing of fission tracks in apatite 3. Variable temperature behaviour. *Chem. Geol. (Isot. Geosci. Sect.)*, 73, 25-38.
- Gleadow, A.J.W. and Duddy, I.R. (1981) A natural long-term track annealing experiment for apatite. *Nuclear Tracks*, 5, 169-174.
- Gleadow, A.J.W., Duddy, I.R. and Lovering, J.F. (1983) Fission track analysis; a new tool for the evaluation of thermal histories and hydrocarbon potential. *APEA J*, 23, 93-102.
- Gleadow, A.J.W., Duddy, I.R., Green, P.F. and Lovering, J.F. (1986) Confined fission track lengths in apatite - a diagnostic tool for thermal history analysis. *Contr. Min. Petr.*, 94, 405-415.
- Green, P.F. (1988) The relationship between track shortening and fission track age reduction in apatite: Combined influences of inherent instability, annealing anisotropy, length bias and system calibration. *Earth Planet. Sci. Lett.*, 89, 335-352.
- Green, P.F., Duddy, I.R., Gleadow, A.J.W., Tingate, P.R. and Laslett, G.M. (1986) Thermal annealing of fission tracks in apatite 1. A qualitative description. *Chem. Geol. (Isot. Geosci. Sect.)*, 59, 237-253.
- Green, P.F., Duddy, I.R., Gleadow, A.J.W. and Lovering, J.F. (1989a) Apatite Fission Track Analysis as a paleotemperature indicator for hydrocarbon exploration. In: Naeser, N.D. and McCulloh, T. (eds.) *Thermal history of sedimentary basins - methods and case histories*, Springer-Verlag, New York, 181-195.
- Green, P.F., Duddy, I.R., Laslett, G.M., Hegarty, K.A., Gleadow, A.J.W. and Lovering, J.F. (1989b) Thermal annealing of fission tracks in apatite 4. Quantitative modelling techniques and extension to geological timescales. *Chem. Geol. (Isot. Geosci. Sect.)*, 79, 155-182.
- Green, P.F., Laslett, G.M. and Duddy, I.R. (1993) Mechanisms and kinetics of apatite fission track annealing: Discussion. *American Mineralogist*, 78, 441-445.
- Hurford, A.J. (1986) Cooling and uplift patterns in the Lepontine Alps, South Central Switzerland and an age of vertical movement on the Insubric fault line. *Contrib. Mineral. Petrol.*, 92, 413-427.
- Laslett, G.M., Kendall, W.S., Gleadow, A.J.W. and Duddy, I.R. (1982) Bias in measurement of fission track length distributions. *Nuclear Tracks*, 6, 79-85.
- Laslett, G.M., Green, P.F., Duddy, I.R. and Gleadow, A.J.W. (1987) Thermal annealing of fission tracks in apatite 2. A quantitative analysis. *Chem. Geol. (Isot. Geosci. Sect.)*, 65, 1-13.

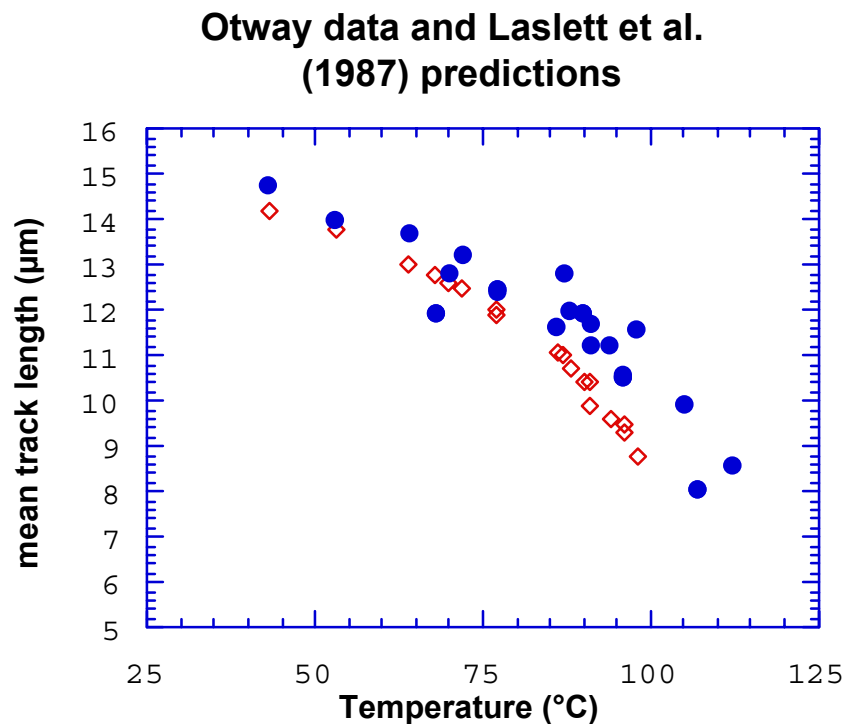


Figure C.1a Comparison of mean track length (solid circles) measured in samples from four Otway Basin reference wells (from Green et al, 1989a) and predicted mean track lengths (open diamonds) from the kinetic model of fission track annealing from Laslett et al. (1987). The predictions underestimate the measured values, but they refer to an apatite composition that is more easily annealed than the majority of apatites in these samples, so this is expected.

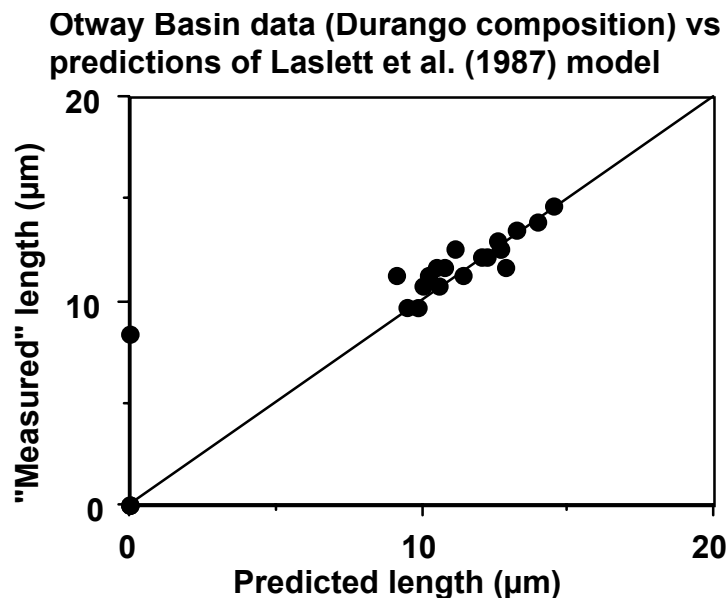


Figure C.1b Comparison of the mean track length in apatites of the same Cl content as Durango apatite from the Otway Group samples illustrated in figure C.1a, with values predicted for apatite of the same composition by the model of Laslett et al. (1987). The agreement is clearly very good except possibly at lengths below $\sim 10 \mu\text{m}$.

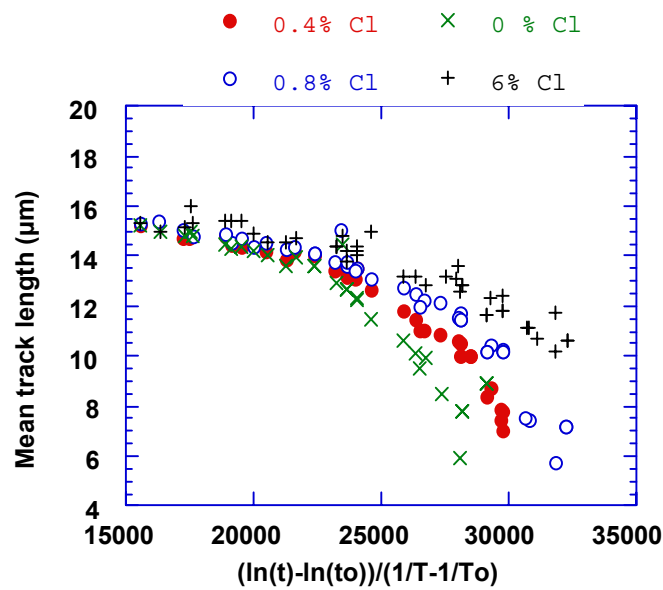


Figure C.2 Mean track length in apatites with four different chlorine contents, as a combined function of temperature and time, to reduce the data to a single scale. Fluorapatites are more easily annealed than chlorapatites, and the annealing kinetics show a progressive change with increasing Cl content.

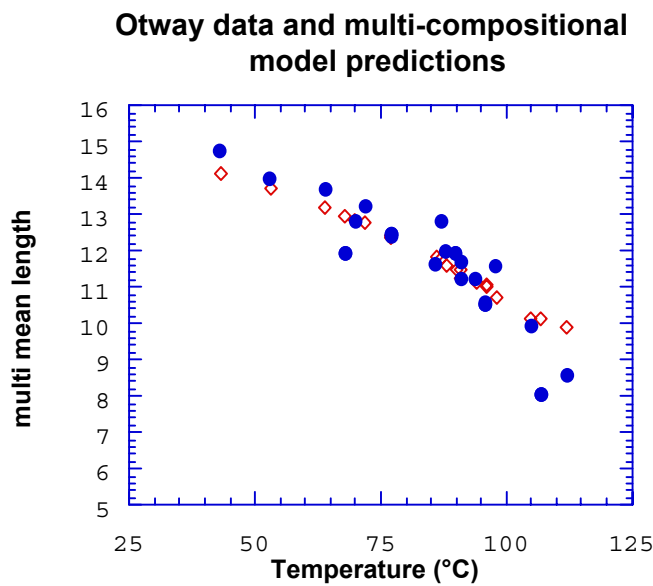
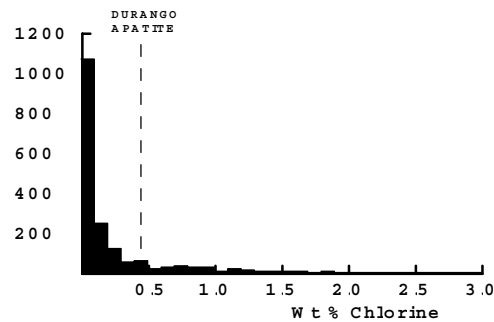


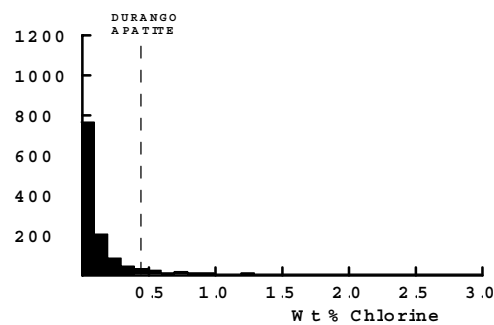
Figure C.3 Comparison of measured mean track length (solid circles) in samples from four Otway Basin reference wells (from Green et al, 1989a) and predicted mean track lengths (open diamonds) from the new multi-compositional kinetic model of fission track annealing described in Section C.3. This model takes into account the spread of Cl contents in apatites from the Otway Group samples and the influence of Cl content on annealing rate. The agreement is clearly very good over the range of the data.



All samples



"Normal sandstones"



Volcanogenic sandstones

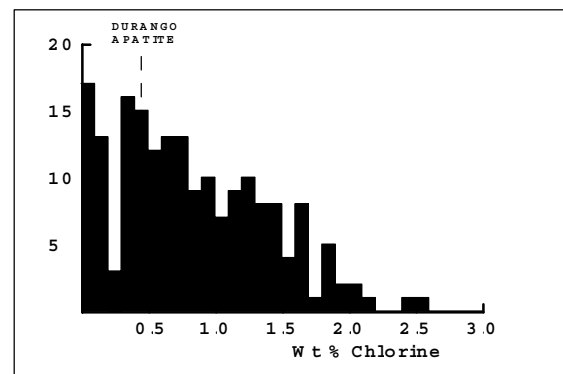


Figure C.4 **a:** Histogram of Cl contents (wt%) in over 1750 apatite grains from over 100 samples of various sedimentary and igneous rocks. Most samples give Cl contents below ~0.5 wt %, while those apatites giving higher Cl contents are characteristic of volcanogenic sandstones and basic igneous sources.

b: Histogram of Cl contents (wt%) in 1168 apatite grains from 61 samples which can loosely be characterised as "normal sandstone". The distribution is similar to that in the upper figure, except for a lower number of grains with Cl contents greater than ~1%.

c: Histogram of Cl contents (wt%) in 188 apatite grains from 15 samples of volcanogenic sandstone. The distribution is much flatter than the other two, with much higher proportion of Cl-rich grains.

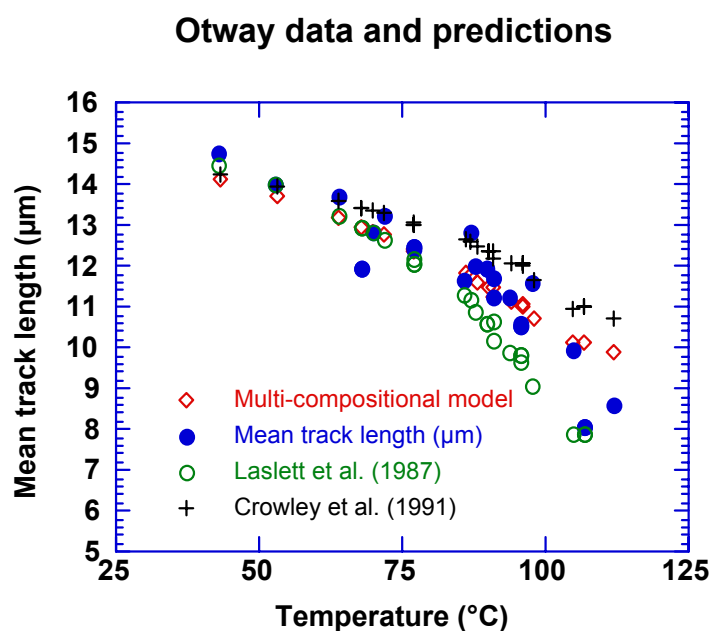


Figure C.5 Comparison of mean track length in samples from four Otway Basin reference wells (from Green et al., 1989a) and predicted mean track lengths from three kinetic models for fission track annealing. The Crowley et al. (1991) model relates to almost pure Fluorapatite (B-5), yet overpredicts mean lengths in the Otway Group samples which are dominated by Cl-rich apatites. The predictions of that model are therefore not reliable.

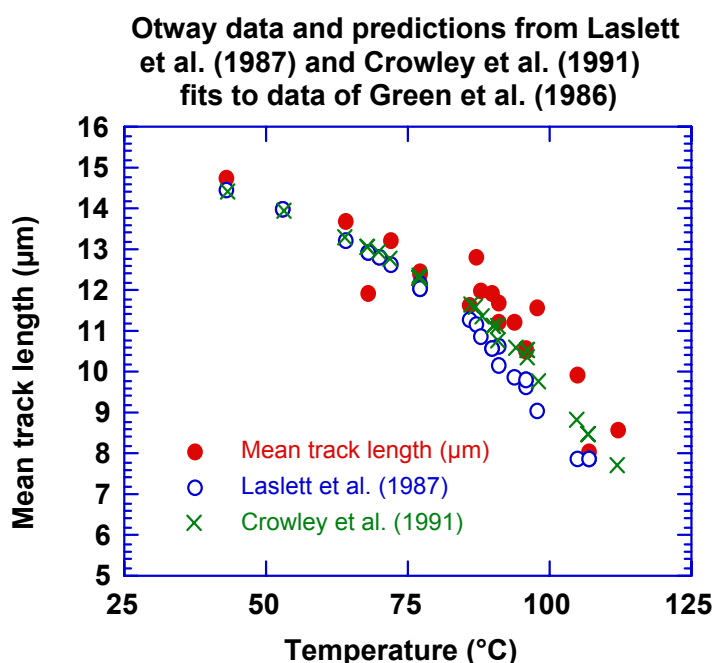
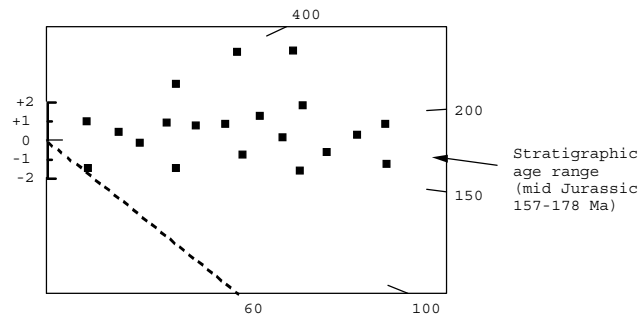


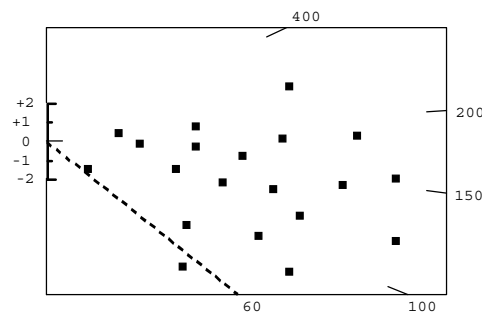
Figure C.6 Comparison of mean track length in samples from four Otway Basin reference wells with values predicted from Laslett et al. (1987) and the model fitted to the annealing data of Green et al. (1986) by Crowley et al. (1991). The predictions of the two models are not very different.



Little or no post-depositional annealing ($T < 60^\circ\text{C}$)



Moderate post-depositional annealing ($T \sim 90^\circ\text{C}$)



Total post-depositional annealing ($T > 110^\circ\text{C}$)

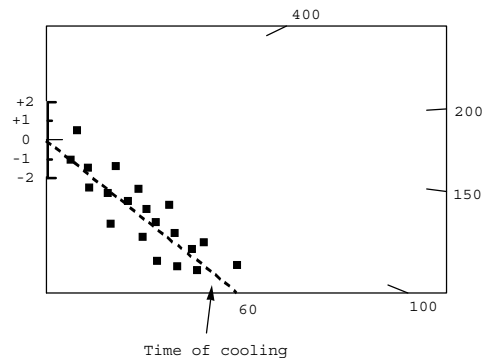


Figure C.7

Radial plots of single grain age data in three samples of mid-Jurassic sandstone that have been subjected to varying degrees of post-depositional annealing prior to cooling at ~ 60 Ma. The mid-point of the stratigraphic age range has been taken as the reference value (corresponding to the horizontal).

The upper diagram represents a sample which has remained at paleotemperatures less than $\sim 60^\circ\text{C}$, and has therefore undergone little or no post-depositional annealing. All single grain ages are either compatible with the stratigraphic age (within $y = \pm 2$ in the radial plot) or older than the stratigraphic age ($y_i > 2$).

The centre diagram represents a sample which has undergone a moderate degree of post-depositional annealing, having reached a maximum paleotemperature of around $\sim 90^\circ\text{C}$ prior to cooling. While some of the individual grain ages are compatible with the stratigraphic age ($-2 < y_i < +2$) and some may be significantly greater than the stratigraphic age ($y_i > 2$), a number of grains give ages which are significantly less than the stratigraphic age ($y < 2$).

The lower diagram represents a sample in which all apatite grains were totally annealed, at paleotemperatures greater than $\sim 110^\circ\text{C}$, prior to rapid cooling at ~ 60 Ma. All grains give fission track ages compatible with a fission track age of ~ 60 Ma (i.e., all data plot within ± 2 of the radial line corresponding to an age of ~ 60 Ma), and most are significantly younger than the stratigraphic age.



MAXIMUM TEMPERATURES NOW

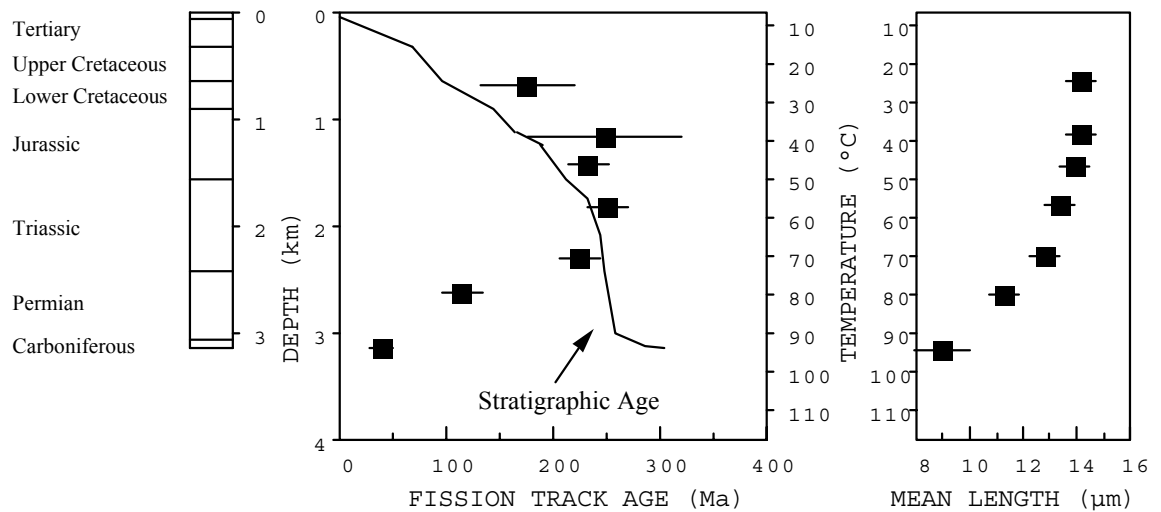


Figure C.8a Typical pattern of AFTA parameters in a well in which samples throughout the entire section are currently at their maximum temperatures since deposition. Both the fission track age and mean track length undergo progressive reduction to zero at temperatures of ~100 - 110°C, the actual value depending on the range of apatite compositions present.

HOTTER IN THE PAST

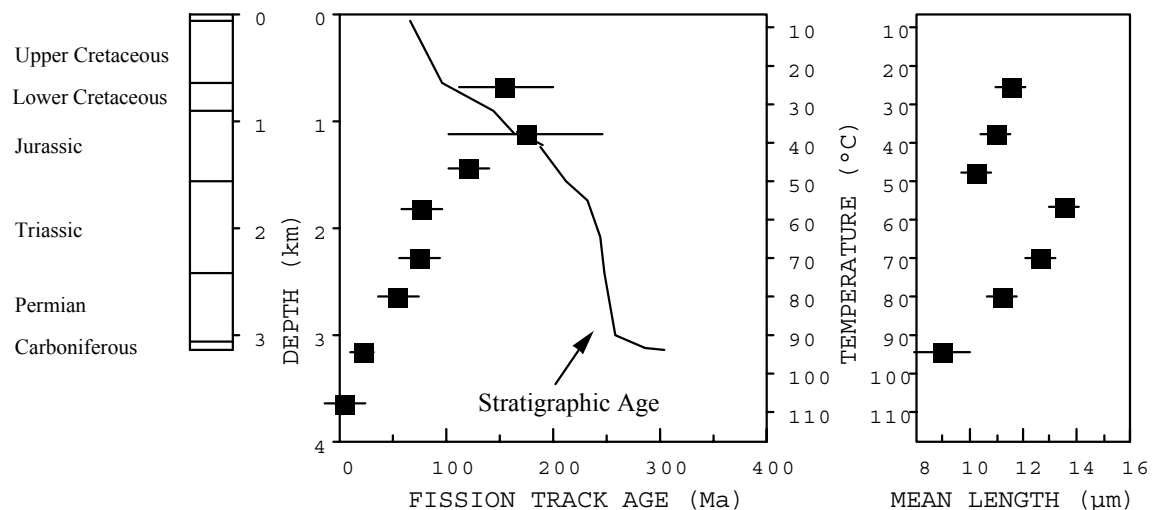


Figure C.8b Typical pattern of AFTA parameters in a well in which samples throughout the section were exposed to elevated paleotemperatures after deposition (prior to cooling in the Early Tertiary, in this case). Both the fission track age and mean track length show more reduction at temperatures of ~40 to 50°C than would be expected at such temperatures. At greater depths (higher temperatures), the constancy of fission track age and the increase in track length are both diagnostic of exposure to elevated paleotemperatures. See Appendix C for further discussion

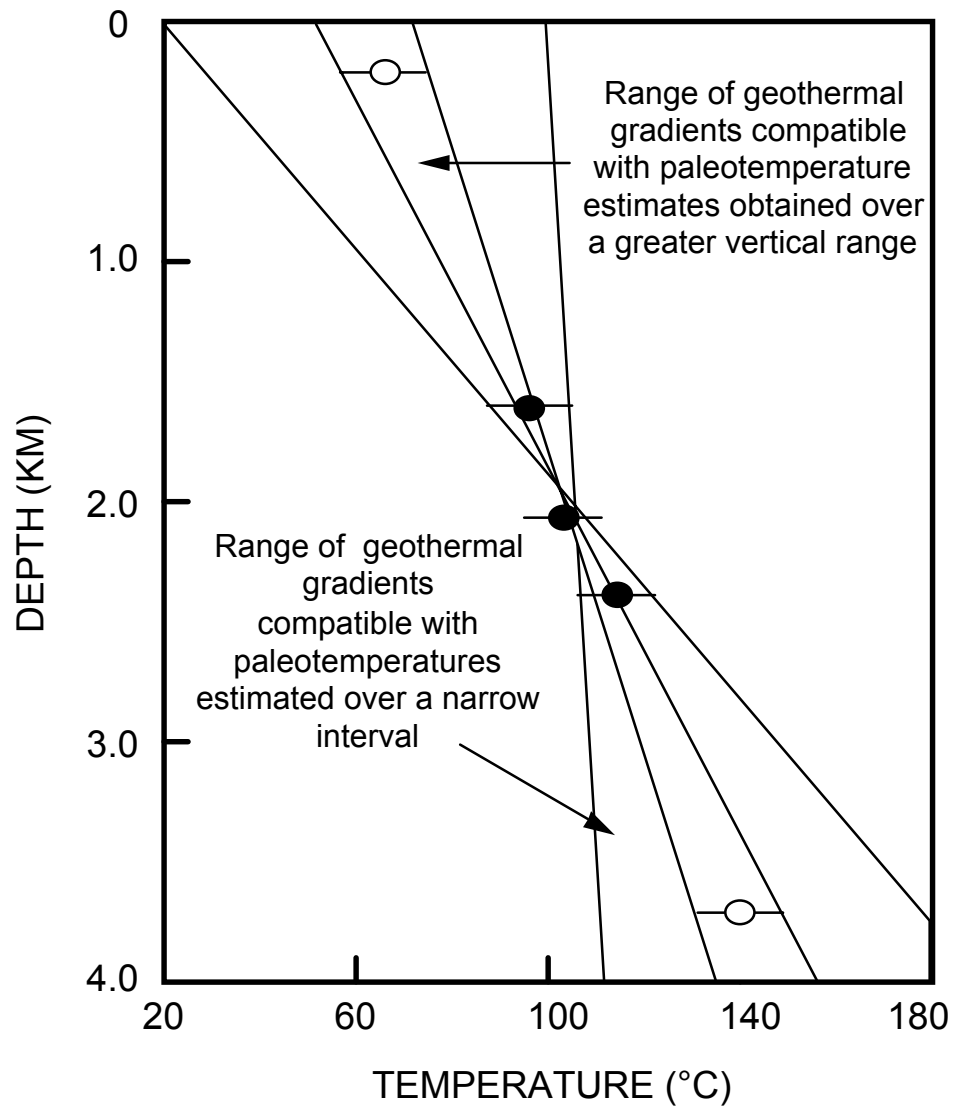


Figure C.9 It is important to obtain paleotemperature constraints over as great a range of depths as possible in order to provide a reliable estimate of paleogeothermal gradient. If paleotemperatures are only available over a narrow depth range, then the paleogeothermal gradient can only be very loosely constrained.

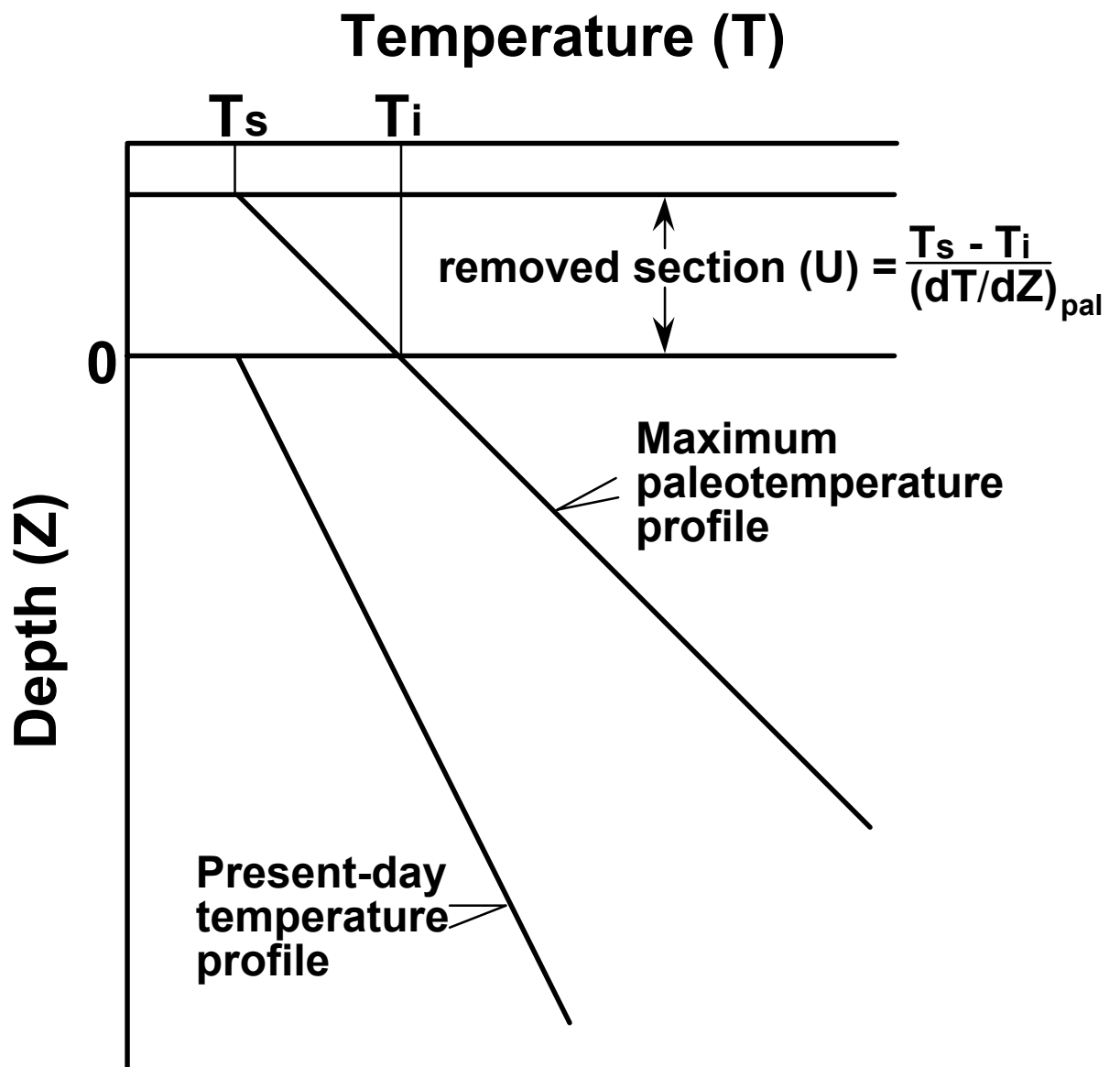


Figure C.10 If the paleogeothermal gradient can be constrained by AFTA and VR, as explained in the text, then for an assumed value of surface temperature, T_s , the amount of section removed can be estimated, as shown.



APPENDIX D

Vitrinite Reflectance Measurements

D.1 New vitrinite reflectance determinations

New vitrinite reflectance data were collected as part of this study, with details of determinations described in sections D.1 and D.2 below.

Samples

Samples were submitted for vitrinite reflectance determination to Keiraville Konsultants, Australia. Results and sample details are summarised in Table D.2, while supporting data, including maceral descriptions and raw data sheets, are presented in the following pages.

Equipment

Leitz MPV1.1 photometer equipped with separate fluorescence illuminator, Swift point counter. Reflectance standards: spinel 0.42%, YAG 0.91%, GGG 1.72%, SiC standard for cokes and masked uranyl glass for measurement of intensity (I) in fluorescence mode. With the Keiraville Konsultants equipment, it is possible to alternate from reflectance to fluorescence mode to check for associated fluorescing liptinite, or importantly with some samples, to check for bitumen impregnation, or the presence, intensity, and source of oil-cut.

Sample preparation

Samples are normally mounted in cold setting polyester resin and polished using Cr₂O₃ and MgO polishing powders. Epoxy resins or araldite can be used if required. "Whole rock" samples are normally used but demineralisation can be undertaken. Large samples of coals and cokes can be mounted and examined.

Vitrinite Reflectance measurement

The procedure used generally follows Australian Standard (AS) 2486, but has been slightly modified for use with dispersed organic matter (DOM). For each sample, a minimum of 25 fields is measured (the number may be less if vitrinite is rare or if a



limited number of particles of vitrinite is supplied, as may be the case with hand-picked samples). If wide dispersal of vitrinite reflectances is found, the number of readings (N) is increased until a stable mean is obtained.

Vitrinite identification is made primarily on textural grounds, and this allows an independent assessment to be made of cavings and re-worked vitrinite populations. Histograms are only used for population definition when a cavings population significantly overlaps the range of the indigenous population. Where such data provides additional information, the mean maximum reflectance of inertinite and/or the mean maximum reflectance of liptinite (exinite) is reported. For each field, the maximum reflectance position is located and the reading recorded. The stage is then rotated by 180° which should give the same reading. In practice, the readings are seldom identical because of stage run-out and slight surface irregularities. If the readings are within $\pm 5\%$ relative, they are accepted. If not, the cause of the difference is sought and the results rejected. The usual source of differences is surface relief. The measurement of both maxima results in a total of 50 measurements being taken for the 25 fields reported. Thus, the 50 readings consist of 25 pairs of closely spaced readings which provide a check on the levelling of the surface and hence additional precision.

As the vitrinite reflectance measurements are being made, the various features of the samples are noted on a check sheet to allow a sample description to be compiled. When the reflectance measurements are complete, a thorough check is made of liptinite fluorescence characteristics. At the same time, organic matter abundance is estimated using a global estimate, a grain count method or point count method as required.

Data presentation

Individual sample results are reported in the following format:

KK No.	Depth (ft)	R_{Vmax}^{*1}	Range ^{*2}	N ^{*3}
x10324	3106	0.79	0.64 - 0.91	25

*1 Mean of all the maximum reflectance readings obtained.

*2 Lowest Rmax and highest Rmax of the population considered to represent the first generation vitrinite population.

*3 Number of fields measured (Number of measurements = 2N because 2 maximum values are recorded for each field)

***Methods - Organic matter abundance and type.***

After completion of vitrinite reflectance readings, the microscope is switched to fluorescence-mode and an estimate made of the abundance of each liptinite maceral. Fluorescence colours are also noted (BG 3 long UV excitation, TK400 dichroic mirror and a K490 barrier filter). The abundances are estimated using comparison charts. The categories used for liptinite (and other components) are:

Descriptor	%	Source potential
Absent	0	None
Rare	<0.1	Very poor
Sparse	$0.1 < x < 0.5$	Poor to fair
Common	$0.5 < x < 2.0$	Fair to good
Abundant	$2.0 < x < 10.0$	Good to very good
Major	$10.0 < x < 40.0$	Very good (excellent if algal)
Dominant	>40.0	Excellent

Dispersed Organic Matter (DOM) composition

At the same time as liptinite abundances are estimated, total DOM, vitrinite and inertinite abundances are estimated and reported in the categories listed above. Liptinite (exinite) fluorescence intensity and colour, lithology and a brief description of organic matter type and abundance are also recorded in a further column. Coal is described separately from dispersed organic matter (DOM). These data can be used to estimate the specific yield of the DOM and form a valuable adjunct to TOC data.

Lithological composition

The lithological abundances are ranked. For cuttings, these data can be useful in conjunction with geophysical logs in assessing the abundance and nature of cavings. For cores, it provides a record of the lithology examined and of the lithological associations of the organic matter.

Coal abundance and composition

Where coals are present, their abundance is recorded and their composition is reported as microlithotypes thus:

Coal major, Vitrinite>Inertinite>Exinite, Clarodurite>vitrite>clarite>inertite.



These data give an approximate maceral composition and information about the organic facies of the coal. Where coal is a major or dominant component, and more precise maceral composition data are required, point count analyses should be requested. However, the precision of the original sampling is commonly a limiting factor in obtaining better quality data.

Abundance factor analysis

Especially where cuttings samples are used, abundance factor analyses are used to obtain an assessment of the maceral assemblages in the various lithologies. This can be done by a combination analysis using a point counter, but a large number of categories is required, and the precision is low if DOM is less than about 10%. For an abundance factor analysis (for core, 50 microscope fields of view) we assess the abundance of DOM, coal and shaly coal in 50 grains. The data can be used to plot DOM and coal abundance profiles.

Analyst/Advisor: Professor A.C. Cook

Prior to transmittal of final results, all samples are examined and checked by A.C. Cook who has more than 30 years' experience of work on coals, cokes, source rocks and source rock maturation.

D.2 Integration of vitrinite reflectance data with AFTA

Vitrinite reflectance is a time-temperature indicator governed by a kinetic response in a similar manner to the annealing of fission tracks in apatite as described in Appendix C. In this study, vitrinite reflectance data are interpreted on the basis of the distributed activation energy model describing the evolution of VR with temperature and time described by Burnham and Sweeney (1989), as implemented in the BasinMod™ software package of Platte River Associates. In a considerable number of wells from around the world, in which AFTA has been used to constrain the thermal history, we have found that the Burnham and Sweeney (1989) model gives good agreement between predicted and observed VR data, in a variety of settings.

As in the case of fission track annealing, it is clear from the chemical kinetic description embodied in equation 2 of Burham and Sweeney (1989) that temperature is more important than time in controlling the increase of vitrinite reflectance. If the Burham and Sweeney (1989) distributed activation energy model is expressed in the form of an Arrhenius plot (a plot of the logarithm of time versus inverse absolute temperature),



then the slopes of lines defining contours of equal vitrinite reflectance in such a plot are very similar to those describing the kinetic description of annealing of fission tracks in Durango apatite developed by Laslett et al. (1987), which is used to interpret the AFTA data in this report. This feature of the two quite independent approaches to thermal history analysis means that for a particular sample, a given degree of fission track annealing in apatite of Durango composition will be associated with the same value of vitrinite reflectance regardless of the heating rate experienced by a sample. Thus paleotemperature estimates based on either AFTA or VR data sets should be equivalent, regardless of the duration of heating. As a guide, Table D.1 gives paleotemperature estimates for various values of VR for two different heating times.

One practical consequence of this relationship between AFTA and VR is, for example, that a VR value of 0.7% is associated with total annealing of all fission tracks in apatite of Durango composition, and that total annealing of all fission tracks in apatites of more Chlorine-rich composition is accomplished between VR values of 0.7 and ~0.9%.

Furthermore, because vitrinite reflectance continues to increase progressively with increasing temperature, VR data allow direct estimation of maximum paleotemperatures in the range where fission tracks in apatite are totally annealed (generally above ~110°C) and where therefore AFTA only provides minimum estimates. Maximum paleotemperature estimates based on vitrinite reflectance data from a well in which most AFTA samples were totally annealed will allow constraints on the paleogeothermal gradient that would not be possible from AFTA alone. In such cases the AFTA data should allow tight constraints to be placed on the time of cooling and also the cooling history, since AFTA parameters will be dominated by the effects of tracks formed after cooling from maximum paleotemperatures. Even in situations where AFTA samples were not totally annealed, integration of AFTA and VR can allow paleotemperature control over a greater range of depth, e.g. by combining AFTA from sand-dominated units with VR from other parts of the section, thereby providing tighter constraint on the paleogeothermal gradient.

References

- Burnham, A.K. and Sweeney, J.J. (1989) A chemical kinetic model of vitrinite reflectance maturation. *Geochim. et Cosmochim. Acta*, 53, 2649-2657.
- Laslett, G.M., Green, P.F., Duddy, I.R. and Gleadow, A.J.W. (1987) Thermal annealing of fission tracks in apatite 2. A quantitative analysis. *Chem. Geol. (Isot. Geosci.Sect.)*, 65, 1-13.



Table D.1: Paleotemperature - vitrinite reflectance nomogram based on Equation 2 of Burnham and Sweeney (1989)

Paleotemperature (°C / °F)	Vitrinite Reflectance (%)	
	1 Ma Duration of heating	10 Ma Duration of heating
40 / 104	0.29	0.32
50 / 122	0.31	0.35
60 / 140	0.35	0.40
70 / 158	0.39	0.45
80 / 176	0.43	0.52
90 / 194	0.49	0.58
100 / 212	0.55	0.64
110 / 230	0.61	0.70
120 / 248	0.66	0.78
130 / 266	0.72	0.89
140 / 284	0.81	1.04
150 / 302	0.92	1.20
160 / 320	1.07	1.35
170 / 338	1.23	1.55
180 / 356	1.42	1.80
190 / 374	1.63	2.05
200 / 392	1.86	2.33
210 / 410	2.13	2.65
220 / 428	2.40	2.94
230 / 446	2.70	3.23

**Table D.2: Vitrinite reflectance sample details and results - well samples from Irish Rockall Trough boreholes (Geotrack Report #777)**

Sample number	Depth (m)	Sample type	Stratigraphic Subdivision	Stratigraphic age (Ma)	Present temperature ^{*1} (°C)	VR (Range) %	N
16/28-sb01 GC777-2.1	147	core	Maastrichtian?	70-65	9	-	
83/20-sb01 GC777-3.1	118	core	Coniacian? - Turonian	89-87	9	0.36 (0.25-0.46)	39
83/24-sb02 GC777-11.1	45	core	Mid to Upper Cretaceous	130-65	6	-	

Note: Some samples may contain both vitrinite and inertinite. Only vitrinite data is shown.

^{*1} See Appendix A for discussion of present temperature data.



GC777					IRELAND, ATLANTIC MARGIN B/H 83/20-sb01
KK #	Depth(m)				Sample description including liptinite fluorescence, maceral abundances, mineral fluorescence
Ref #.	/Type	\overline{R}_{vmax}	Range	N	
T7023	177	0.36	0.25-0.46	39	JURASSIC Sparse sporinite yellow to orange, sparse cutinite yellow, sparse liptodetrinite yellow to orange. (Silty calcareous sandstone. Dom abundant, V>>L>I. Vitrinite abundant, liptinite sparse, inertinite sparse to absent. Abundant reworked coals, mostly of high rank and showing significant bireflectance. Some grains are profoundly weathered. Mineral fluorescence weakly patchy moderate orange. Pyrite common.)
Ctgs 3.1	R _{reworked coal}	1.37	0.87-2.30	22	

Three blocks were prepared but all contain abundant vitrinite and are generally similar. The wisps of plant impressions seen in the bedding planes are preserved as telovitrinite with lesser amounts of detrovitrinite. Most of the telovitrinite is associated with carbonate. Reworked coal occurs as abundant coarse sand-sized grains ranging up to 0.8 mm in diameter. The rank range in the provenance was relatively high, ranging from less than 0.9% to over 2%. Some grains show severe weathering, but others are relatively fresh. Although the classic Carboniferous megaspore and densospore assemblages are not present there is little doubt the coals are Carboniferous in age.

GC777					IRELAND, ATLANTIC MARGIN B/H 83/28-1
KK #	Depth(m)				Sample description including liptinite fluorescence, maceral abundances, mineral fluorescence
Ref #.	/Type	\overline{R}_{vmax}	Range	N	
T7064 Core 2.1	147.2	-	-	-	MAASTRICHTIAN OR OLDER Liptinite absent. (Sandstone with dominant carbonate cement. Dom absent. All maceral group absent and sample is barren of organic matter. Mineral fluorescence absent from quartz grains, moderate to strong orange from carbonate. Pyrite absent.)
GC777					IRELAND, ATLANTIC MARGIN B/H 24-2
KK #	Depth(m)				MID CRETACEOUS Liptinite absent. (Sandstone with dominant carbonate cement. Dom absent. All maceral group absent and sample is barren of organic matter. Mineral fluorescence absent from quartz grains, moderate orange from carbonate. Abundant grains of sand sized iron oxides, common disseminated iron oxides. Pyrite absent.)
Ref #.	/Type	\overline{R}_{vmax}	Range	N	
T7065 Core 11.1	45.4	-	-	-	

Samples are barren. The amount of carbonate matrix is very high. Organic matter may have been lost when the carbonate was emplaced. It is probable however, that the sample with abundant iron oxides lacked organic matter at the depositional stage.